UNIVERSITY OF CALIFORNIA, SAN DIEGO

Single neuron modeling and data assimilation in BNST neurons

A dissertation submitted in partial satisfaction of the
requirements for the degree
Doctor of Philosophy

in

Physics with Specialization in Computational Science

by

Reza Farsian

Committee in charge:

Professor Henry D. I. Abarbanel, Chair
Professor Timothy Gentner
Professor Benjamin Grinstein
Professor Michael Holst
Professor Oleg Shpyrko

2013

The dissertation of Reza Farsian is approved, and it is acceptable in quality and form for publication on microfilm and electronically:

_____

_____

_____

_____

_____

Chair

University of California, San Diego

2013

DEDICATION

To Setareh and Kazem,
for their love and support.

EPIGRAPH

Blessed is the gambler
Who has lost everything
Except the desire
To gamble
Once more
—Rumi

TABLE OF CONTENTS

Signature Page . . . iii

Dedication . . . iv

Epigraph . . . v

Table of Contents . . . vi

List of Figures . . . ix

List of Tables . . . xii

Acknowledgements . . . xiii

Vita and Publications . . . xiv

Abstract of the Dissertation . . . xv

Chapter 1 Preface . . . 1

Chapter 2 Biophysical Models of Single Neuron . . . 4
- 2.1 Inrtoduction . . . 4
  - 2.1.1 Cell Membrane and Ions . . . 4
  - 2.1.2 Nernst Potential . . . 5
  - 2.1.3 Equilibrium Potential . . . 6
- 2.2 Model of Ion Channels . . . 7
  - 2.2.1 Transition Rates . . . 8
  - 2.2.2 Gating Variables . . . 10
  - 2.2.3 Steady State and Time Constant . . . 11
- 2.3 Hodgkin-Huxley Model . . . 13
  - 2.3.1 Electrical Circuit Model of a Neuron . . . 13
  - 2.3.2 Original Hodgkin-Huxley Model . . . 18
- 2.4 Constant Field Equation . . . 19
- 2.5 Zoo of Ionic Channels . . . 20
  - 2.5.1 Na Currents . . . 20
  - 2.5.2 K Currents . . . 21
  - 2.5.3 Ca Currents . . . 21
  - 2.5.4 Ca-activated channels . . . 21

Chapter 3 Parameter Estimation and Synchronization . . . 22
3.1 Introduction . . . 22
3.2 Parameter and State Estimation . . . 22
3.3 Chaos and Sensitivity on Initial Conditions . . . 25
3.4 Synchronization . . . 27
3.5 R-value Test . . . 29

Chapter 4 Twin Experiments . . . 30
4.1 Introduction . . . 30
4.2 Standardized Single Neuron Model . . . 30
4.3 Electrophysiological Experiments . . . 31
4.3.1 Voltage Clamp . . . 32
4.3.2 Current Clamp . . . 32
4.4 Currents . . . 33
4.4.1 Transient sodium current $I_{Na,t}$ . . . 33
4.4.2 Delayed rectifier potassium current I_{KDR} . . . 35
4.4.3 Inwardly rectifying potassium current I_{IR} . . . 36
4.4.4 Potassium current I_A . . . 40
4.4.5 Leak current I_{leak} . . . 41
4.5 Twin experiment Results . . . 41
4.5.1 Five dimensional model . . . 42
4.5.2 Seven Dimensional Model . . . 42
4.6 Summary . . . 57

Chapter 5 Estimation of BNST Neurons . . . 61
5.1 Introduction . . . 61
5.2 Model Construction . . . 61
5.3 Control Term and Cost Function . . . 63
5.4 Estimation and Prediction Workflow . . . 63
5.5 Type II BNST Neuron 1 . . . 64
5.6 Type II BNST Neuron 2 . . . 66
5.7 Summary . . . 75

Chapter 6 Statistical Path Integral Method . . . 83
6.1 Introduction . . . 83
6.2 Probabilistic Formulation . . . 83
6.2.1 Metropolis-Hastings . . . 86
6.2.2 Hybrid Monte Carlo . . . 87
6.2.3 Langevin Monte Carlo . . . 90
6.3 Estimation and Prediction in Colpitts Oscillator . . . 91
6.3.1 Number of Measured States . . . 91
6.3.2 Results . . . 92
6.4 Metropolis Coupled Markov Chain Monte Carlo . . . 93

Appendix A Phenomenological Current Equations 95
A.1 Current List 95
A.2 Voltage Equation 95
A.3 Transient sodium channel $I_{Na,t}$ 96
A.4 Persistence sodium channel $I_{Na,p}$ 97
A.5 Delayed rectifier potassium current I_K 98
A.6 Transient outward potassium current I_A 99
A.7 Slowly inactivating delay potassium current $I_{A,slow}$ 101
A.8 Inwardly rectifying potassium current I_{IR} 102
A.9 Low-threshold calcium current I_T 103

Appendix B Standardization of some currents 105
B.1 Delayed rectifier potassium current I_K 105
B.2 Transient outward potassium current I_A 106
B.3 Low-threshold calcium current I_T 107

Appendix C Detailed Model for Type II BNST Neurons 113
C.1 Steady states 113
C.2 Time constant 114

Bibliography 115

LIST OF FIGURES

Figure 2.1: Free energy 9
Figure 2.2: Opening and closing transition rate $\alpha(V)$ and $\beta(V)$ 10
Figure 2.3: Typical shape and range of steady states of activating and inactivating gates m (blue) and h (green) 12
Figure 2.4: Representation of Hodjkin-Huxley model as an electrical circuit 14

Figure 3.1: Lorenz attractor 25
Figure 3.2: Sensitivity to initial conditions in lorenz system 26
Figure 3.3: Surface of cost function 28

Figure 4.1: Current clamp simulation. Current base is at 0 mV, a 100 ms long step is applied starting at -50pA to 50pA at 10pA steps . . 34
Figure 4.2: Time constant of activation (blue) and inactivation (green) gating variables of $I_{Na,t}$ current. 35
Figure 4.3: Steady states of activation (blue) and inactivation (green) gating variables of $I_{Na,t}$ current. 36
Figure 4.4: $I_{Na,t}$ of a voltage clamp simulation with voltage base at -70mV, where a 100 ms step voltage was applied from -50mV to 20mV at 10mV steps 37
Figure 4.5: Time constant of activation gating variable of I_{KDR} current. . . 37
Figure 4.6: Steady states of activation gating variable of I_{KDR} current. . . 38
Figure 4.7: I_{KDR} of a voltage clamp simulation with voltage base at -70mV, where a 100 ms step voltage was applied from -50mV to 20mV at 10mV steps 38
Figure 4.8: Steady states of activation gating variable of I_{IR} current. 39
Figure 4.9: I_{IR} of a voltage clamp simulation with voltage base at -70mV, where a 100 ms step voltage was applied from -50mV to 20mV at 10mV steps 39
Figure 4.10: I_A of a voltage clamp simulation with voltage base at -70mV, where a 100 ms step voltage was applied from -50mV to 20mV at 10mV steps 41
Figure 4.11: HH-like model twin experiment including $I_{Na,T}$, I_{KDR}, I_{IR}, and I_l. Original and estimated trace for V 44
Figure 4.12: HH-like model twin experiment including $I_{Na,T}$, I_{KDR}, I_{IR}, and I_l. Original and estimated traces for all gating particles 45
Figure 4.13: Comparison of prediction and original voltage trace 45
Figure 4.14: Comparison of prediction and original gating variables trace . . 46
Figure 4.15: R value for the measurement time window 46
Figure 4.16: HH-like model twin experiment including $I_{Na,T}$, I_{KDR}, I_{IR}, I_A, and I_l. Original and estimated trace for V 47

Figure 4.17: HH-like model twin experiment including $I_{Na,T}$, I_{KDR}, I_{IR}, I_A, and I_l. Original and estimated trace for m 48
Figure 4.18: HH-like model twin experiment including $I_{Na,T}$, I_{KDR}, I_{IR}, I_A, and I_l. Original and estimated trace for h 49
Figure 4.19: HH-like model twin experiment including $I_{Na,T}$, I_{KDR}, I_{IR}, I_A, and I_l. Original and estimated trace for n 49
Figure 4.20: HH-like model twin experiment including $I_{Na,T}$, I_{KDR}, I_{IR}, I_A, and I_l. Original and estimated trace for r 50
Figure 4.21: HH-like model twin experiment including $I_{Na,T}$, I_{KDR}, I_{IR}, I_A, and I_l. Original and estimated trace for a 50
Figure 4.22: HH-like model twin experiment including $I_{Na,T}$, I_{KDR}, I_{IR}, I_A, and I_l. Original and estimated trace for b 51
Figure 4.23: R value for the measurement time window 51
Figure 4.24: HH-like model twin experiment including $I_{Na,T}$, I_{KDR}, I_{IR}, I_A, and I_l. Original and estimated trace for V 52
Figure 4.25: HH-like model twin experiment including $I_{Na,T}$, I_{KDR}, I_{IR}, I_A, and I_l. Original and estimated trace for m 52
Figure 4.26: HH-like model twin experiment including $I_{Na,T}$, I_{KDR}, I_{IR}, I_A, and I_l. Original and estimated trace for h 53
Figure 4.27: HH-like model twin experiment including $I_{Na,T}$, I_{KDR}, I_{IR}, I_A, and I_l. Original and estimated trace for n 53
Figure 4.28: HH-like model twin experiment including $I_{Na,T}$, I_{KDR}, I_{IR}, I_A, and I_l. Original and estimated trace for r 54
Figure 4.29: HH-like model twin experiment including $I_{Na,T}$, I_{KDR}, I_{IR}, I_A, and I_l. Original and estimated trace for a 54
Figure 4.30: HH-like model twin experiment including $I_{Na,T}$, I_{KDR}, I_{IR}, I_A, and I_l. Original and estimated trace for b 55
Figure 4.31: R-value for the measurement time window 55
Figure 4.32: HH-like model twin experiment including $I_{Na,T}$, I_{KDR}, I_{IR}, I_A, and I_l. Original and estimated trace for V 57
Figure 4.33: HH-like model twin experiment including $I_{Na,T}$, I_{KDR}, I_{IR}, I_A, and I_l. Original and estimated traces for all gating particles . . 58
Figure 4.34: R-value for the measurement time window 59
Figure 4.35: HH-like model twin experiment including $I_{Na,T}$, I_{KDR}, I_{IR}, I_A, and I_l. Original and estimated voltage traces 59
Figure 4.36: HH-like model twin experiment including $I_{Na,T}$, I_{KDR}, I_{IR}, I_A, and I_l. Original and estimated traces for all gating particles . . 60

Figure 5.1: Comparison of Data, estimation, and prediction 69
Figure 5.2: Comparison of Data, estimation, and prediction 70
Figure 5.3: Comparison of Data, estimation, and prediction 71
Figure 5.4: Comparison of Data, estimation, and prediction 72
Figure 5.5: Comparison of Data, estimation, and prediction 73

Figure 5.6: Comparison of Data, estimation, and prediction 74
Figure 5.7: Comparison of Data, estimation, and prediction 76
Figure 5.8: Comparison of Data, estimation, and prediction 77
Figure 5.9: Comparison of Data, estimation, and prediction 78
Figure 5.10: Comparison of Data, estimation, and prediction 79
Figure 5.11: Comparison of Data, estimation, and prediction 80

Figure 6.1: Colpitts Oscillator 92
Figure 6.2: Minima of A_0 for Colpitts oscillator with 3 and 4 parameters . . 93
Figure 6.3: Estimation and prediction of state variables of Colpitts oscillator. (All state variables and time have arbitrary units) 94

Figure B.1: Comparison of phenomenological and standardized curves for I_K 110
Figure B.2: Comparison of phenomenological and standardized curves for I_A 111
Figure B.3: Comparison of phenomenological and standardized curves for I_T 112

LIST OF TABLES

Table 2.1: List of concentration and reversal potential of some ions 6

Table 4.1: List of ionic currents used in twin experiments 33
Table 4.2: Parameters of $I_{Na,t}$ 34
Table 4.3: Parameters of I_{KDR} 35
Table 4.4: Parameters of I_{IR} 36
Table 4.5: Parameters of I_A 40
Table 4.6: Parameters of I_{leak} 41
Table 4.7: List of currents (5D) 42
Table 4.8: Estimated parameters of 5-D model 43
Table 4.9: List of currents (7D) 43
Table 4.10: Estimated parameters of 7-D model 56

Table 5.1: List of Ion Channels 62
Table 5.2: Summary of runs 64
Table 5.3: Run7-Sweep1 65
Table 5.4: Run1-Sweep1 65
Table 5.5: Run8-Sweep1 65
Table 5.6: Estimated parameter summary 67
Table 5.6: Summary of runs 81
Table 5.7: Parameter bounds for run1 81
Table 5.8: Estimated parameters in run 1 82

Table 6.1: Estimated Parameters for Colpitts Oscillator 93

ACKNOWLEDGEMENTS

First and foremost, I would like to thank my advisor, professor Henry D. I. Abarbanel, for all his support, motivation, and patience the past few years. This work would not have been possible without his intellectual guidance and passion for science.

Many thanks to my dissertation committee members Professor Timothy Gentner, Professor Benjamin Grinstein, Professor Michael Holst, and Professor Oleg Shpyrko for their valuable time and guidance.

I would also like to thank my experimental collaborator and mentor, Dr. Attila Szücs, for sharing his vast knowledge of electrophysiological experiments. His endless enthusiasm for neurophysiological experiment and elegant methods has been one of my greatest motivators as a graduate student. A great part of this work would have been impossible without his help.

I would like to acknowledge Professor Frank Wuerthwein, who was the reason I moved to UCSD. His guidance and support throughout my first few years as a graduate student was essential in my academic life.

Thanks to all my friends on and off campus for all the great memories the past few years.

VITA

2006	B. S. in Physics *with distinction*, University of Michigan, Ann Arbor
2008	M. S. in Physics, University of California, San Diego
2010	Ph. D. Candidate in Physics with Specialization in Computational Science, University of California, San Diego
2006-2012	Graduate Teaching Assistant, University of California, San Diego
2006-2012	Graduate Research Assistant, University of California, San Diego
2013	Ph. D. Physics with Specialization Computational Science

PUBLICATIONS

H. D. I. Abarbanel, D. R. Creveling, R. Farsian, and M. Kostuk, 2009 "Dynamical State and Parameter Estimation", *SIAM J. on Applied Dynamical Systems*, 8, pp. 1341-1381

H. D. I. Abarbanel, R. Farsian, A. Szucs, "Characterizations of Type II and III neurons of Bed Nucleus of Stria Terminalis of the Rat", *In preparation*

H. D. I. Abarbanel, R. Farsian, C. D. Meliza, D. Margoliash, A. Nogaret, "Modeling and Parameter Estimation of HVc Neurons in Zebra Finches", *In preparation*

ABSTRACT OF THE DISSERTATION

Single neuron modeling and data assimilation in BNST neurons

by

Reza Farsian

Doctor of Philosophy in Physics with Specialization in Computational Science

University of California, San Diego, 2013

Professor Henry D. I. Abarbanel, Chair

Neurons, although tiny in size, are vastly complicated systems, which are responsible for the most basic yet essential functions of any nervous system. Even the most simple models of single neurons are usually high dimensional, nonlinear, and contain many parameters and states which are unobservable in a typical neurophysiological experiment. One of the most fundamental problems in experimental neurophysiology is the estimation of these parameters and states, since knowing their values is essential in identification, model construction, and forward prediction of biological neurons.

Common methods of parameter and state estimation do not perform well for neural models due to their high dimensionality and nonlinearity. In this dissertation, two alternative approaches for parameters and state estimation of biological

neurons have been demonstrated: dynamical parameter estimation (DPE) and a Markov Chain Monte Carlo (MCMC) method. The first method uses elements of chaos control and synchronization theory for parameter and state estimation. MCMC is a statistical approach which uses a path integral formulation to evaluate a mean and an error bound for these unobserved parameters and states.

These methods have been applied to biological system of neurons in Bed Nucleus of Stria Termialis neurons (BNST) of rats. State and parameters of neurons in both systems were estimated, and their value were used for recreating a realistic model and predicting the behavior of the neurons successfully. The knowledge of biological parameters can ultimately provide a better understanding of the internal dynamics of a neuron in order to build robust models of neuron networks.

Chapter 1

Preface

One of the most fundamental problems in experimental neurophysiology is the identification of different ion channels and their dynamics in a neuron. In a typical single neuron experiment, membrane potential and injected current can be observed, but the amount of different ionic currents and their specific parameters is usually not measurable. The identification of these hidden parameters and states has been traditionally done by performing current clamp experiments. This method uses step currents of various magnitudes to depolarize and hyperpolarize neurons and record their membrane potential. This data is analyzed by naked eye and only an experienced neurophysiologist would be able to identify the signature of various currents. An alternative approach uses pharmacological blockers to deactivate specific channels, and provides information about the remaining ones. The main disadvantage of this method is the unknown effect these blockers can have on the dynamics of the cell. In both methods, it is not possible to measure the amount of currents present, or identify hidden parameters or states.

The main purpose of my dissertation research has been to develop quantitative methods of parameters and states estimation in neural systems. Most of my research has been done in direct collaboration with an experimental groups University of California, San Diego. This lab works on Bed Nucleus of Stria Termialis (BNST) of rats. These neurons are a part of the extended amygdala and play an important role in the regulation of stress and reward related behavior. The neurons from BNST are categorized into three types. I have mainly analyzed type

II and III neurons for their consistent behavior.

We have developed two methods to solve the above problem, namely, dynamical parameter estimation (DPE) method and a Markov Chain Monte Carlo (MCMC) approach. The first method uses elements of chaos control theory for estimation of parameters and states. The conventional approaches of parameter and state estimation, such as least square optimization, fail in a nonlinear regime due to embedded instabilities in the search space. DPE, however, can handle nonlinear systems by coupling data to the model of such systems (Chapter 3). This method also uses a new cost function designed to guarantee that the coupling to the model does not override the mathematical form of the equations of motion.

To ensure the robustness of DPE, we used lower dimensional chaotic and nonlinear systems such as Lorenz and Colpitts oscillator as test examples. In a chaotic system, the number of observables needs to be at least equal to the number of positive Lyaponov exponents for the estimation procedure to work. There is only one positive Lyaponov exponent in both Lorenz and Colpitts models, hence, one observable is sufficient for a successful estimation. Using these models, data was synthetically generated and one of the states was picked as the "observable". The time series from this state was treated as "data" for the estimation method. This procedure is also known as a *twin experiment.* After DPE successfully reproduced all parameters and hidden states of these systems, we shifted our focus on twin experiments of neuron models (Chapter 4).

I worked directly with each experimental group to taylor realistic biophysical models for specific neuron types, and used these models to estimate the hidden parameter and states. In each case, the model and its estimated parameters were used to predict the behavior of the neuron outside of the estimation window. This led to several successful predictions of neurons' membrane potential (Chapter 5).

Although the analysis of neural data using DPE has generated outstanding results, this method has two main disadvantages. It does not incorporate model error, and the final results of estimation have no error bounds on them. In order to avoid these problems, we have incorporated statistical methods of parameters and state estimation using various MCMC methods. These methods are used for

integration of a path integral defined for each model. The action of this path integral is small when the estimated states and measurements are close, and these states follow the given dynamics within a defined bound. Due to statistical nature of the MCMC method, the convergence is not as fast as DPE.

Chapter 2

Biophysical Models of Single Neuron

2.1 Inrtoduction

Neurons dynamic, just as any other biological system, are highly complex. Several models describe the function of neurons and generation of action potential and sub-threshold behavior. In this chapter, our main focus is on single compartmental models of neurons. Different conductance based models are introduced, and a standardized form is introduced which will be used throughout our studies of neurons.

2.1.1 Cell Membrane and Ions

Like other biological cells, neurons have a lipid bilayer which allows different concentration of ions inside and outside of the cell. The plasma membrane is selectively permeable to specific ions such as Na^+, K^+, Cl^-, and Ca^{2+}. The concentration difference of the ions inside and outside of the cell determines neuron's membrane potential, which is responsible for electric properties of the neuron. Na^+, Cl^-, and Ca^{2+} ions have a greater concentration outside the cell, and K^+ ions has a greater concentration inside the cell. These ionic concentrations are, however, subject to change due to the movement of these charged particles. The

inflow and outflow of ions is regulated via pore-forming proteins better known as ionic channels. When the cell membrane is sitting at a specific voltage ions will flow in and out until the cell reaches *equilibrium potential* (See section 2.1.3). If the neuron stays at this the extracellular and intracellular concentrations of ions remains unchanged. As the membrane potential deviates from equilibrium, however, the membrane's permeability to ions will also change, hence, currents of ions start flowing in and out of the cell until equilibrium is reached again.

Consider K^+ ions around an open ion channel that allows them to freely move in and out of the neuron. Due to diffusion, ions will be flowing down the concentration gradient, therefore, K^+ ions will be flowing outside of the cell. As these charged particles accumulate outside of the cell, the arriving ions have to face more positive ions, therefore, the outward flow of K^+ ions will slow down. Eventually, the current of ions will cease and the neuron's membrane will be at a new potential.

2.1.2 Nernst Potential

The two main forces which move ions across membrane are the difference in ionic concentration and electric potential across the membrane If we define the flux of ions diffusing from the high concentrate side of the membrane to the low concentration side as J_{diff}, and the flux of ions drifting from one side to the other due the electric potential difference as J_{diff}, then the total flux J can be written as:

$$J = J_{drift} + J_{diff} \tag{2.1}$$

The above equation can be rewriting as total current I:

$$I = -\left(uZ^2F[C]\frac{\partial V}{\partial x} + uZRT\frac{\partial [C]}{\partial x}\right) \tag{2.2}$$

where u is μ/N_A molar mobility, μ is mobility, Z is the valence of the ion, $[C]$ is ionic concentration, R is the gas constant, F is Faraday's constant, N_A is Avogadro's

number, and I is surface current density. Equation (2.2) is also known as Nernst-Plank equation.

When the forces resulting from ionic concentration difference and electric potential difference are equal and in opposite directions, the total current of an ion type would be zero. When this equilibrium state is reached, the membrane potential of the neuron is equal to *Nernst potential* of a specific ion type. In the case of potassium ions, Nernst potential of K^+ is given by the following equation:

$$E_{\mathrm{K}} = \frac{RT}{ZF} \ln \left[\frac{[\mathrm{K}^+]_o}{[\mathrm{K}^+]_i} \right] \tag{2.3}$$

E_{K} is also known as the *reversal potential* of K^+ ions. The value of Nernst potential depends valence of the ion and the intracellular and extracellular concentration, therefore, each ion has a specific reversal potential. Note that this is not independent of neuron type, since the concentrations of ions are different for different neurons. A list of typical extracellular and intracellular concentration of ions and their reversal potentials are given in table (2.1).

Table 2.1: List of concentration and reversal potential of some ions

Ion	Extracellular Concentration (mM)	Intracellular Concentration (mM)	Reversal Potential (at $36°C$) (mV)
K^+	5 to 20	140 to 400	-150 to -80
Na^+	145 to 460	5 to 50	+50 to +90
Ca^{2+}	1 to 2	1 to 2 $\times 10^{-4}$	+110 to +130
Cl^-	110 to 540	4 to 100	-90 to -40

2.1.3 Equilibrium Potential

In a realistic representation of a neuron, several ionic channels exist which allow different types of ions to enter and exit the cell. This creates a more complicated picture than what we described in the case of a single ion channel in previous section. The overall potential of a neuron depends on all ionic channels, the concentration of ions inside and outside of the cell, and the ionic currents. If the

ions are allowed to flow freely, after a long enough time, the ionic currents would be zero and the neuron would be at *equilibrium potential* or *resting potential* V_r. Given the concentration of ions across the cell membrane, the value of V_r is given by Goladman-Hodgkin-Kats (GHK) equation:

$$V_r = \frac{RT}{ZF} \ln \left[\frac{\sum_x P_x [x]_o}{\sum_x P_x [x]_i} \right] \tag{2.4}$$

where P_x is the permeability of the ion x. For example, in the presence of Na^+, K^+, and Cl^- ions, the neuron will have a resting membrane potential given by the following equation.

$$V_r = \frac{RT}{ZF} \ln \left[\frac{P_{\mathrm{K}}[\mathrm{K}^+]_o + P_{\mathrm{Na}}[\mathrm{Na}^+]_o + P_{\mathrm{Cl}}[\mathrm{Cl}^-]_i}{P_{\mathrm{K}}[\mathrm{K}^+]_i + P_{\mathrm{Na}}[\mathrm{Na}^+]_i + P_{\mathrm{Cl}}[\mathrm{Cl}^-]_o} \right] \tag{2.5}$$

In a typical neuron, the resting membrane potential can be anywhere between -80 to -60 mV.

2.2 Model of Ion Channels

The presence of long protein in the neuron membrane make it permeable to specific ions as described in section 2.1.1 Ion channels are selectively allow one or more types of ions to freely move through their water-filled pores. These channels are sensitive to electric potential of the membrane and their permeability changes with voltage.

To simplify the modeling of ion channels, we assume that a channel can either be in open state O, or closed state C. At any given time, there is a probability associated with each of these states. Depending on these probabilities, an ensemble of channels will have some fraction of it in open state and the rest in closed state. Individual channels, however, go from open state to closed and vice versa with some transition rate. We define these two transition rates as α to go from closed to open state, and β to go from open to closed state.

$$C \underset{\beta}{\overset{\alpha}{\rightleftarrows}} O$$

2.2.1 Transition Rates

A free energy is associated with transition between open and closed states. (Figure 2.1) The shape of this free energy is usually a function of membrane potential and has a complicated form. Transition rates, α and β, are proportional to an exponential functions of the free energy barrier's amplitude based on the theory of reaction rates.

$$\begin{aligned} \alpha(V) &\propto \exp\left[-\Delta G_\alpha(V)/RT\right] \\ \beta(V) &\propto \exp\left[-\Delta G_\beta(V)/RT\right] \end{aligned} \tag{2.6}$$

where ΔG_α and ΔG_β are the height of free energy barrier going from closed to open state and open to closed state respectively. Free energy G is usually a complicated function of membrane voltage, therefore, ΔG is not easily determined. We can use a Taylor expansion of this function around voltage V to approximate the shape of ΔG:

$$\Delta G(V) = c_0 + c_1 V + c_2 V^2 + O(V^3) \tag{2.7}$$

where c_0, c_1, c_2, ... are constants. Using this equation along with the expression for α we have:

$$\alpha(V) = \exp\left[-(c_0 + c_1 V + c_2 V^2 + O(V^3))/RT\right] \tag{2.8}$$

Here we will keep only the linear terms and drop out all other terms in the above expansions. Therefore, we can re-write the transition rates.

$$\begin{aligned} \alpha(V) &= a_0 e^{-a_1 V} \\ \beta(V) &= b_0 e^{-b_1 V} \end{aligned} \tag{2.9}$$

where a_0, a_1, b_0, and b_1 are new constants, and both α and β are functions of membrane voltage. Constants a_0 and b_0 are independent of membrane voltage and are equal to each other when in the absence of membrane potential. The constants

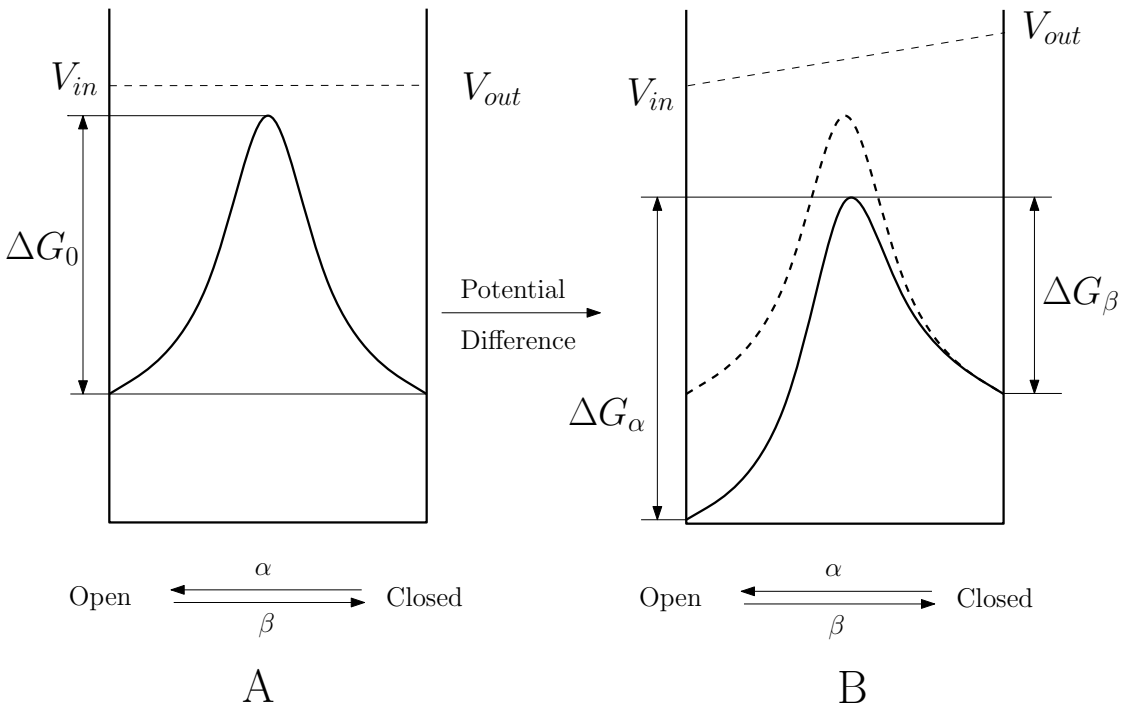

Figure 2.1: Free energy

inside the exponential function, however, do depend on the voltage. a_1 and b_1 are equal when the potential difference across the membrane is zero, hence, the opening rate α is identical to the closing rate β. Defining the height of the energy barrier in the absence of membrane potential as ΔG_0, we have:

$$\begin{aligned} \alpha(V) &= k_0 e^{-\Delta G_0(V)/RT} \\ \beta(V) &= k_0 e^{-\Delta G_0(V)/RT} \end{aligned} \tag{2.10}$$

where both a_0 and b_0 are defined as k_0 here.

When a potential difference is applied across the membrane, there is a shift in free energy barrier height, which makes transition rates asymmetric. Figure (2.1) represents how the presence of voltage membrane affects the free energy. Equation (2.10) transforms to:

$$\begin{aligned} \alpha(V) &= k_0 e^{-(\Delta G_\alpha(V)/RT)} \\ \beta(V) &= k_0 e^{-(\Delta G_\beta(V)/RT)} \end{aligned} \tag{2.11}$$

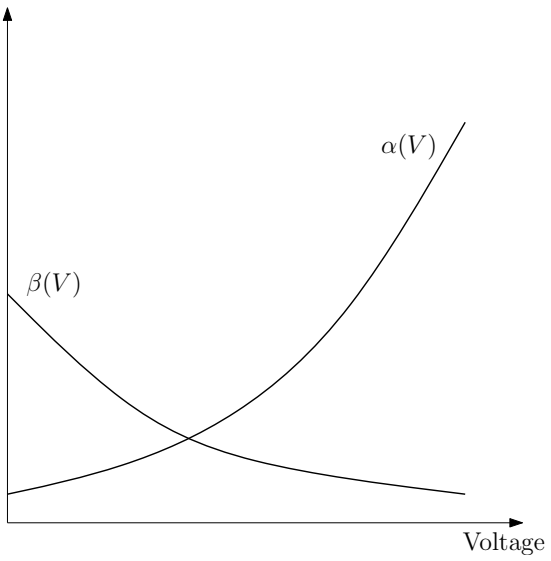

Figure 2.2: Opening and closing transition rate $\alpha(V)$ and $\beta(V)$

2.2.2 Gating Variables

All of the above can be applied to any single channel; however, if we consider an ensemble of similar channels the same transition rates can be used. Here we define m as the ratio of channels which are open.

$$m = \frac{[O]}{[C] + [O]} \tag{2.12}$$

where $[O]$ denotes the number of open channels and $[C]$ denotes the number of closed ones. m is often referred to as *gating variable* of a channel.

At any given time t, the fraction of channels which are open is $m(t)$, and since there are only two possible states, the fraction of closed channels are $(1 - m(t))$. The open channels are going from open to closed state at a transition rate $\beta(V)$, and the closed channels are going from closed to open state at a rate $\alpha(V)$. Therefore, the rate at which $m(t)$ is changing over time is the fraction of channels going from closed to open minus the closed channels which are opening. This time evolution can be mathematically represented as an ordinary differential equation for the gating variable $m(t)$:

$$\frac{dm}{dt} = \alpha(V) \cdot (1 - m) - \beta(v) \cdot m \tag{2.13}$$

An alternative way to interpret gating variable m is to take is as a probability of a single channel being open or closed. m is a function of voltage and time, where the voltage dependence is imbedded in opening and closing transition rates $\alpha(V)$ and $\beta(V)$. Depending on the parameters a_1 and b_1 in equation (2.9), $\alpha(V)$ and $\beta(V)$ may increase or decrease as a higher value of voltage. a_1 and b_1 always have opposite signs meaning as $\alpha(V)$ increases $\beta(V)$ will decrease or vice versa.

Gating variables can be categorized into two groups *activating* and *inactivating* gating variables. A gating variable is activating if its opening rate $\alpha(V)$ increases with voltage, meaning at higher voltages a channel is more probable to be open. In contrast, in an inactivating gating variable $\alpha(V)$ decreases as voltage increases, hence, the channel has a higher probability of being closed at higher voltage values. Traditionally, activating gating variables are represented by m, and deactivating gating variables are represented by h. A Channel can have one of both of these gating variables. (See section 2.5)

2.2.3 Steady State and Time Constant

When a neuron is kept at a constant voltage, after a long enough time m will reach a steady state, denoted as m_∞. Using equation (2.13), and the fact that at steady state the change in m is zero ($dm/dt = 0$), we have:

$$m_\infty = \frac{\alpha(V)}{\alpha(V) + \beta(V)} \tag{2.14}$$

This equation can be re-written:

$$\frac{dm}{dt} = \left[\frac{\alpha}{\alpha + \beta} - m\right] \cdot (\alpha + \beta) \tag{2.15}$$

The first term in the bracket is equal to m_∞, and the inverse of the last term, $(\alpha + \beta)$, has dimensions of time. $1/(\alpha + \beta)$ is defined as the activating time constant of gating variable m, and is denoted as τ_m. The time evolution of m in equation (2.13) can be rewritten in terms of m_∞ and τ_m.

$$\frac{dm(t)}{dt} = \frac{m_\infty(V) - m(t)}{\tau_m(V)} \tag{2.16}$$

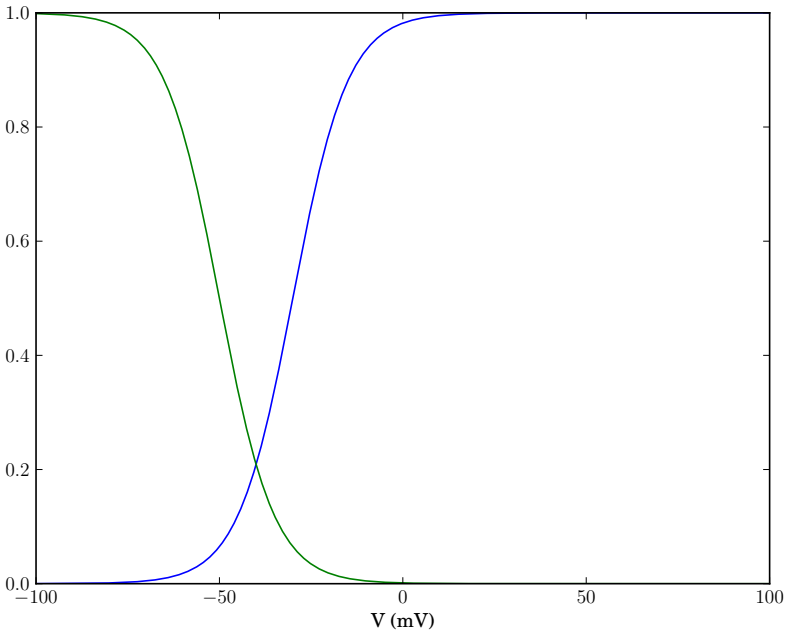

Figure 2.3: Typical shape and range of steady states of activating and inactivating gates m (blue) and h (green)

where,

$$\tau_m(V) = \frac{1}{\alpha(V) + \beta(V)} \tag{2.17}$$

Note that both m_∞ and τ_m are functions of membrane voltage. Steady state and time constant of m can be re-written using the exponential form of transition rates from equation (2.9).

$$m_\infty(V) = \frac{1}{1 + \exp[-(V - v_0)/k_0]} \tag{2.18}$$

$$\tau_m(V) = \frac{1}{\exp[-(V - v_1)/k_1] + \exp[-(V - v_2)/k_2]} \tag{2.19}$$

with v_i and k_i where $i = 0, 1, 2$ as new parameters. The steady state of a gating variable has the shape of a sigmoidal function given by equation (2.18). Time constant is a measure of how quickly a gating variable responds to a change in voltage. The functional form of τ_m is usually bell-shaped.

For activating gating variables m, the value of m_∞ at high values of V is either close or equal to one. At low voltage values, the steady state is near zero at lower voltage. Inactivating gating variables h respond in the exact opposite way to voltage change as expected. Figure (2.3) shows steady states of a typical activating and inactivating gating variables.

12

2.3 Hodgkin-Huxley Model

Main neuron features such as spike generation and sub-threshold behavior can can be modeled using simple electrical elements such as resistors and capacitors. Although the resistive behavior of the membrane is not ohmic, in cases where the intracellular and extracellular concentrations of a type of ion are not dramatically different, the cell's membrane can be assumed to operate as a linear resistor. The presence of ions and potential difference across the cell membrane can be represented as cell capacitance C_m. The flow of these charged particles across the membrane is regulated by ion channels which are permeable to specific kind of ions. The activity of these ion channels can be represented as an electrical resistor and can be represented mathematically as following:

$$I_{ion} = g_{ion}(V - E_{ion}) \tag{2.20}$$

The dynamics of these currents depend on the type of channel and its kinetic as described in section 2.2.

2.3.1 Electrical Circuit Model of a Neuron

Figure (2.4) represents a simple circuit model of an idealized point neuron including three different currents and a cell capacitance. Capacitance C_m and leak current I_L describe the passive behavior of a neuron, and are responsible for sub-threshold of a neuron. Sodium and potassium currents, I_{Na} and I_{K}, are required for action potential generation.

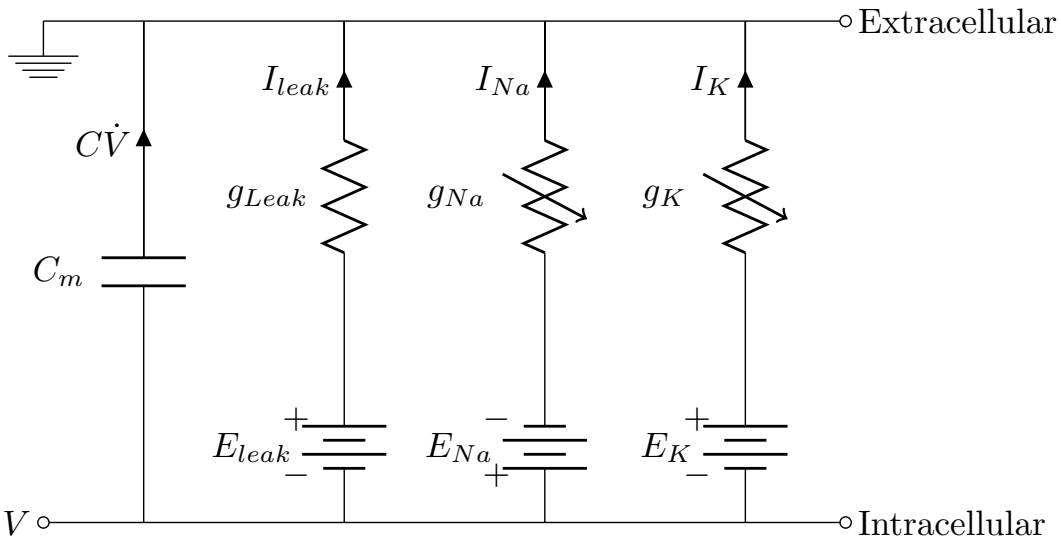

Figure 2.4: Representation of Hodjkin-Huxley model as an electrical circuit

In the definition of membrane voltage, the extracellular environment is treated as ground.

$$V = V_{\text{in}} - V_{\text{out}} \tag{2.21}$$

We can use Kirchhoff's voltage law to find I_{Na} in terms of sodium conductance and reversal potential. Starting from inside the cell where the potential is defined to be V. This potential drops by Nernst potential of Na^+ ions and conductance of sodium channel.

$$I_{\text{Na}} = g_{\text{Na}}(V - E_{\text{Na}}) \tag{2.22}$$

The above equation is only true when the direction of current is defined outward. Changing this direction will obviously introduce a negative to the right-hand side of this formula. A similar formula can be written for potassium and leak currents, I_{L} and I_{K}. The change of membrane voltage introduces another current proportional to the membrane capacitance C_m. Adding up all these currents according to Kirchhoff's current law, we get an expression which described the evolution of membrane potential over time.

$$C_m \frac{dV}{dt} = -\underbrace{g_{\mathrm{Na}}(V - E_{\mathrm{Na}})}_{I_{\mathrm{Na}}} - \underbrace{g_{\mathrm{K}}(V - E_{\mathrm{K}})}_{I_{\mathrm{K}}} - \underbrace{g_{\mathrm{L}}(V - E_{\mathrm{L}})}_{I_{\mathrm{L}}} \tag{2.23}$$

Here, C_m is the membrane capacitance, and its value is close to 1.0 with units of $\mu F/cm^2$. g_{Na}, g_{K} and g_{L} are conductances in mS/cm^2. Reversal potentials E_{Na}, E_{K}, and E_{L} represent the equilibrium potentials for Na^+, K^+ and leak currents and have units of mV. The units of time are ms over which the voltage is changing.

Na and K Currents and Gating Variables

Sodium and potassium ion conductances, g_{Na} and g_{K}, are not constants. This is a representative of the voltage gated nature of these currents. Ion conductance can be represented using the following general form:

$$g_{\mathrm{ion}}(V) = \bar{g}_{\mathrm{ion}} m^a(V) h^b(V) \tag{2.24}$$

where $\bar{g}_{\mathrm{ion}}$ is the maximal conductance, m and h are activating and deactivating gating variables, and a and b are the corresponding powers of those gating variables.

The gating variables follow similar dynamics described in section 2.2. The equation of motion for a gating variable $X(t)$ is:

$$\frac{dX(t)}{dt} = \frac{X_\infty - X(t)}{\tau_X}$$

where $X(t)$ is the probability of a channel being open at time t. X_∞ and τ_X are commonly functions of membrane voltage. Given this formalism, the potassium and sodium ion currents can be written as:

$$I_{\mathrm{Na}} = \bar{g}_{\mathrm{Na}} m^3 h (E_{\mathrm{Na}} - V) \tag{2.25}$$

$$I_{\mathrm{K}} = \bar{g}_{\mathrm{K}} n^4 (E_{\mathrm{K}} - V) \tag{2.26}$$

Here $\bar{g}_{\mathrm{Na}}$ and $\bar{g}_{\mathrm{K}}$ are maximal conductances, m and n are activating gating variables for sodium and potassium channels respectively, and h is the only deactivating gating variable which is present in sodium channel. m^3h term can be interpreted as 3 activating gates present versus one deactivating gate in a sodium channel. Same

interpretation is valid for n^4 term in potassium current equation. The equation of motion of these three gating variables are of general form described above.

$$\frac{dm}{dt} = \frac{m_\infty(V) - m}{\tau_m(V)} \tag{2.27}$$

$$\frac{dh}{dt} = \frac{h_\infty(V) - h}{\tau_h(V)} \tag{2.28}$$

$$\frac{dn}{dt} = \frac{n_\infty(V) - h}{\tau_n(V)} \tag{2.29}$$

These equations together with equation (2.23) are referred to as Hodgkin-Huxley model. Kinetics of steady states and time constant have similar forms to that of equations (2.18) and (2.19).

Alternatively, the dynamical equations of m, h, and n can be written in terms of opening and closing transition rates, α and β. The three differential equations follow the general form introduced in equation (2.13).

$$\begin{aligned} \frac{dm}{dt} &= \alpha_m(V)(1-m) - \beta_m(V) \cdot m \\ \frac{dh}{dt} &= \alpha_h(V)(1-h) - \beta_h(V) \cdot h \\ \frac{dn}{dt} &= \alpha_n(V)(1-n) - \beta_n(V) \cdot n \end{aligned} \tag{2.30}$$

This is the formalism adopted by Hodgkin and Huxley in their original paper of 1952. Section 2.3.2 provides a detailed discussion of this model.

Passive Properties

In the absence of sodium and potassium currents, the neuron behaves as a simple RC circuit and equation (2.23) will reduce to:

$$C_m \frac{dV}{dt} = g_{\mathrm{L}}(E_{\mathrm{L}} - V) \tag{2.31}$$

This equation represents a battery (E_{L}) and resistor in series connected to a capacitor (C_m) in parallel. Leak current represents the pore channels that are always open and are responsible for constant leakage of ions across the membrane.

The passive flux of ions through different ion leak channels is represented as one *leak channel*. Cell's permeability to each ion can be represented as a constant leak conductance for that ion. If g^*_{ion} represents the conductance of a specific ions leak channel, the reversal potential of the combined leak channel E_{L} can be written as:

$$E_{\text{L}} = \frac{\sum_{\text{ion}} g^*_{ion} E_{\text{ion}}}{\sum_{\text{ion}} g^*_{\text{ion}}} \tag{2.32}$$

This is equivalent to resting potential of a neuron described by Goladman-Hodgkin-Kats equation (2.4). The total conductance of a leak channel is equal to sum of all present leak channels, $g_{\text{L}} = \sum_{\text{ion}} g_{\text{ion}}$. The permeability of the membrane to specific ion is an intrinsic property of the neuron, hence, both g_{L} and E_{L} are constant and independent of membrane voltage.

Injected Current

In addition to the intrinsic leak and ionic currents of a neuron, an external current can be injected into a cell. This current is usually referred to as *injected current*, I_{inj}, and can be added to equation (2.23).

$$C_m \frac{dV}{dt} = g_{\text{Na}}(E_{\text{Na}} - V) + g_{\text{K}}(E_{\text{K}} - V) + g_{\text{L}}(E_{\text{L}} - V) + I_{\text{inj}} \tag{2.33}$$

In the absence of I_{inj}, neuron's potential will eventually reach its resting value V_r. Injected current is a driving force which can bring a neuron to different voltage regions. The response of a neuron to various types of injected currents facilitates characterization of a neuron. If a constant injected current is applied the resting potential will change to:

$$V_r = \frac{g_{\text{Na}} E_{\text{Na}} + g_{\text{K}} E_{\text{K}} + g_{\text{L}} E_{\text{L}} + I_{\text{inj}}}{g_{\text{Na}} + g_{\text{K}} + g_{\text{L}}} \tag{2.34}$$

A positive current will result in a higher resting potential V_r, in this case the neuron has been *depolarized* On there other hand, a negative current will lower V_r and *hyperpolarizes* the neuron.

Input Resistance

Another intrinsic property of a neuron is the total resistance of the membrane commonly referred to as *membrane input resistance*, R_{inp}. Given the total area of the cell A in cm^2, and conductance of the leak current g_{L} in mS/cm^2, R_{inp} is equal to:

$$R_{\text{inp}} = \frac{1}{Ag_{\text{L}}} \tag{2.35}$$

and has units of $k\Omega$.

2.3.2 Original Hodgkin-Huxley Model

In this section, we will introduce the original Hodgkin-Huxley model with its exact functional forms and parameter values. This model was was first published by Hodgkin and Huxley in 1952. In their study, Hodgkin and Huxley used data from giant squid axon, and constructed a phenomenological model based on their observations. Their model had voltage and three gating particles as the state variables described by the following equations:

$$\begin{aligned}
\frac{dV}{dt} &= \frac{1}{C_m}\Big[- \bar{g}_{\text{Na}} m^3 h (V - E_{\text{Na}}) - \bar{g}_{\text{K}} n^4 (V - E_{\text{K}}) - \bar{g}_{\text{L}} (V - E_{\text{L}}) \Big] \\
\frac{dm}{dt} &= \alpha_m(V)(1 - m) - \beta_m(V) \cdot m \\
\frac{dh}{dt} &= \alpha_h(V)(1 - h) - \beta_h(V) \cdot h \\
\frac{dn}{dt} &= \alpha_n(V)(1 - n) - \beta_n(V) \cdot n
\end{aligned} \tag{2.36}$$

The evolution of gating variables m, h, and n are described in terms of transition rates α and β here. The voltage dependence functional form these transition rates are described in following equation set (2.37). All of the specific parameter values in these equations are purely phenomenological and were estimated to match the observed data.

$$\alpha_m(V) = \frac{-0.1(V-25)}{\exp[-(V-25)/4]-1} \qquad \beta_m(V) = 4\exp[-V/18]$$
$$\alpha_h(V) = 0.07\exp[-V/20] \qquad \beta_h(V) = \frac{1}{1+\exp[-(V+30)/10]}$$
$$\alpha_n(V) = \frac{-0.01(V+10)}{\exp[-(V+10)/10]-1} \qquad \beta_n(V) = 0.125\exp[-V/80] \tag{2.37}$$

2.4 Constant Field Equation

Hodgkin-Huxley model is a sufficient model for ions whose intracellular and extracellular concentrations are not dramatically different. This is usually the case for ions such as Na^+, K^+, and Cl^-. For Ca^{2+}, however, the inside and outside concentrations can be several orders of magnitude different. (See table 2.1). Under these conditions, we cannot assume that the membrane acts as an ohmic resistor, and a different formulation of ion currents is necessary. In this regime, current equation (2.20) cannot properly represent the ion current. The ohmic current equation is replaced with *constant field equation*:

$$I_{\text{ion}} = \bar{P}_{\text{ion}} m^a h^b G(V, [\text{ion}]_o, [\text{ion}]_i) \tag{2.38}$$

where $\bar{P}_{\text{ion}}$ is the maximum permeability of an ion. m and h are activating and inactivating gating variables, respectively, a and b are the corresponding powers of those gating variables. The gating variables follow similar dynamics as explained in section 2.2. G is a function of membrane potential and ion concentrations inside and outside the cell.

$$G(V, [\text{ion}]_o, [\text{ion}]_i) = \frac{Z^2F^2V}{RT} \times \frac{[\text{ion}]_i - [\text{ion}]_o \exp(-ZFV/RT)}{1-\exp(-ZFV/RT)} \tag{2.39}$$

where Z is the valence of the ion, [ion] is ionic concentration inside or outside the neuron, R is the ideal gas constant, F is Faraday's constant, and T is temperature. Equation (2.38) and (2.39) are also known as Goldman-Hodgking-Katz (GHK) equations. These equations are usually used when a more precise model of ion

current is desired. Nernst equation (2.3) is an approximation to GHK equations and is only used in cases where the ion concentrations are not considerably different across the membrane.

In Hodgkin-Huxley model, the only state variables are voltage and gating variables, and we have assumed that ionic concentrations inside and outside of the cell are approximately constant over time. Ionic concentrations show up explicitly in GHK models, and are introduced as new state variables. For ions such as Ca^{2+}, the extracellular does not change significantly over time. The intracellular concentration of Ca^{2+} ions, however, changes due to calcium currents and active transport of these ions.

2.5 Zoo of Ionic Channels

The main features of a neuron such as spiking and sub-threshold behavior can be modeled using a simple Hodgkin-Huxley neuron. Kinetic parameters in sodium and potassium currents, I_{Na} and I_{K}, are responsible for spike generation, shape, and height of the spike. Leak current, on the other hand, models the passive behavior of the cell in sub-threshold regions. In our study of real neurons, however, we had to add other currents in order to capture the real behavior of a neuron.

2.5.1 Na Currents

Two types of Na currents, transient sodium and persistent sodium currents, exist in a large family of neurons. The main different between these two currents are the activation time and their magnitude. Transient sodium current, $|_{\mathrm{Na},T}$ is a fast current that inactivates within a few milliseconds. This current is present in all neurons and is essential for spike generation. Persistent sodium current, $I_{\mathrm{Na},P}$, is a slower current which contributes to stead state firing.

2.5.2 K Currents

Potassium currents are a large and diverse family of currents. The main current which is essential in spike generation is delayed rectifier potassium current I_{KDR}. The activation time of this current is slower than $I_{\mathrm{Na},T}$, and is responsible for depolarization of neuron's membrane potential during an action potential.

Hyperpolarization-activated current, h current, is a special type of current which activate with hyper polarization of a neuron. Features of this current can be observed in sub-threshold region of voltage. This current is important in the rhythmic generation of oscillation and the slow depolarization of cell.

2.5.3 Ca Currents

Calcium currents are present in almost all neurons. We have used two main types of Ca currents, hight threshold Ca current I_L and low-threshold Ca current I_T. High-threshold current I_L is activated at -40 mV, in contrast, low-threshold current I_T is activated at around -65 mV.

2.5.4 Ca-activated channels

The activation of some channels are sedative to Ca^{2+} ions. This current is activated by increase of intracellular concentration of Ca^{2+} ions.

Chapter 3

Parameter Estimation and Synchronization

3.1 Introduction

One of the most important problems scientists face in dealing with complex biological systems is identifying the hidden parameters and states of such systems. Conventional methods of system verification fail in extremely nonlinear regimes. In this chapter, we will discuss method methods that can be used for parameter and state estimation of highly nonlinear and chaotic systems.

3.2 Parameter and State Estimation

A dynamical system can be described by a set of first order ordinary differential equations (ODE) as shown in equation (3.1). The state variables of this D dimensional dynamical system are represented by vector $\mathbf{x} = \{x_1, x_2, \ldots, x_D\}$, and L parameters q are denoted by vector $\mathbf{q} = \{q_1, q_2, \ldots, q_L\}$. $\mathbf{F}$ are the set of functions which dictate the time evolution of state variables $\mathbf{x}$, and can take any mathematical form.

$$\frac{d\mathbf{x}}{dt} = \mathbf{F}\Big(\mathbf{x}, \mathbf{p}\Big) \tag{3.1}$$

Parameter vector $\mathbf{p}$, by definition, is a constant over time:

$$\frac{d\mathbf{p}}{dt} = 0 \tag{3.2}$$

In a real experimental system, only a few of the state variables are observable. Imagine only the first state variable, x_1, is observable and we are interested in finding the value of the unobserved state variables and parameters. We can re-write the original equations in terms of the observable state x_1, and all other states which are unobservable, $\mathbf{x}_\perp$:

$$\begin{aligned} \frac{dx_1}{dt} &= F_1\Big(x_1, \mathbf{x}_\perp, \mathbf{p}\Big) \\ \frac{d\mathbf{x}_\perp}{dt} &= \mathbf{F}_1\Big(x_1, \mathbf{x}_\perp, \mathbf{p}\Big) \end{aligned} \tag{3.3}$$

In the case of a Hodgkin-Huxley like model, x_1 would be membrane voltage which is directly measured in a lab experiment, and $\mathbf{x}_\perp$ are gating variables which cannot be directly observed. The assumption is that we are able to construct a model based on our physical knowledge of the system which describes the above experimental system. As a first step, we will assume that it is possible to design a model which has the exact same form as the one described in equation (3.3). This new system is the model that would be used for our estimation procedure. The state variable of the new system are $\mathbf{y}$ and its parameters are $\mathbf{q}$.

$$\begin{aligned} \frac{dy_1}{dt} &= F_1\Big(y_1, \mathbf{y}_\perp, \mathbf{q}\Big) \\ \frac{d\mathbf{y}_\perp}{dt} &= \mathbf{F}_1\Big(y_1, \mathbf{y}_\perp, \mathbf{q}\Big) \end{aligned} \tag{3.4}$$

If we have information on x_1 between time 0 and T, then the objective is to estimate the time series of all hidden states $x_\perp$ and q.

Since any real measurement is taken at discrete time we need to discretize the above equations. If we have $N+1$ measurements, then equations (3.3) and (3.4) can be discretized using the following general form:

$$\mathbf{x}(n+1) = \mathbf{F}\Big(\mathbf{x}(n), \mathbf{p}\Big) \tag{3.5}$$

where $\mathbf{G}$ is the discretization rule and n is any time point between 0 and $N+1$. Equation (3.5) is an exact mapping from time point n to $n+1$. In other words, $\mathbf{x}(n+1)$ has will have the exact value starting with identical $\mathbf{x}(n)$.

Our estimation, therefore, is a search over initial conditions $\mathbf{y}(0)$ and $\mathbf{q}$. The only given initial condition is $\mathbf{x}(0)$ and all other initial conditions are not given. Once all initial conditions for the experimental system $\mathbf{x}$ and model $\mathbf{y}$ are the same and parameters $\mathbf{p}$ and $\mathbf{q}$ match, our estimation problem is solved.

One approach is to design a cost function to minimize the distance between the two systems. A conventional cost function is a least square distance between the two systems as shown in equation (3.6).

$$C\Big(\mathbf{q}, \mathbf{y}(0)\Big) = \frac{1}{2T}\int_0^T dt\Big(x_1(t) - y_1(t)\Big)^2 \tag{3.6}$$

This equation can be written for discrete time as the following:

$$C\Big(\mathbf{q}, \mathbf{y}(0)\Big) = \frac{1}{2N}\sum_{n=0}^{N}\Big(x(n) - y(n)\Big)^2 \tag{3.7}$$

Various optimization routines are used to minimize the above cost function. The global minima of cost function C happens at the point where $\mathbf{q}$ and $\mathbf{p}$ are equal, and the two systems start at the same initial conditions. By looking for minima of C, we are essentially searching for zeros of cost function's derivatives with respect to parameters and initial conditions.

$$\frac{dC\Big(\mathbf{q}, \mathbf{y}(0)\Big)}{dp} = 0 \tag{3.8}$$

$$\frac{dC\Big(\mathbf{q}, \mathbf{y}(0)\Big)}{d\mathbf{y}(0)} = 0 \tag{3.9}$$

These derivatives involve the following terms:

$$\frac{\partial \mathbf{y}(t)}{\partial \mathbf{q}} \quad \text{and} \quad \frac{\partial \mathbf{y}(t)}{\partial \mathbf{y}(0)}$$

The time evolution of these derivatives is:

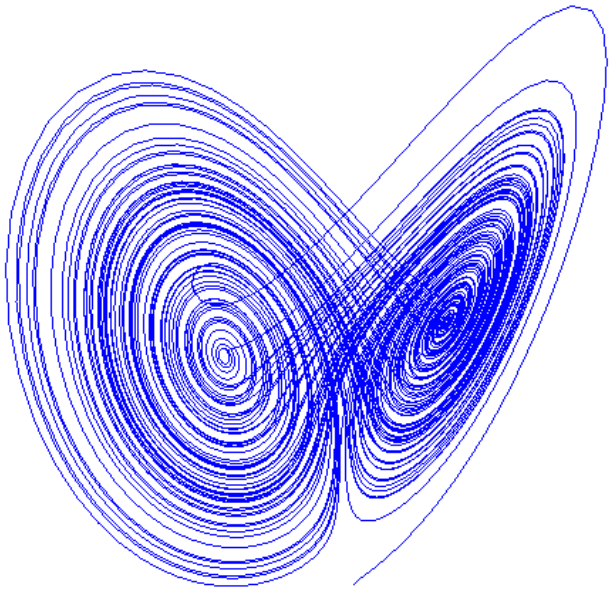

Figure 3.1: Lorenz attractor

$$\begin{aligned} \frac{d}{dt}\Big(\frac{\partial \mathbf{y}(t)}{\partial \mathbf{q}}\Big) &= \frac{\partial \mathbf{F}(y,p)}{\partial \mathbf{y}(t)}\Big(\frac{\partial \mathbf{y}(t)}{\partial \mathbf{q}}\Big) + \frac{\partial \mathbf{F}(\mathbf{y},\mathbf{q})}{\partial \mathbf{q}} \\ \frac{d}{dt}\Big(\frac{\partial \mathbf{y}(t)}{\partial \mathbf{q}}\Big) &= \frac{\partial \mathbf{F}(y,p)}{\partial \mathbf{y}(t)}\Big(\frac{\partial \mathbf{y}(t)}{\partial \mathbf{y}(0)}\Big) \end{aligned} \tag{3.10}$$

where

$$\frac{\partial \mathbf{F}(y,p)}{\partial \mathbf{y}(t)} \quad \text{and} \quad \frac{\partial \mathbf{F}(y,p)}{\partial \mathbf{y}(t)}$$

is the Jacobian of the system. The second formula in equation (3.10) clearly shows that if this Jacobian has positive Lyapunov exponents, the sensitivity of time evolution of a chaotic system grow exponentially.

3.3 Chaos and Sensitivity on Initial Conditions

The method described in last section is a conventional method used in many disciplines of science for estimating a systems parameters and states. This approach, however, does not perform very well when the equations of an experi-

mental system is highly nonlinear or chaotic. As an example we will use the famous Lorenz system to demonstrate this fact.

Lorenz system is a 3 dimensional ODE system, introduced by Edward Lorenz in 1963 as a simplification of atmospheric convection. (Equation 3.11)

$$\begin{aligned} \frac{dx}{dt} &= \sigma(y - x) \\ \frac{dy}{dt} &= Rx - y - xz \\ \frac{dz}{dt} &= xy - bz \end{aligned} \tag{3.11}$$

For the following set of parameter values this system is chaotic.

$$\sigma = 10 \quad R = 28 \quad b = \frac{3}{8} \tag{3.12}$$

Figure (3.1) shoes the famous *butterfly* attractor for this system.

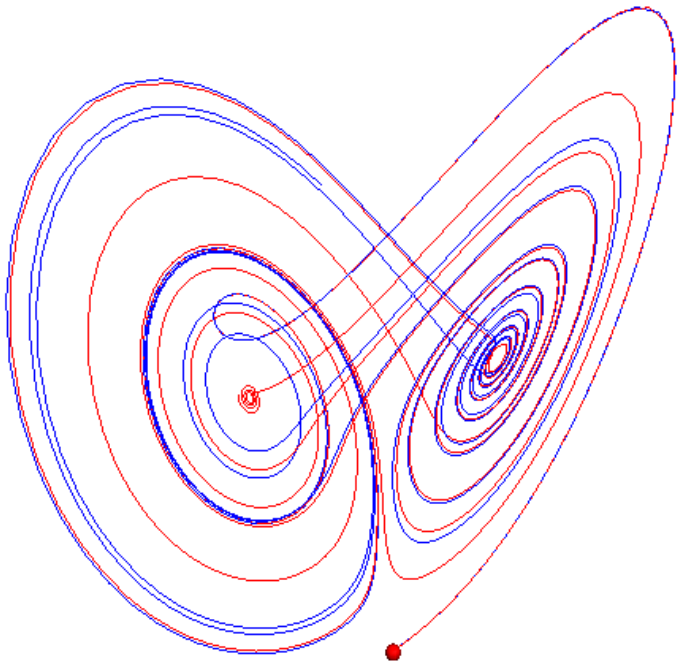

Figure 3.2: Identical Lorenz systems (red and blue) starting at slightly different initial point diverge quickly due to chaos

Chaos refers to the characteristic of dynamical systems where little changes in initial conditions is magnified in the state of the system at a later time. This is due to the presence of positive eigenvalues in the Jacobian of these systems, also referred to as Lyapunov exponents. If there are two systems following Lorenz equations of motion (equation 3.11) but have slightly different initial conditions, as shown in figure (3.2), the trajectory of the two systems will diverge very quickly.

The sensitivity on initial condition in chaotic systems makes the search over the cost function manifold extremely hard. The surface of the cost function has many sharp local minima, and any search routine will get stuck in those minima. The probability of finding the global minima, hence the correct values of parameters and states is very small.

3.4 Synchronization

One method to get around the above problem is to synchronize the two chaotic systems. We can couple the measured state x_1 of our experimental system to the equations of motion of the constructed model ([15], [3]). Equation (3.4) will take the following form:

$$\begin{aligned} \frac{dy_1}{dt} &= F_1\Big(y_1, \mathbf{y}_\perp, \mathbf{q}\Big) + K(x_1 - y_1) \\ \frac{d\mathbf{y}_\perp}{dt} &= \mathbf{F}_1\Big(y_1, \mathbf{y}_\perp, \mathbf{q}\Big) \end{aligned} \tag{3.13}$$

where the coupling term, K, determines the strength coupling x_1 to $\mathbf{y}$ equations of motion. The presence of this new term changes the Jacobain of the system. The new eigen values of this Jacobian are usually known as conditional Lyapunov exponents (CLE). A large enough K will make all CLEs non-positive, therefore, eliminating all instability due to little changes in initial conditions. We took K to be a constant here, but it be taken to be a function of time.

Figure (3.3) shows the regularization of cost function as control term grows. In this picture two Hogdkin-Huxley models were used. The only difference between these two models were values of their capacitance C_1 and C_2. The two systems

will synchronize when $C_1 = C_2$. In the absence of K, it will be much harder to search for the right values of C_2. Larger values of K, however, smooth the cost function which can be search over easier.

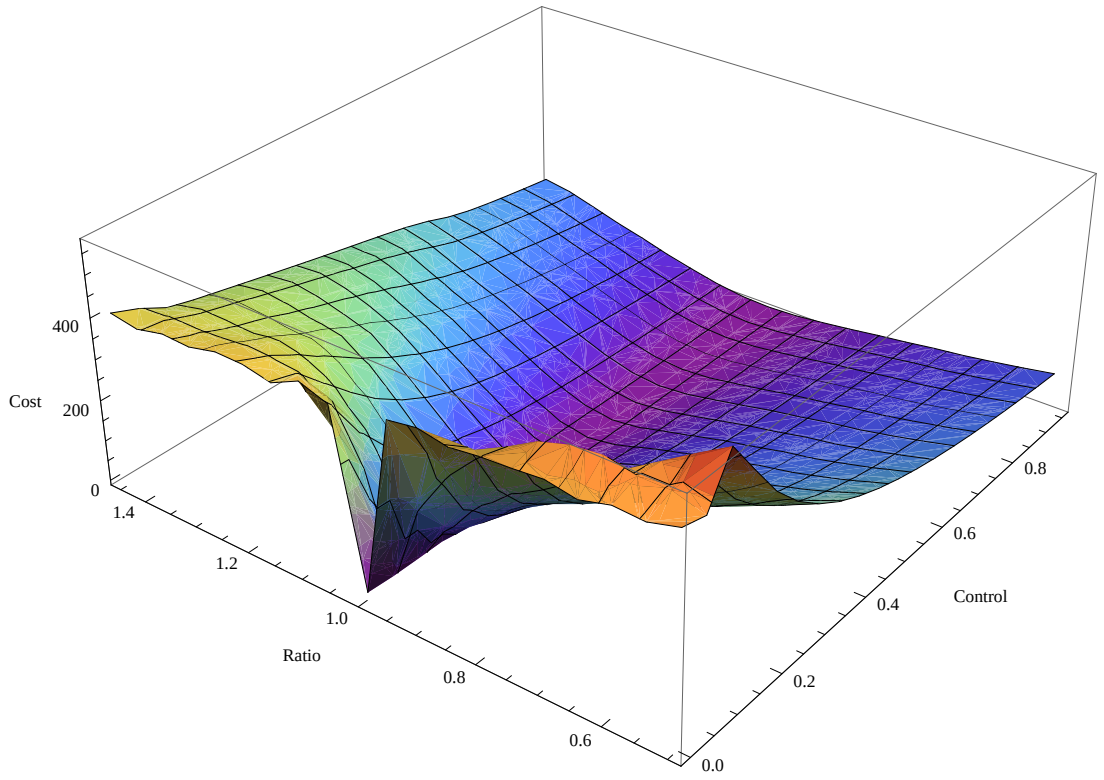

Figure 3.3: Surface of the cost function as the control changes between 0 and 1 and the ratio of C/C' changes between 0.5 and 1.5

If the value of K is too small, it would not eliminate positive Lyapunov exponents. In contrast, if this value is too large, the mathematical form of equations in the experimental system and model does not play a role. We need to find the smallest value of K that makes all CLEs non-positive. This can be achieved by introducing a new term into the cost function:

$$\begin{aligned} C\Big(\mathbf{q}, \mathbf{y}(0)\Big) &= \frac{1}{2T}\int_0^T dt\Big(x_1(t) - y_1(t)\Big)^2 + K^2(t) \\ &= \frac{1}{2N}\sum_{n=0}^{N}\Big(x(n) - y(n)\Big)^2 \end{aligned} \tag{3.14}$$

in continuos and discrete time.

3.5 R-value Test

Very large values of K will make x_1 and y_1 synchronous regardless of the mathematical form of their models. As discussed in previous chapter, one method to ensure this value does not get too large is to penalize for it in the cost function. If we do not know the exact form of the experimental equation, however, we would like to have a method to compare the size of control term to the output of the model. We use the following quantity R to ensure that the values of K is not too large compared to the

$$R(t) = \frac{F_1^2\Big(\mathbf{y}(t), \mathbf{q}\Big)}{F_1^2\Big(\mathbf{y}(t), \mathbf{q}\Big) + K^2(t)\Big(x_1 - y_1\Big)^2} \tag{3.15}$$

The value of R is between zero and one. If K is much larger than $\mathbf{F}_1$, the system is being mainly driven by the control term. When the equations of motion of the two systems are identical or close to each other, K will be small. Hence, the value of R would be close to unity.

Chapter 4

Twin Experiments

4.1 Introduction

Twin experiment is a method to verify a new estimation procedure. The basic idea is to generate synthetic *data*, and use the *data* to estimate the hidden parameters and states. In this chapter, we have constructed several neuron models with various currents. These models are the basis of our *twin experiments*.

The neuron models are integrated forward using a Runge-Kutta integration method. We call this our *experimental system*. Using the exact form of equations as in experimental system, we construct our *estimation system*. The output voltage of the experimental system is coupled to the estimation model. The estimation model, however, has no information about the gating variables and parameters. At this point, we apply our synchronization method along with an optimization routine to find the minima in the cost function. The estimated parameters and state are then compared to their true values.

4.2 Standardized Single Neuron Model

In chapter 2, we discussed the biophysics of single neurons and various models which can describe its dynamics. Several different Hodgkin-Huxley like models were used in previous chapter to show how the method of synchronization can help with parameter and state estimation. These models, however, are purely

phenomenological and the kinetics take several different form. In order to have a consistent model, we have generalized the form of our kinetics in all the models that will be discussed in this chapter.

In general, steady state of gating variables have a sigmoidal shape, and the time constant is a bell-shaped curve as a function of voltage. (See 2.2.3) This is true for most of the currents that we have analyzed, hence, we have been able to use a standardized model based on the original Hodgkin-Huxley model.

Equation 4.1 shows the generalized form of a single neuron model that will be used in this chapter and also chapter 5.

$$\frac{dV}{dt} = \frac{1}{C_m}\left[\sum_j I_j + I_{DC} + I_{inj}\right] \tag{4.1}$$

Here X and Y are gating variables for activation and inactivation of different channels. Current I_j is defined as:

$$I_j = \bar{g}_j X^\lambda Y^\gamma (E_j - V) \tag{4.2}$$

$\bar{g}_j$ is the maximal conductance for each channel, and E_j is the reversal potential for the corresponding ion. The dynamical equation of the gating variable X could be written as the following:

$$\dot{X} = (X_\infty(V) - X)/\tau_X(V) \tag{4.3}$$

where steady state, $X_\infty(V)$, and time constant, $\tau_X(V)$, are defined as:

$$\begin{aligned} X_\infty(V) &= \frac{1}{2}\left[1 + \tanh\left(\frac{V - v_X}{dv_X}\right)\right] \\ \tau_X(V) &= tX_0 + tX_1\left[1 - \tanh^2\left(\frac{V - v_{Xt}}{dv_{Xt}}\right)\right] \end{aligned}$$

4.3 Electrophysiological Experiments

In the absence of injected current, a neuron's voltage will reach equilibrium over long enough time. To study the behavior and dynamics of a neuron, however, we are interested in variations in sub-threshold behavior and features of action

potentials. In our analysis of neuron models, we have used two main techniques used by experimental electrophysiologists as described in the following sections.

4.3.1 Voltage Clamp

When the voltage of a neuron is kept constant, there will be different currents flowing in and out of the cell in order to compensate for this fixed voltage. Mathematically, the derivative of voltage in equation (4.1) will be zero, and all the ionic currents on the right hand side have to balance each other out. When a neuron is at rest the amounts of ionic flow is a constant. If a non-zero voltage is applied to cell, ion channels open and a flow of different ions will move across the membrane. These currents will eventually reach equilibrium at a new value. This is also known as a *voltage clamp* experiment, and was originally also used by Hodgkin and Huxley in the construction of their model. The shape and sign of the current reveals informations about a specific channel such as presence of activating or deactivating gating particles. This method has been used in our model construction, to show a more biologically basis for currents.

4.3.2 Current Clamp

A slightly different way to study a neuron is to control the injected current and let the membrane voltage to change and compensate the injected current. In this experimental method, also known as *current clamp*, square waves of current with different amplitude is applied. If the amplitude of these waves is big enough, it will produce spikes. When a current with positive sign is applied the neuron is *depolarized*. In contrast, applying a negative current to a neuron is called *hyperpolarizing* it. Applying a complicated wave form is also common, especially when trying to estimate parameters of a model. Complicated wave forms can push the neuron the different parts of its state space.

In a simple case, where Hodgkin-Huxley model reduces to an RC circuit in the absence of gated ion channels (such as Na and K), voltage can be simplified to equation (2.31). When a constant non-zero current is applied to the neuron, the

response is that of an RC circuit. These are the growing and decaying curves that can be observed when a neuron is depolarized or hyper-polarized.

$$V(t) = V_0 + (V_r - V_0) \exp\left[\frac{-t}{\tau}\right] \tag{4.4}$$

4.4 Currents

Table 4.1: List of ionic currents used in twin experiments

Current	form
$I_{Na,t}$	$\bar{g}_{Na,t} m^3 h (E_{Na} - V)$
I_{KDR}	$\bar{g}_{KDR} n^4 (E_K - V)$
I_{IR}	$\bar{g}_{IR} r (E_K - V)$
I_A	$\bar{g}_A a^3 b (E_K - V)$
I_{leak}	$\bar{g}_{leak} (E_{leak} - V)$

Table (4.1) shows a list of currents used in this chapter. A detailed description of these currents and their dynamics is given in the following sections.

4.4.1 Transient sodium current $I_{Na,t}$

Current equation:

$$I_{Na,t} = \bar{g}_{Na,t} m^3 h (E_{Na} - V) \tag{4.5}$$

Table 4.2: Parameters of $I_{Na,t}$

$gbarNa$	50
ENa	55
vm	-30
dvm	15
$tm0$	0.1
$tm1$	1.5
vmt	-40
$dvmt$	30
vh	-50
dvh	-15
$th0$	1
$th1$	10
vht	-50
$dvht$	40

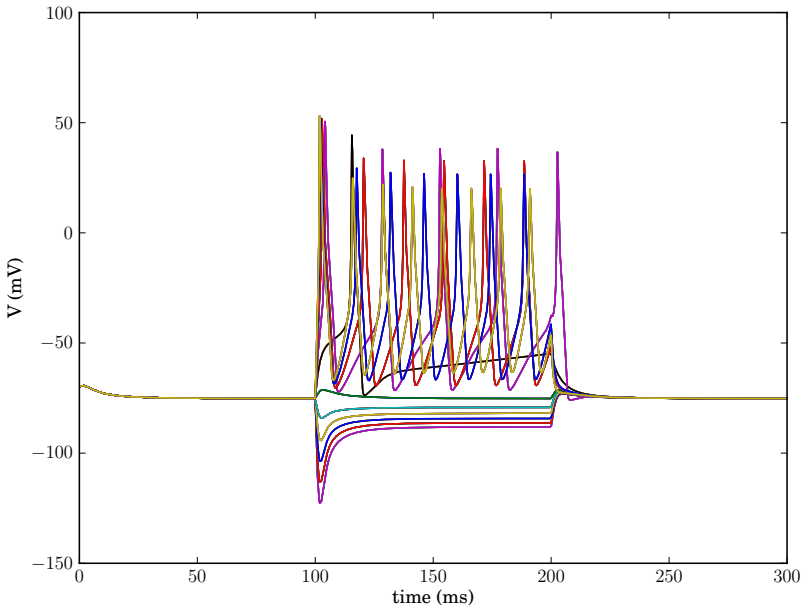

Figure 4.1: Current clamp simulation. Current base is at 0 mV, a 100 ms long step is applied starting at -50pA to 50pA at 10pA steps

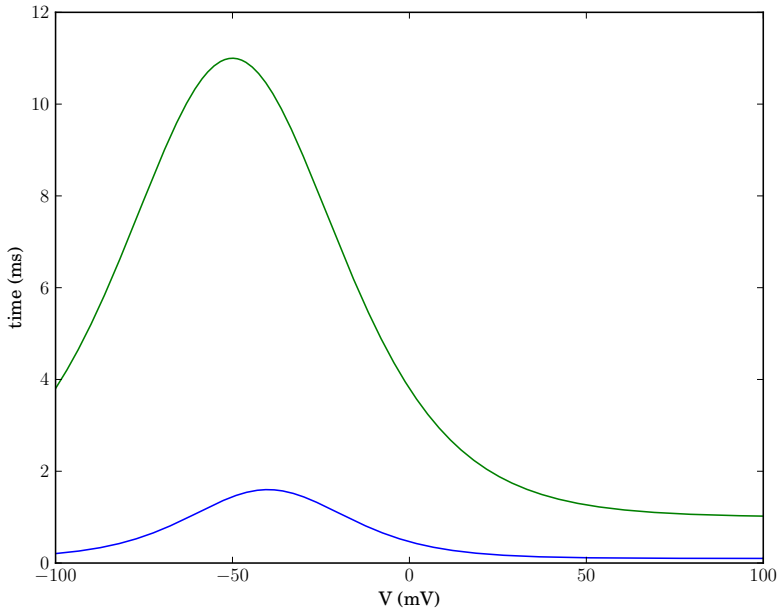

Figure 4.2: Time constant of activation (blue) and inactivation (green) gating variables of $I_{Na,t}$ current.

4.4.2 Delayed rectifier potassium current I_{KDR}

Current equation:

$$I_{KDR} = \bar{g}_{KDR} n^4 (E_K - V) \tag{4.6}$$

Table 4.3: Parameters of I_{KDR}

$gbarK$	70
EK	-77
vn	-25
dvn	25
$tn0$	1
$tn1$	10
vnt	-75
$dvnt$	50

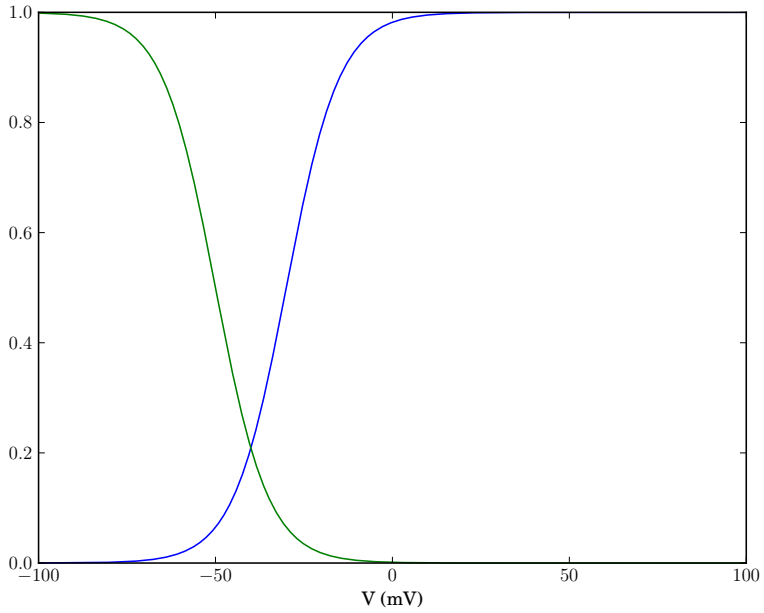

Figure 4.3: Steady states of activation (blue) and inactivation (green) gating variables of $I_{Na,t}$ current.

4.4.3 Inwardly rectifying potassium current I_{IR}

Current equation:

$$I_{IR} = \bar{g}_{IR} r (E_K - V) \tag{4.7}$$

Table 4.4: Parameters of I_{IR}

$gbarKIR$	5
EK	-77
vm	-80
dvm	-15

This current has a time constant which is approximately $15mV$ throughout the interested voltage range. τ_r is written as a constant for this model

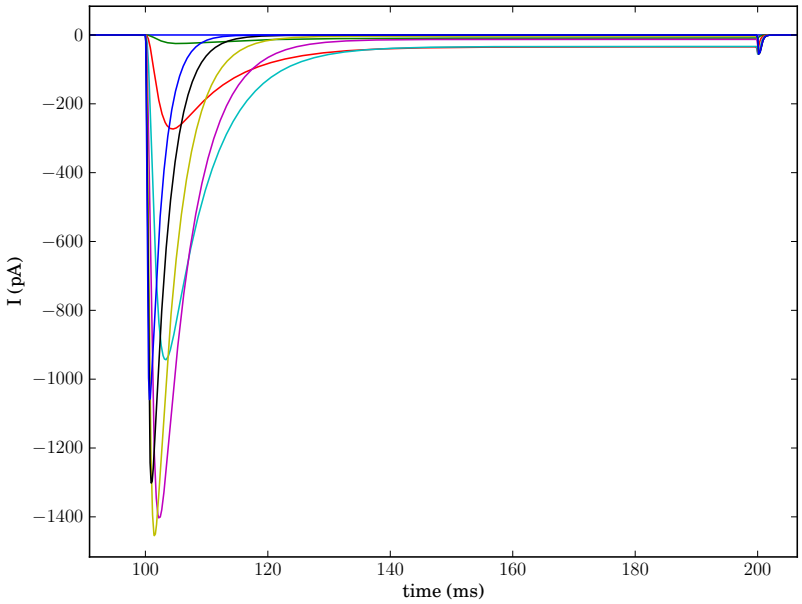

Figure 4.4: $I_{Na,t}$ of a voltage clamp simulation with voltage base at -70mV, where a 100 ms step voltage was applied from -50mV to 20mV at 10mV steps

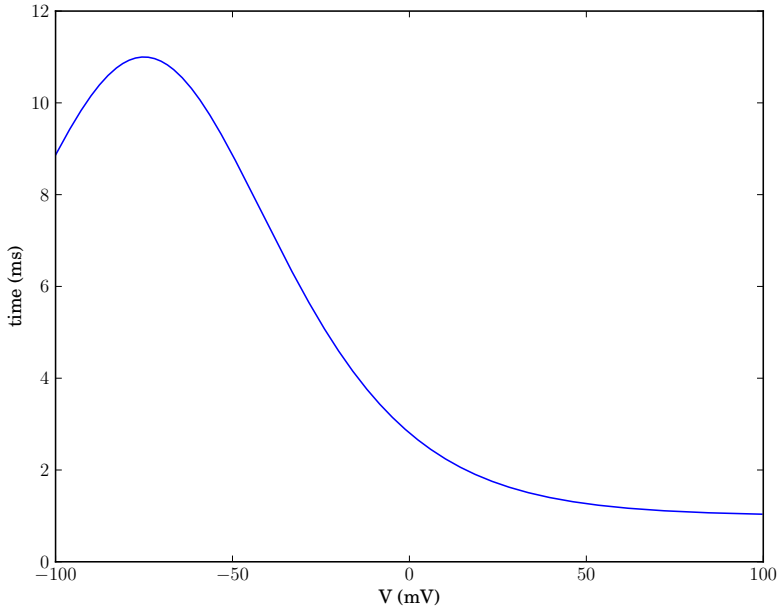

Figure 4.5: Time constant of activation gating variable of I_{KDR} current.

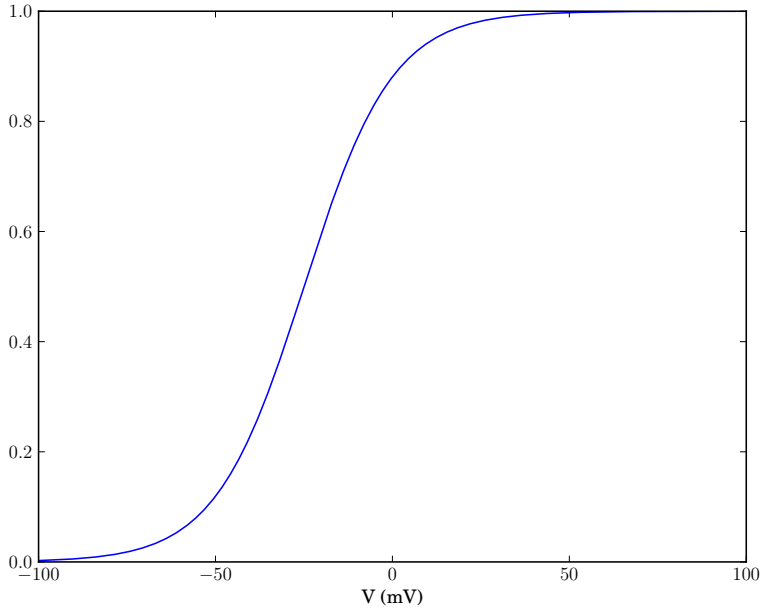

Figure 4.6: Steady states of activation gating variable of I_{KDR} current.

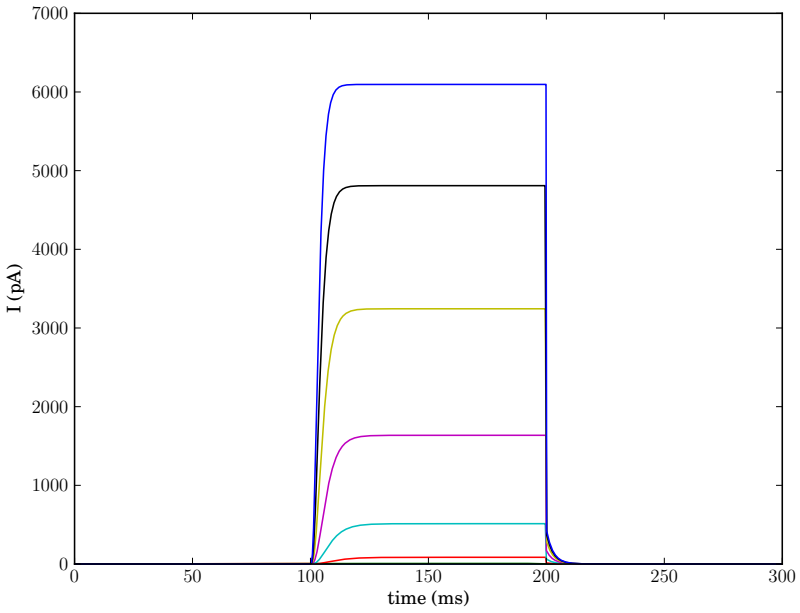

Figure 4.7: I_{KDR} of a voltage clamp simulation with voltage base at -70mV, where a 100 ms step voltage was applied from -50mV to 20mV at 10mV steps

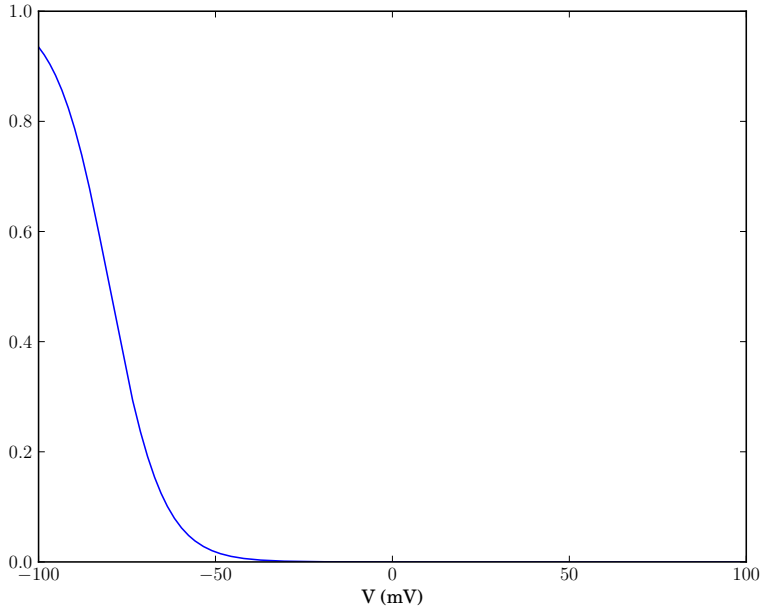

Figure 4.8: Steady states of activation gating variable of I_{IR} current.

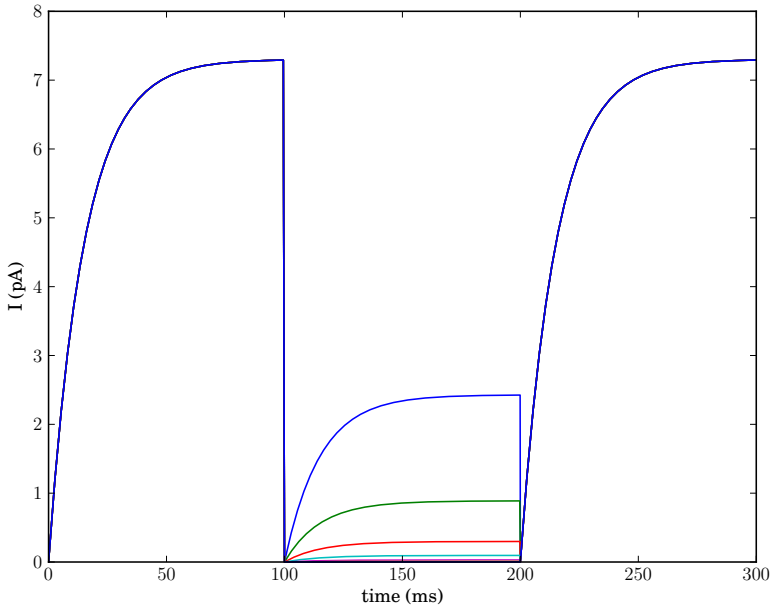

Figure 4.9: I_{IR} of a voltage clamp simulation with voltage base at -70mV, where a 100 ms step voltage was applied from -50mV to 20mV at 10mV steps

4.4.4 Potassium current I_A

Current equation:

$$I_{IR} = \bar{g}_A a^3 b(E_K - V) \tag{4.8}$$

Table 4.5: Parameters of I_A

$gbarA$	20
va	-30
dva	15.
$ta0$	0.1
$ta1$	1.5
vat	-40
$dvat$	30
vb	-55
dvb	-15.
$tb0$	1.
$tb1$	10.
vbt	-50
$dvbt$	90

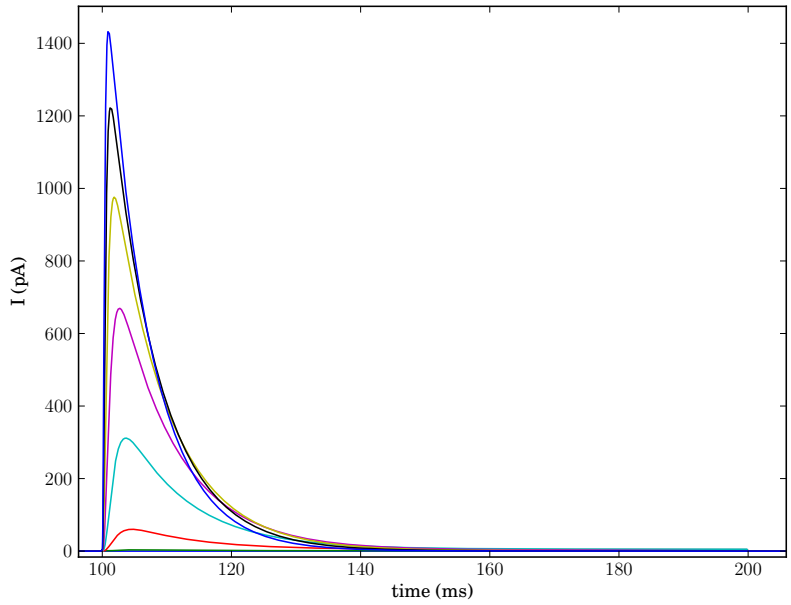

Figure 4.10: I_A of a voltage clamp simulation with voltage base at -70mV, where a 100 ms step voltage was applied from -50mV to 20mV at 10mV steps

4.4.5 Leak current I_{leak}

Current equation:

$$I_{leak} = \bar{g}_{leak}(E_{leak} - V) \tag{4.9}$$

Table 4.6: Parameters of I_{leak}

gl	.4
El	-30

4.5 Twin experiment Results

Using the standardized HH-like model described in this chapter and the their set of parameters, we performed a twin experiment. Data was generated using an RK4 integration scheme, and the voltage from this synthetic data was then fed

into ipOpt along with the injected current. The reversal potentials (E_j), offset current (I_{DC}), and specific cell capacitance (C_m) were taken as known parameters, but all the other parameters in the voltage equation and functions of steady states and time constants were treated as unknown parameters.

4.5.1 Five dimensional model

In this twin experiment, a five dimensional model was constructed using currents in table (4.7). 3,000 data points from the voltage trace of this model were used for this twin experiment at 20 kHz. Estimated and original traces are shown in figures (4.11) and (4.12), and all the observed and unobserved states are matched very well.

The value of estimated and original variables of this model are also given in table (4.7). The estimated parameter values were used and integrated using the same injected current and model. These traces also followed the original traces as well as shown in figures (4.13) and (4.14).

Table 4.7: List of currents (5D)

Current	form
$I_{Na,t}$	$\bar{g}_{Na,t}m^3h(E_{Na}-V)$
I_{KDR}	$\bar{g}_{KDR}n^4(E_K-V)$
I_{IR}	$\bar{g}_{IR}r(E_K-V)$
I_{leak}	$\bar{g}_{leak}(E_{leak}-V)$

4.5.2 Seven Dimensional Model

This seven-dimensional model includes all channels present in the five-dimensional model plus an extra potassium current, I_A. A list of current present in this model are shown in table (4.9). This current has two gating particles a and b, and it appears in the voltage equation exactly in the same form as $I_{Na,t}$ with a different reversal potential. The twin experiment for this model was repeated four times as described in here.

Table 4.8: Estimated parameters of 5-D model

	Parameter	Original Value	Estimated Value	% error
1	gbarNa	50	47.4247	5.150620
2	gbarK	70	71.2515	1.787800
3	gbarKIR	5	4.9675	0.649520
4	gl	0.4	0.4005	0.117025
5	vm	-30	-29.9781	0.072967
6	dvm	15	15.0373	0.248533
7	tm0	0.1	0.1000	0.002030
8	tm1	1.5	1.4973	0.179133
9	vmt	-40	-40.0446	0.111400
10	dvmt	30	30.0917	0.305800
11	vh	-50	-49.0780	1.844000
12	dvh	-15	-14.8195	1.203533
13	th0	1	1.0662	6.623000
14	th1	10	10.0247	0.247300
15	vht	-50	-48.1969	3.606260
16	dvht	40	38.1372	4.656950
17	vn	-25	-24.9394	0.242520
18	dvn	25	25.0769	0.307720
19	tn0	1	0.9850	1.502870
20	tn1	10	10.0078	0.077800
21	vnt	-75	-75.5836	0.778133
22	dvnt	50	50.7642	1.528320
23	vm	-80	-79.9055	0.118075
24	dvm	-15	-14.9998	0.001067
25	mTau	15	14.9779	0.147067

Table 4.9: List of currents (7D)

Current	form
$I_{Na,t}$	$\bar{g}_{Na,t}m^3h(E_{Na}-V)$
I_{KDR}	$\bar{g}_{KDR}n^4(E_K-V)$
I_{IR}	$\bar{g}_{IR}r(E_K-V)$
I_A	$\bar{g}_A a^3 b(E_K-V)$
I_{leak}	$\bar{g}_{leak}(E_{leak}-V)$

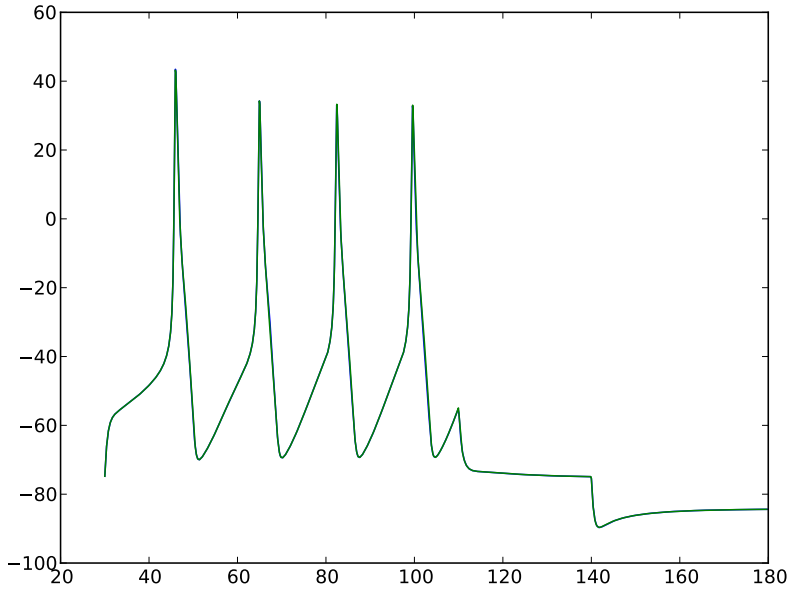

Figure 4.11: HH-like model twin experiment including $I_{Na,T}$, I_{KDR}, I_{IR}, and I_l. Original and estimated trace for V

Run 1

7,000 data points have been used at 100 kHz (0.01 ms) for this estimation. Figures (4.16) to (4.22), show the first four estimated (blue) and original (green) state variables It is clear from these results that only voltage is estimated well here, and the original state variables and parameters were not recreated successfully.

It is very interesting that R-value, figure (4.15), is almost always one throughout the estimation. The estimated hidden states, however, are not nearly perfect. This is a good example of solution degeneracy as the dimension of the search space increases increases. The optimization has solved the problem, but the solution it provides is different than true solution.

Run 2

A second estimation was done on the same model described above. For this estimation I included three spikes (one more spike compared to run 1) and a region

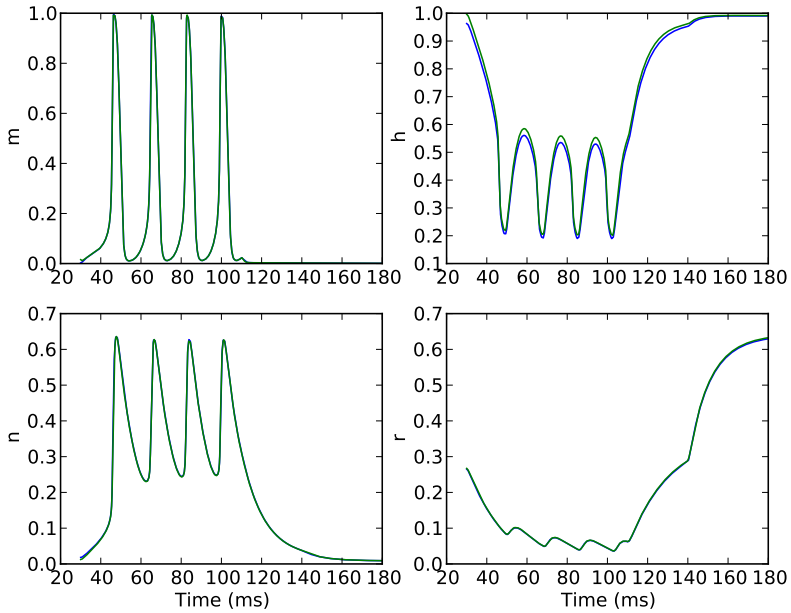

Figure 4.12: HH-like model twin experiment including $I_{Na,T}$, I_{KDR}, I_{IR}, and I_l. Original and estimated traces for all gating particles

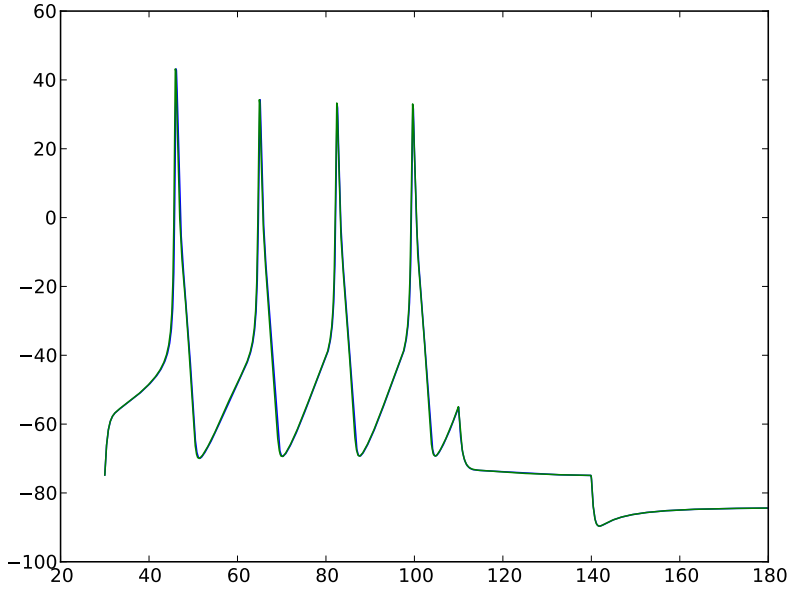

Figure 4.13: Comparison of prediction and original voltage trace

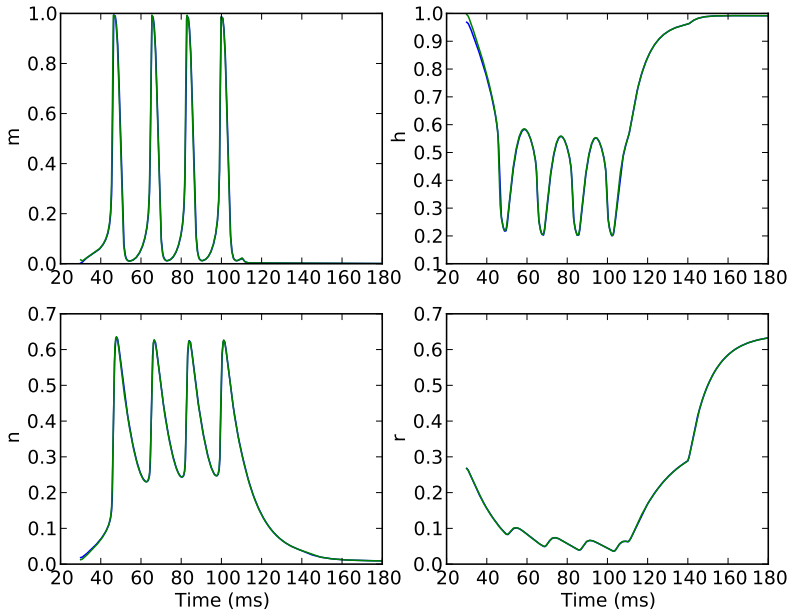

Figure 4.14: Comparison of prediction and original gating variables trace

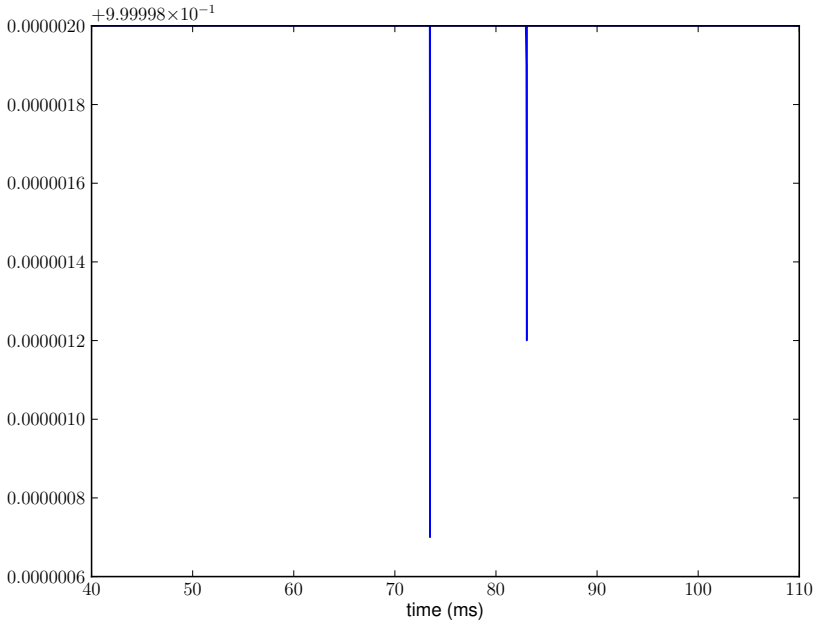

Figure 4.15: R value for the measurement time window

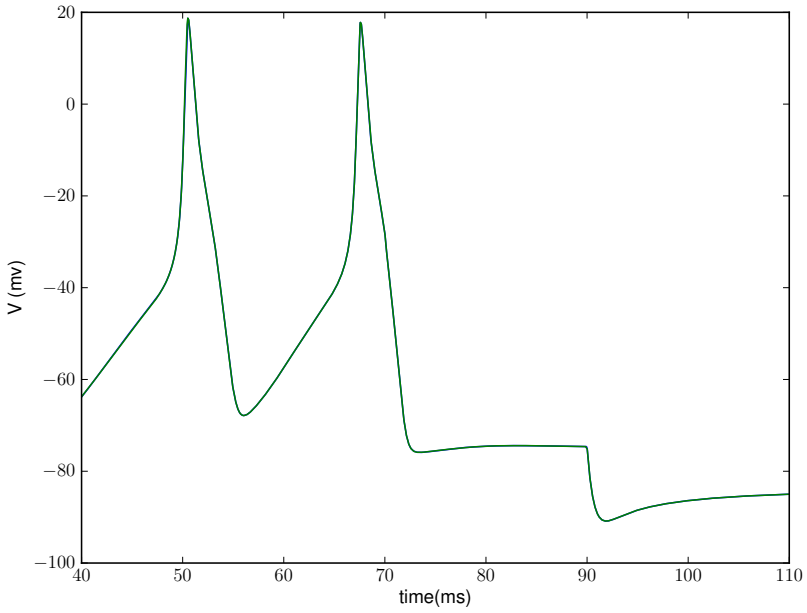

Figure 4.16: HH-like model twin experiment including $I_{Na,T}$, I_{KDR}, I_{IR}, I_A, and I_l. Original and estimated trace for V

of hyperpolarization. The bound on some of the parameters was widened to avoid the estimation of those ending up at the boundaries. 10,000 data points were used in this estimation is 10,000, which is 3,000 more than the run 1. The time step is set at 0.01 ms as before. The estimation of V, figure (4.24), is still excellent. Also, R-value, figure (4.23), is essentially one throughout the estimation window. The estimation of hidden state has definitely improved compared to the previous run, as can be verified from figures (4.25) to (4.30).

Run 3

In this run, 16,000 data points were used at 100kHz frequency. Figure (4.32) and (4.33), show the estimated (blue) and original (green) state variables Table (4.10) shows the values of original and estimated parameters. Although, many of the parameters are not matching very well to the original values, the estimated traces match very well with the original traces of the state variables. As expected, R-value is always at 1 as shown in figure (4.31).

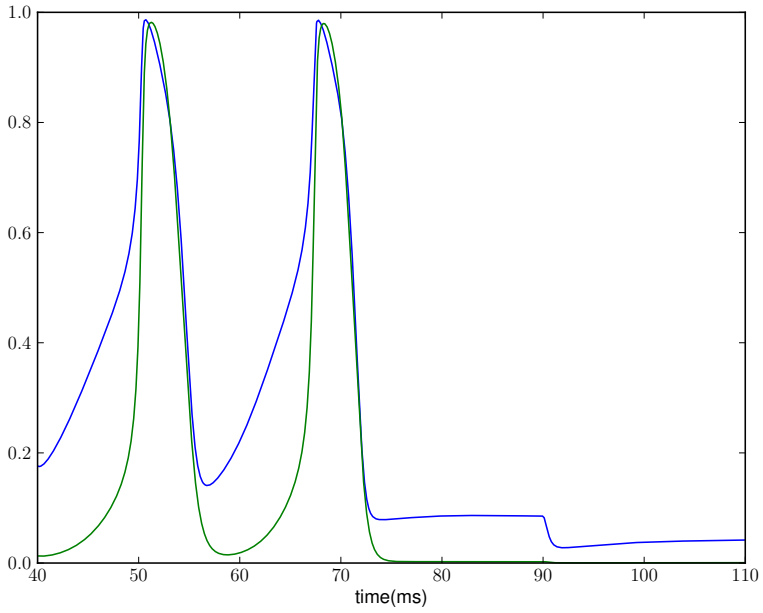

Figure 4.17: HH-like model twin experiment including $I_{Na,T}$, I_{KDR}, I_{IR}, I_A, and I_l. Original and estimated trace for m

The estimated parameters in table (4.10) was then used and the equations were integrated using the same injected current and initial condition. The integration did not produce a similar path, which might be due to the difference in the value of many estimated parameters, and use of a different numerical integration scheme.

Run 4

In this twin experiment, instead of using a step current for polarization and depolarization, a Lorenz current is used as an injected current. 24,000 data points were used at 100kHz. Figure (4.35) and (4.36), show the estimated (blue) and original (green) state variables. Figure (4.34) shows the R-value for the estimation time window. Compared to the estimation results using a step current as injected current, the estimation accuracy has diminished here. The estimated value for parameters also did not match the original values very well.

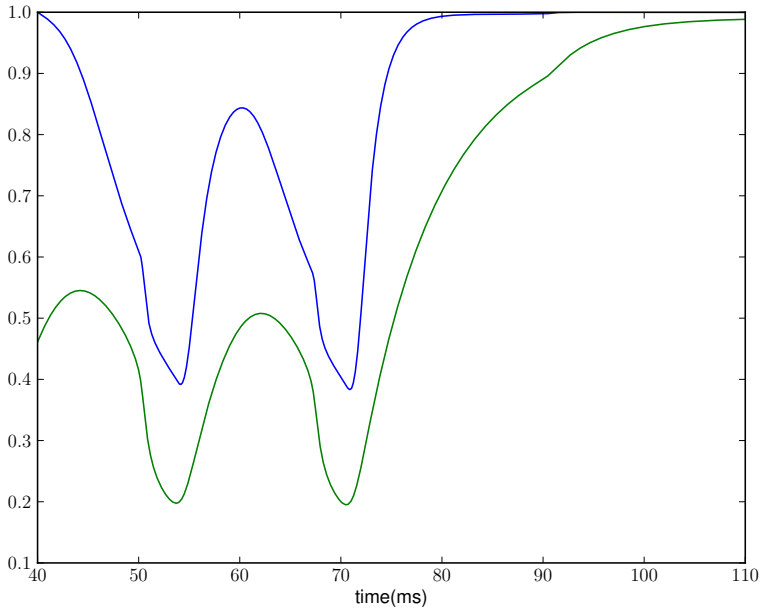

Figure 4.18: HH-like model twin experiment including $I_{Na,T}$, I_{KDR}, I_{IR}, I_A, and I_l. Original and estimated trace for h

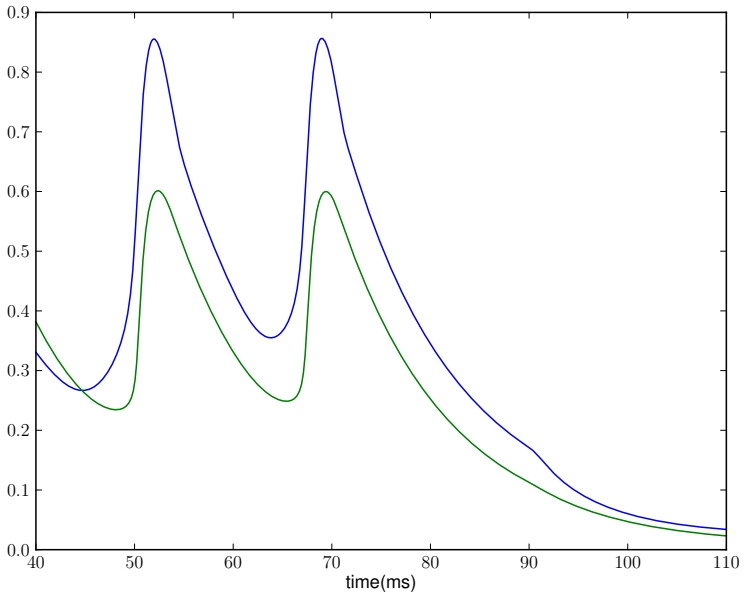

Figure 4.19: HH-like model twin experiment including $I_{Na,T}$, I_{KDR}, I_{IR}, I_A, and I_l. Original and estimated trace for n

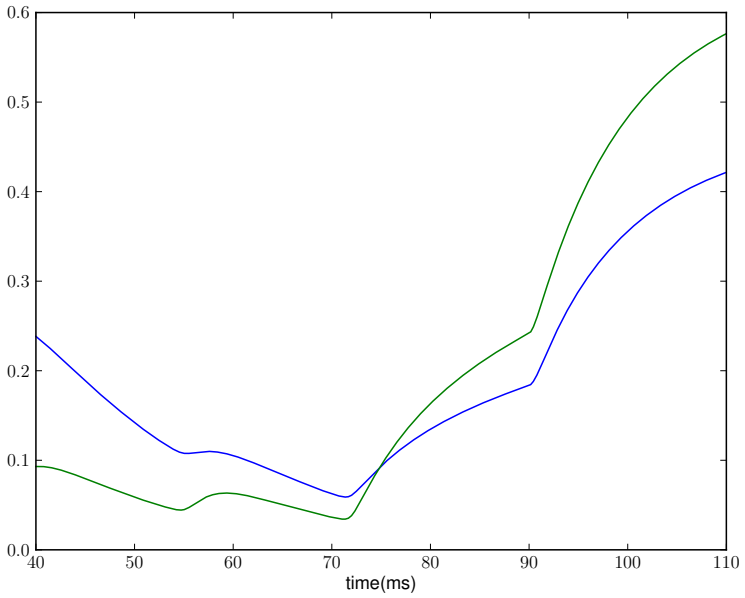

Figure 4.20: HH-like model twin experiment including $I_{Na,T}$, I_{KDR}, I_{IR}, I_A, and I_l. Original and estimated trace for r

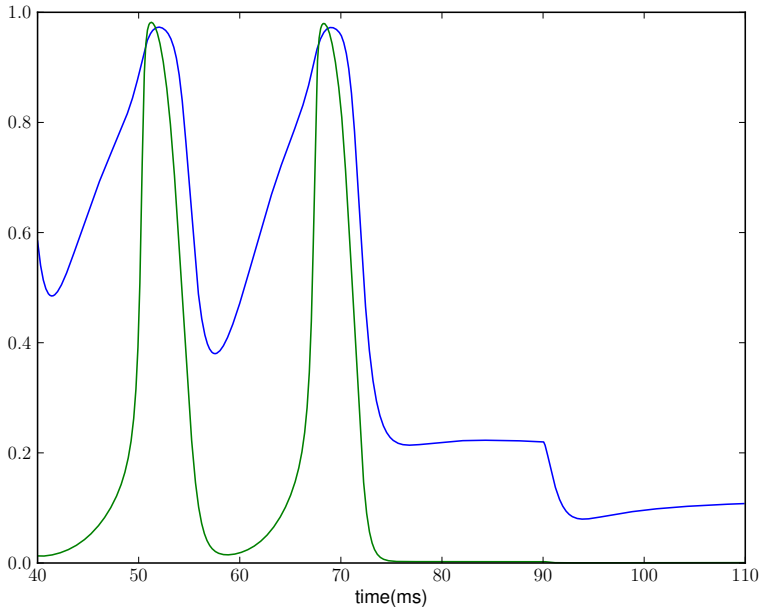

Figure 4.21: HH-like model twin experiment including $I_{Na,T}$, I_{KDR}, I_{IR}, I_A, and I_l. Original and estimated trace for a

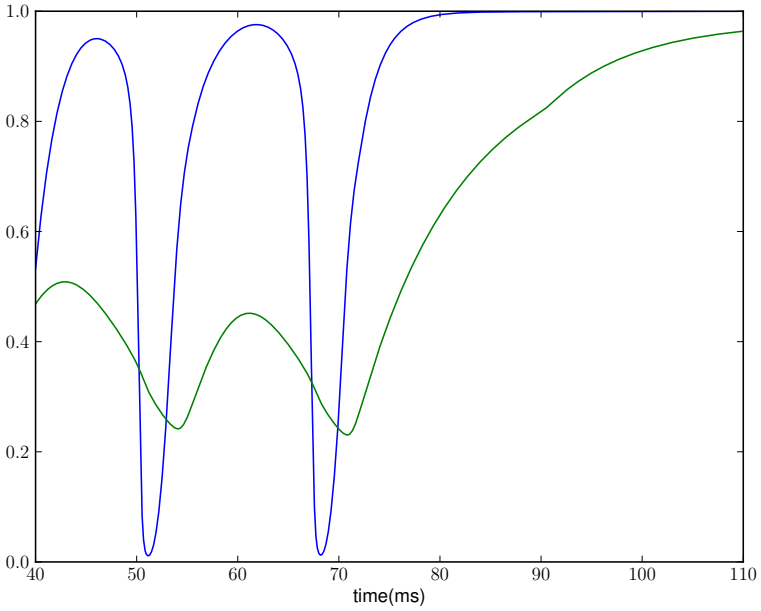

Figure 4.22: HH-like model twin experiment including $I_{Na,T}$, I_{KDR}, I_{IR}, I_A, and I_l. Original and estimated trace for b

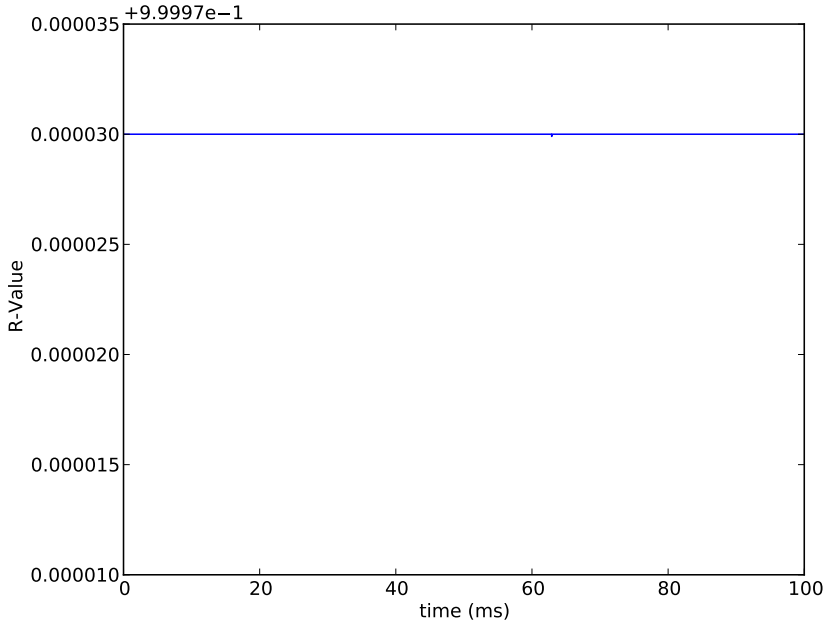

Figure 4.23: R value for the measurement time window

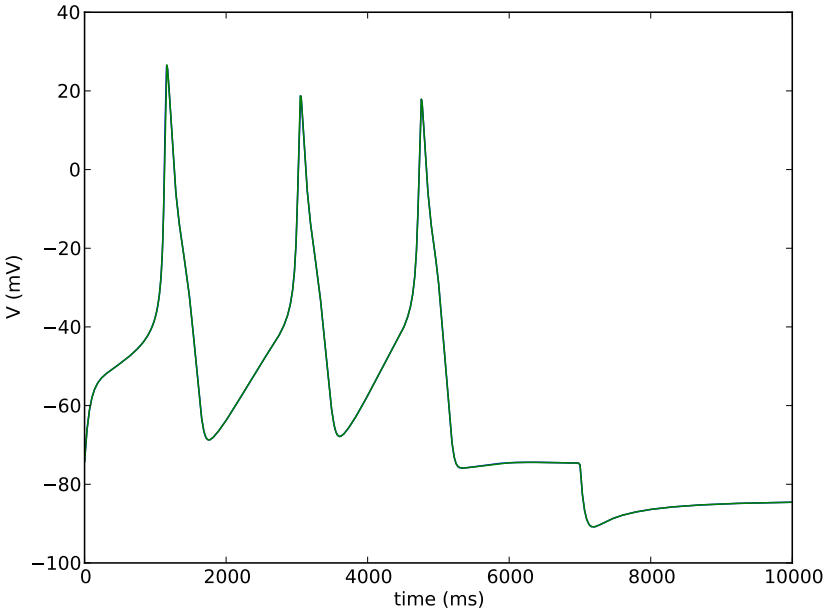

Figure 4.24: HH-like model twin experiment including $I_{Na,T}$, I_{KDR}, I_{IR}, I_A, and I_l. Original and estimated trace for V

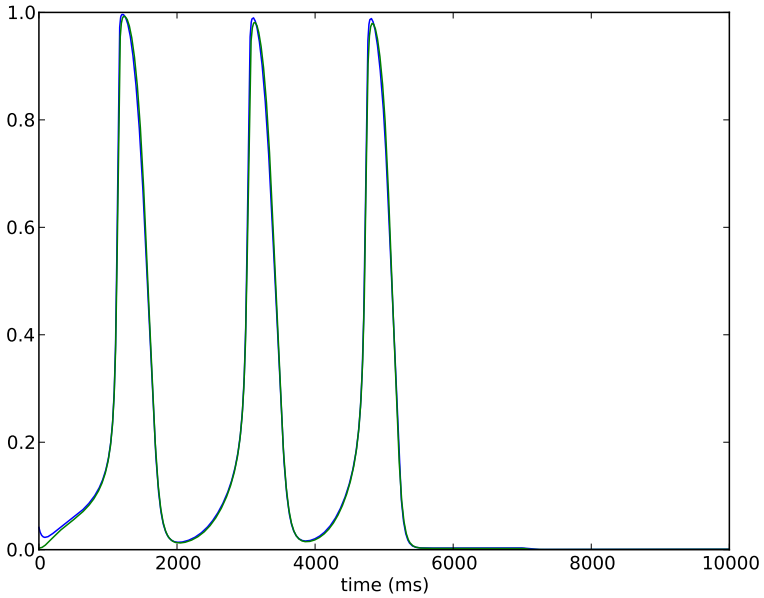

Figure 4.25: HH-like model twin experiment including $I_{Na,T}$, I_{KDR}, I_{IR}, I_A, and I_l. Original and estimated trace for m

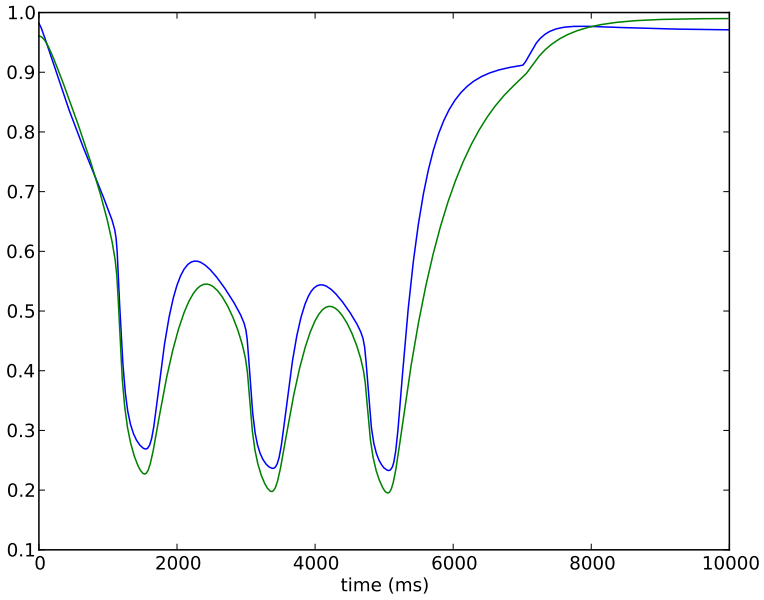

Figure 4.26: HH-like model twin experiment including $I_{Na,T}$, I_{KDR}, I_{IR}, I_A, and I_l. Original and estimated trace for h

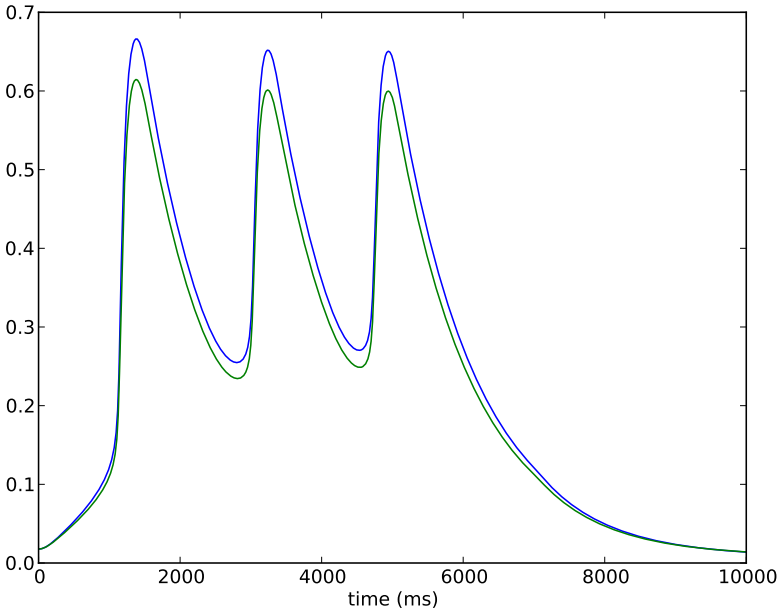

Figure 4.27: HH-like model twin experiment including $I_{Na,T}$, I_{KDR}, I_{IR}, I_A, and I_l. Original and estimated trace for n

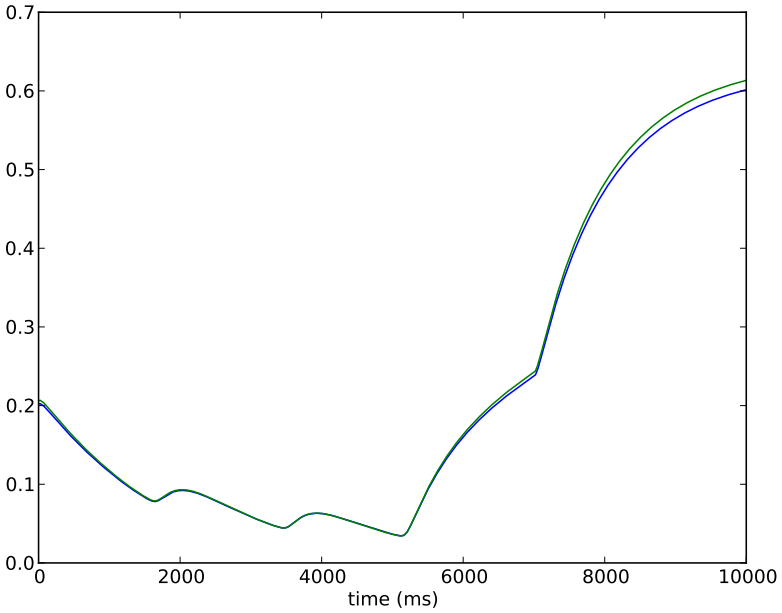

Figure 4.28: HH-like model twin experiment including $I_{Na,T}$, I_{KDR}, I_{IR}, I_A, and I_l. Original and estimated trace for r

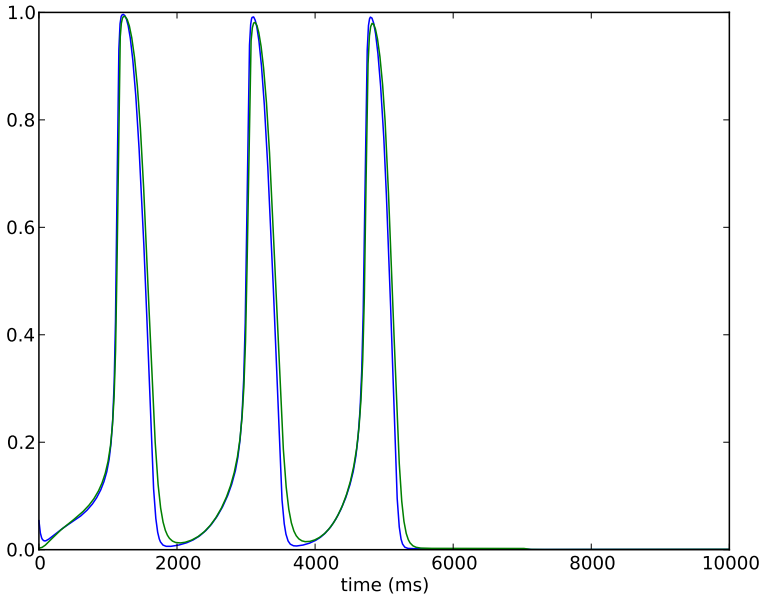

Figure 4.29: HH-like model twin experiment including $I_{Na,T}$, I_{KDR}, I_{IR}, I_A, and I_l. Original and estimated trace for a

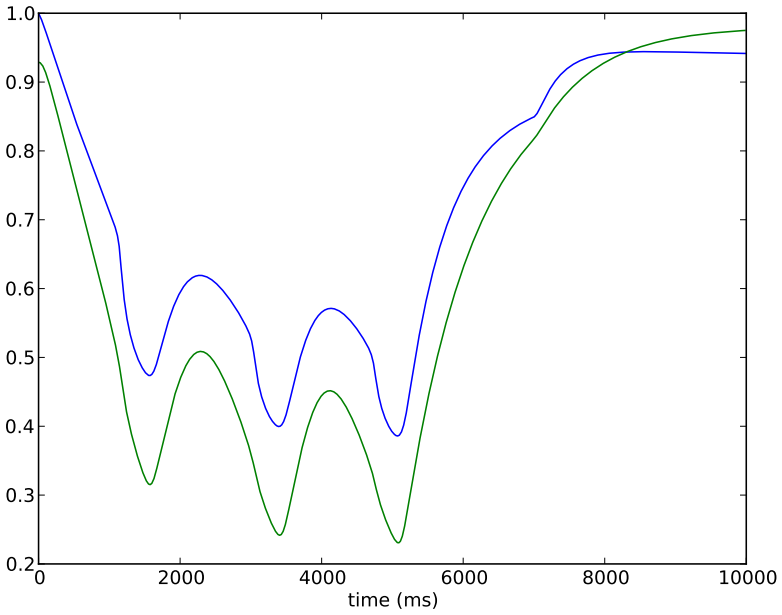

Figure 4.30: HH-like model twin experiment including $I_{Na,T}$, I_{KDR}, I_{IR}, I_A, and I_l. Original and estimated trace for b

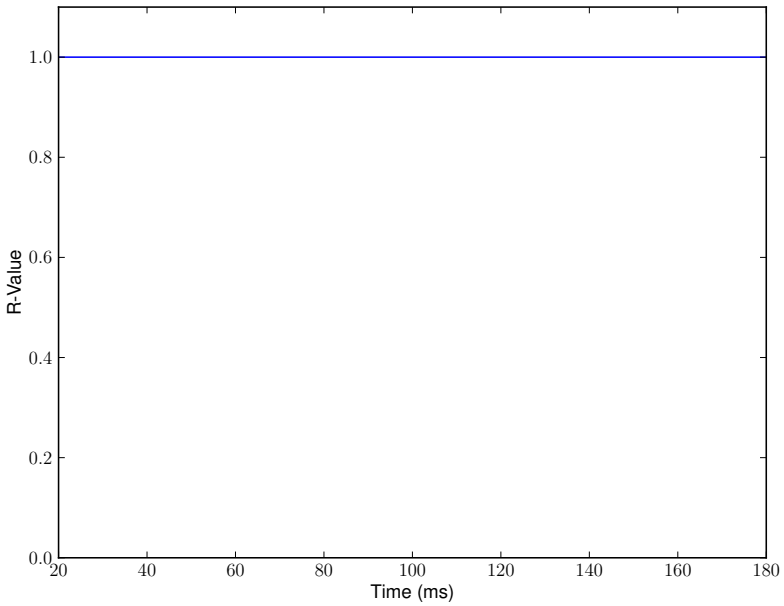

Figure 4.31: R-value for the measurement time window

Table 4.10: Estimated parameters of 7-D model

	Parameter	Real Value	Estimated Value	% error
1	Ifact	1	0.9956	0.44
2	gbarNa	50.000	48.0391	3.92
3	gbarK	70.000	62.2570	11.06
4	gbarKIR	5.000	4.9549	0.9
5	gbarA	20.000	21.1175	5.59
6	gl	0.400	0.3996	0.09
7	vm	-30.000	-30.3020	1.01
8	dvm	0.067	0.0674	0.62
9	tm0	0.100	0.2287	128.74
10	tm1	1.500	1.3928	7.15
11	vmt	-40.000	-40.3513	0.88
12	dvmt	0.033	0.0364	10.29
13	vh	-50.000	-49.3040	1.39
14	dvh	-0.067	-0.0733	9.92
15	th0	1.000	0.3848	61.52
16	th1	10.000	10.6342	6.34
17	vht	-50.000	-54.0721	8.14
18	dvht	0.025	0.0209	16.27
19	vn	-25.000	-25.6666	2.67
20	dvn	0.040	0.0403	0.83
21	tn0	1.000	0.9968	0.32
22	tn1	10.000	10.0195	0.19
23	vnt	-75.000	-74.4855	0.69
24	dvnt	0.020	0.0206	3.07
25	vm	-80.000	-79.9392	0.08
26	dvm	-0.067	-0.0671	0.6
27	mTau	15.000	14.9760	0.16
28	Iva	-30.000	-30.9961	3.32
29	Idva	0.067	0.0647	3.01
30	ta0	0.100	0.0717	28.27
31	ta1	1.500	2.0000	33.33
32	Tva	-40.000	-45.5533	13.88
33	Tdva	0.033	0.0229	31.29
34	Ivb	-55.000	-61.0994	11.09
35	Idvb	-0.067	-0.0505	24.32
36	tb0	1.000	2.0000	100
37	tb1	10.000	13.4789	34.79
38	Tvb	-50.000	-10.0157	79.97
39	Tdvb	0.011	0.0100	10

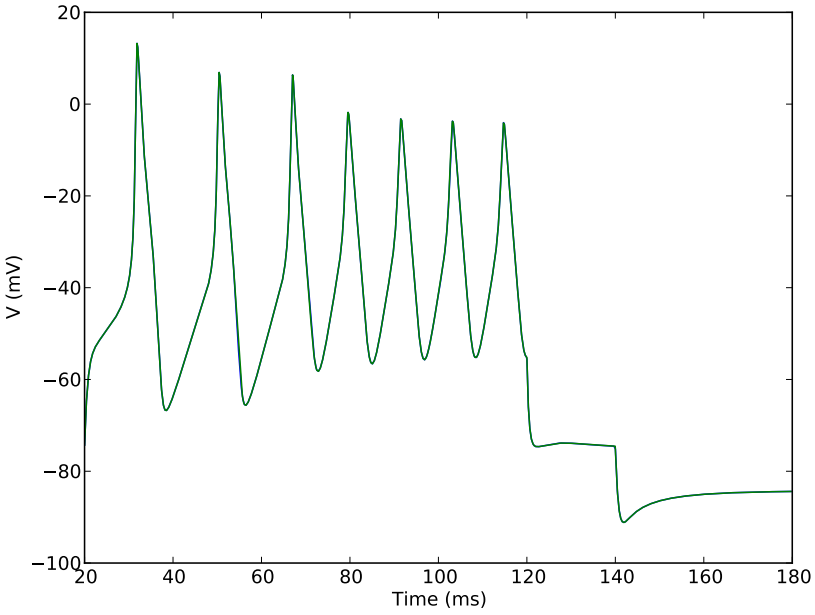

Figure 4.32: HH-like model twin experiment including $I_{Na,T}$, I_{KDR}, I_{IR}, I_A, and I_l. Original and estimated trace for V

4.6 Summary

The various twin experiments performed on neuron models of different dimensions has recreated the hidden parameters and states. As the dimension of the search space increases, however, more data is needed to be coupled to the desinged model to recreate the true values of parameters and states. Based on results from run 1 and 2 of seven-dimensional neuron model, it is not garaunteed that the state and parameters are correctly estimated as the dimension of the estimation problem grows. This is a manifestation of degeneracy in the search space as the model gets more complicated and the number of parameters grow.

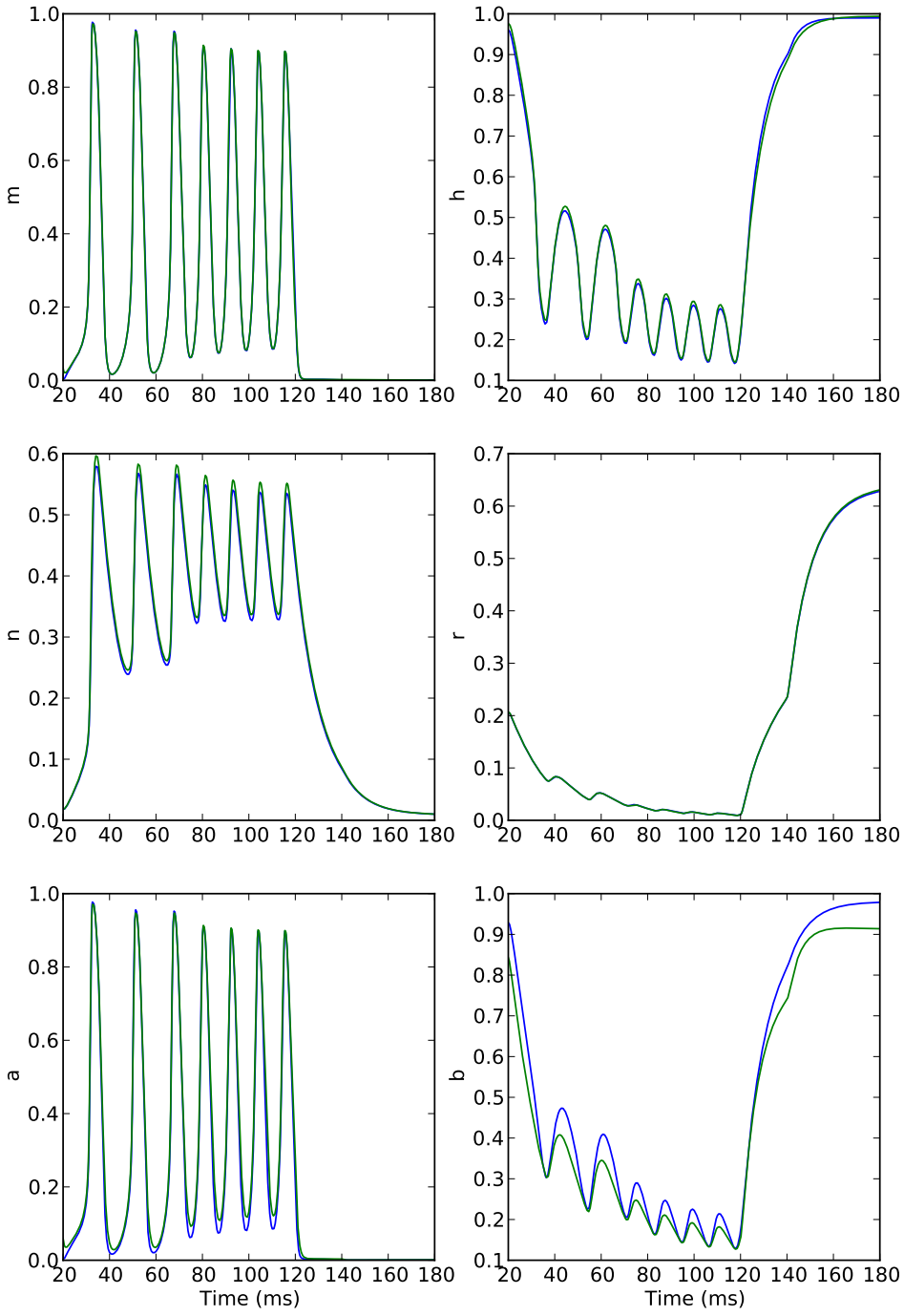

Figure 4.33: HH-like model twin experiment including $I_{Na,T}$, I_{KDR}, I_{IR}, I_A, and I_l. Original and estimated traces for all gating particles

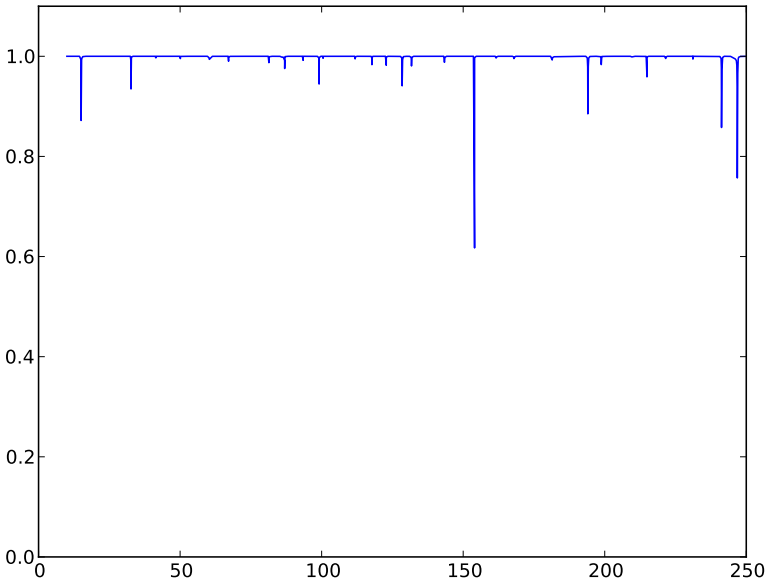

Figure 4.34: R-value for the measurement time window

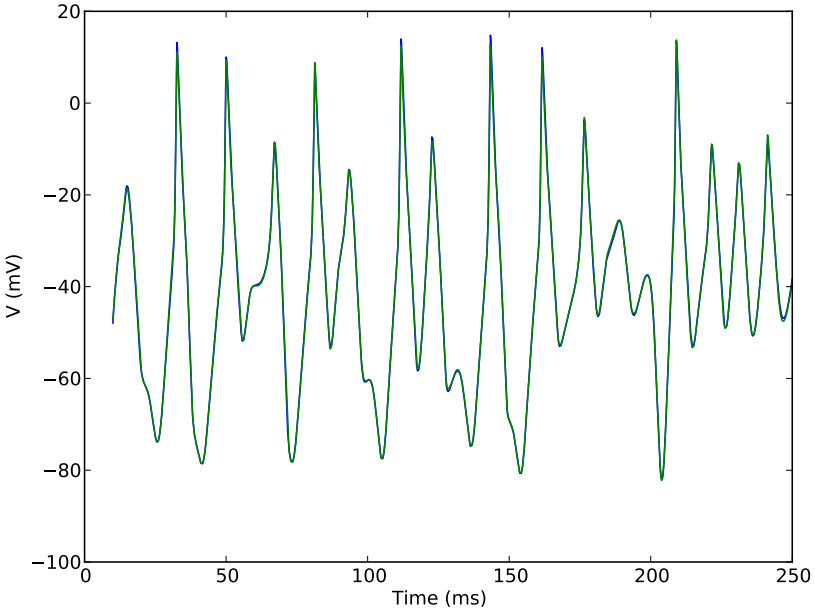

Figure 4.35: HH-like model twin experiment including $I_{Na,T}$, I_{KDR}, I_{IR}, I_A, and I_l. Original and estimated voltage traces

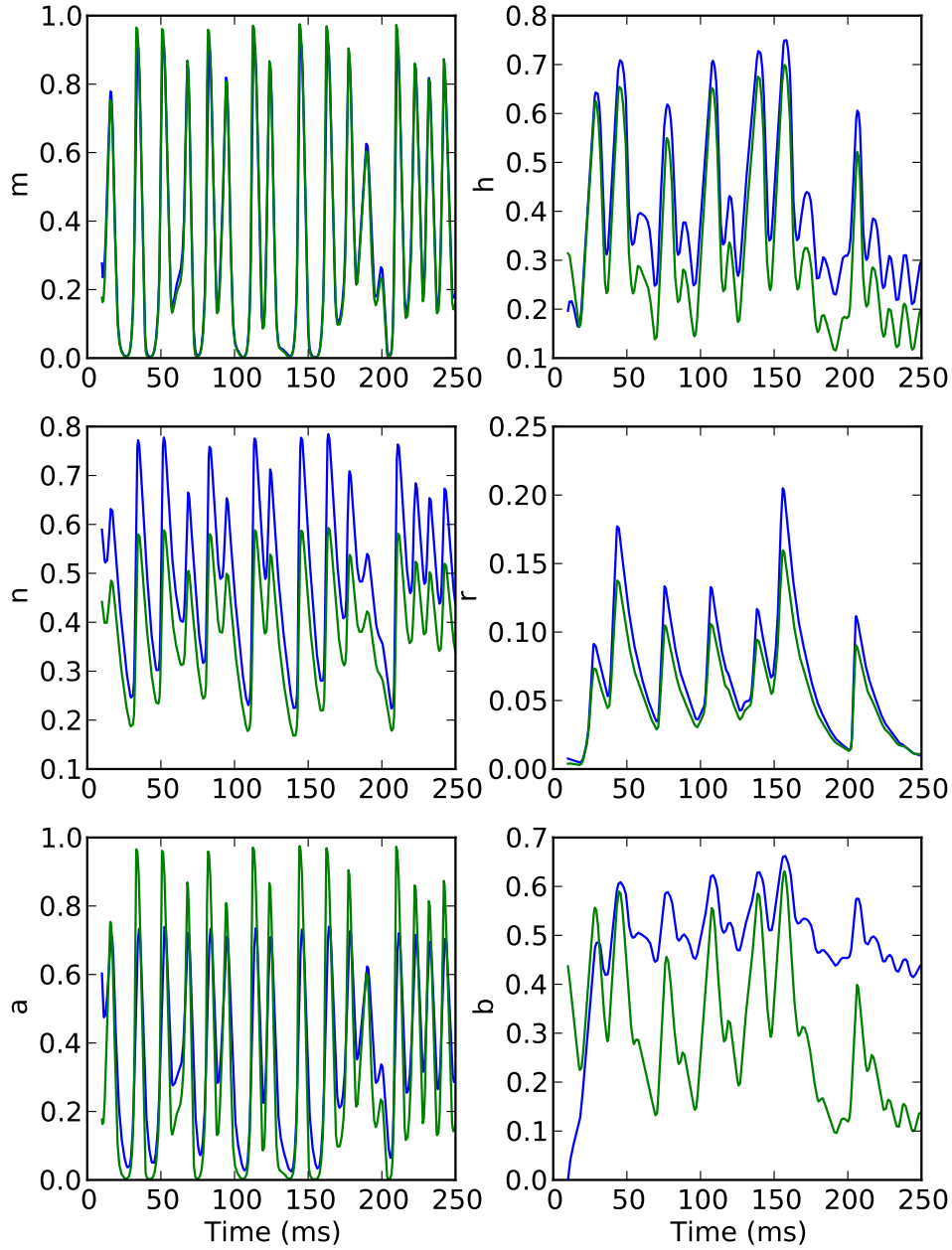

Figure 4.36: HH-like model twin experiment including $I_{Na,T}$, I_{KDR}, I_{IR}, I_A, and I_l. Original and estimated traces for all gating particles

Chapter 5

Estimation of BNST Neurons

5.1 Introduction

Bed Nucleus of Stria Termialis neurons (BNST) neurons are a part of extended amygdala of rats brain. These neurons play an important role in reward related behavior and regularization of stress. Studying the biological properties of these neurons is essential in understanding behavior such as alcoholism and drug addiction.

This family of neurons has three types (I, II, III). Type II and III neurons have the most reproducible voltage traces when presented with similar injected current. We will present results from parameters and state estimations of these neurons. Two type II neurons have been used for estimation analysis and prediction, and a type III neuron is used to investigate the generality of the model used.

5.2 Model Construction

The model for BNST neurons was based on neurophysiological information for each specific neuron ([48], [24]). The main type of ionic channels are that present in the biological neuron were recreated in the model as a current (Table 5.1). The form of the current equation is that of the standardized model introduced in section 4.2.

$$\frac{dV}{dt} = \frac{1}{C_m}\left[\sum_j I_j + \frac{I_{\text{inj}} + V/R_s}{Area}\right] \tag{5.1}$$

where I_j are various currents shown in table (5.1), I_{inj} is injected current, and R_s is the input resistance of the neuron.

The dynamic of calcium currents depend on the extracellular and intracellular ionic concentration of calcium. These ions take a similar form described by equations (2.38) and (2.39), also known as GHK model. We have re-written these equations in a new form:

$$G_{Ca} = V_T \times \frac{g_{out} - g_{in}\exp(-V/V_T)}{\exp(-V/V_T) - 1} \tag{5.2}$$

with the following definitions:

Thermal voltage of Ca^{2+} ions:	V_T	$=$	$k_BT/Z \approx 13mV$
Outer calcium concentration:	g_{out}	$=$	$FP[Ca]_{out}$
Inner calcium concentration:	g_{in}	$=$	$FP[Ca]_{in}$
Membrane permeability:	P		
Faraday Constant:	F		

Table 5.1: List of Ion Channels

Current	Equation		
Transient sodium	I_{NaT}	$=$	$g_{Na}m^3h(E_{Na} - V)$
Persistent sodium	I_{NaP}	$=$	$g_P n(E_{Na} - V)$
Potassium	I_A	$=$	$g_{A1}b^4(E_K - V)$
Direct rectifying potassium	I_{DR}	$=$	$g_{A2}p^4q(E_K - V)$
Calcium activated potassium	I_{K2}	$=$	$g_c u(E_K - V)$
High threshold calcium	I_L	$=$	r^2G_{Ca}
Low threshold calcium	I_T	$=$	stG_{Ca}
Hyperpolarization activated	I_h	$=$	$g_h z(E_h - V)$
Leak	I_L	$=$	$g_L(E_L - V)$

There are a total of 11 gating variables present in this model (m, h, n, b, p, q, u, r, s, t, z). All of these gating variables follow the standard mathematical form described in section 4.2. For a gating variabel X we have:

$$\dot{X} = (X_\infty(V) - X)/\tau_X(V) \tag{5.3}$$

where steady state, $X_\infty(V)$, and time constant, $\tau_X(V)$, are defined as:

$$\begin{aligned} X_\infty(V) &= \frac{1}{2}\left[1+\tanh\left(\frac{V-v_X}{dv_X}\right)\right] \\ \tau_X(V) &= tX_0 + tX_1\left[1-\tanh^2\left(\frac{V-v_{Xt}}{dv_{Xt}}\right)\right] \end{aligned} \tag{5.4}$$

Here v_X, dv_X, v_{Xt}, dv_{Xt},

The above form for time constant of a current is symmetric. In order to incorporate asymmetry of time constant for some currents, an additional term was introduced to equation (5.4).

$$\tau_X(V) = tX_0 + tX_1\left[1-\tanh^2\left(\frac{V-v_{Xt}}{dv_{Xt}}\right)\right] + \frac{\delta_i}{2}\left[a+\tanh\left(\frac{V-v_{Xt}}{dv_{Xt}}\right)\right] \tag{5.5}$$

Appendix C shows the exact form we used in our model.

5.3 Control Term and Cost Function

To couple the measured membrane voltage of the neuron to our model, the following term was added to the end of voltage equation (equation 5.1).

$$K(t,V)\Big(V_{\text{data}} - V\Big) \tag{5.6}$$

where V_{data} is the measured voltage and control term K is a function of voltage and time (equation 5.7).

$$K\Big(t,V\Big) = K\left[1+c_1\left(1+\tanh\left[\frac{V-V_{th}}{5}\right]\right)\right] \tag{5.7}$$

where c_1 is a constant that will set the strength of coupling and was fixed at 5, V_{th} is the spike threshold and was taken to be about 40 mV.

5.4 Estimation and Prediction Workflow

In all of the following runs, an initial learning window was used to estimate the parameters and states of that neuron. These parameters and states are then

used to integrate the model forward. In the prediction window, the control term K is off and the trajectory of the system is purely based on the learned parameters and states.

The data for each neuron is taken at different *sweeps*. These sweeps are the voltage trace of the neuron at different times. The first sweep is always used to learn that parameter values and hidden states. The final values of states from estimation is used as initial condition for forward integration using the model constructed based on estimated parameters.

In sweeps after the first one, a shorter window is used only to estimate the hidden states while parameters are fixed to the values found in sweep one. The initial condition based on estimated states are used again to integrate forward.

5.5 Type II BNST Neuron 1

This is a summary of estimation and prediction runs on BNST neuron *11a08_C2_08_T2*. All the data is recorded at 20 kHz frequency. For all the following runs, the model described in section 5.2 is used. The main difference between these runs are the ranges over which the estimation was done for four parameters Cm, ENa, EK, and El. All runs except run1 include I_{NaP}. For each run, a graph shows the data versus estimation and prediction. The prediction models are all based on parameters found during estimation for that specific run.

Table (5.2) shows a summary for each run, including number of data points used, number of parameters, number of states, and sweep number used.

Table 5.2: Summary of runs

Run #	**Sweep #**	**data points used**	**Starting Point**	**Number of States**	**Number of Parameters**
1	1	50,000	0	11	67
7	1	50,000	0	12	69
8	1	50,000	0	12	69
9	2	20,000	0	12	0
11	4	20,000	0	12	0
13	3	20,000	0	12	0

Run 1

Initial run using the model described in section 5.2. Table 5.3 shows limits on some of the parameters, initial guess, and their estimation.

Table 5.3: Run7-Sweep1

Parameter	Unit	Lower Bound	Upper Bound	Initial Guess	Estimation
Cm	pF	0.3	4	1	0.3
ENa	mV	42	50	50	50
EK	mV	-90	-80	-85	-90
El	mV	-110	-40	-80	-110

Run 7

In this run, I_{NaP} was added to the model used in run 1. Table 5.4 shows limits on some of the parameters, initial guess, and their estimation.

Table 5.4: Run1-Sweep1

Parameter	Unit	Lower Bound	Upper Bound	Initial Guess	Estimation
Cm	pF	0.3	4	1	0.3
ENa	mV	42	50	50	50
EK	mV	-90	-80	-85	-90
El	mV	-110	-40	-80	-81.49492

Run 8

Some of the parameters search limits are changed in this run compared to run 7. (Table 5.5)

Table 5.5: Run8-Sweep1

Parameter	Unit	Lower Bound	Upper Bound	Initial Guess	Estimation
Cm	pF	0.8	1.2	1	0.8
ENa	mV	45	55	50	55.0
EK	mV	-82	-72	-77	-82.0
El	mV	-60	-50	-55	-60

Run 9

In this run, all the parameters found in run 8 are fixed in the model. 20,000 data points were used for the estimation of state variables only. The end point of estimation window was used as initial condition for forward integration. For the value of parameters used in this run, refer to table 5.6 and look for parameters of run 8.

The forward integration based on model contracted from run 8 matches very well with data.

Run 11

The same as run9, except for using sweep 4 of the same neuron.

Run13

The same as run9, except for using sweep 3 of the same neuron.

5.6 Type II BNST Neuron 2

Another type II neuron (*11b09_C1_08_T2*) is used in this section. We have follow a very similar procedure as described in previous section. Once again, all the data is recorded at 20 kHz frequency.

Run1

This is the initial run using the same model used in previous section. Table 5.7 shows limits on some of the parameters. Figure (5.7) shows data, estimation, and prediction for this sweep. Table 5.8, shows the complete list of estimated parameters for this run.

Run 2, 3 and 4

These runs are done on sweep 2, 4, and 5 of the same neuron. In all three runs, the model and estimated parameters of run 1 is used to find initial conditions,

Table 5.6: Estimated parameter summary

Parameter	**Run 1**	**Run 7**	**Run 8**
c1	5	5	5
Cm	0.3	0.3	0.8
gNa	120	120	120
gP	NA	2.548614e-13	2.011884e-13
ENa	50	50	55
gA1	0.04543025	1.202752	3.011381
gA2	54.77707	0.1132848	1.570486
gc	0.07914345	0.04391224	0.07357142
EK	-90	-90	-82
gL	0.01204375	0.06190968	0.133207
EL	-110	-81.49492	-60
gou	0.2140506	0.4275365	0.9662544
gin	0.0001	0.0001	0.0001
gh	0.03689983	0.02003147	0.005466672
Isa	0.1328072	0.1145784	0.04949765
amV1	-27	-27	-27
amV2	6.918695	7.13674	7.518999
amV3	5.283022	5	45
tm0	0.4550618	0.2596156	0.2502509
epsm	0.4096885	0.3491841	0.012
ahV1	-62.153	-68.50788	-64.32899
ahV2	-12.81243	-13.98113	-14.40966
ahV3	20.29448	21.79102	21.52385
th0	0.02	0.02	0.02
epsh	100.6137	107.6997	90.05317
anV1	NA	-55.69083	-55.6469
abV1	-48.64102	-21	-21
abV2	34	5	5
abV3	8.105468	25.12213	24.71878
tb0	0.7043556	0.01	0.01
epsb	14.97476	4.646471	4.43374
apV1	-22.01061	-52.05146	-45.79392
apV2	19.54994	48	48
apV3	5	11.22868	5.701622
tp0	1.094631	1.036469	1.300378
epsp	23	12.78726	9.694104

Table 5.6: Continued

Parameter	Run 1	Run 7	Run 8
aqV1	-57.69772	-35	-63.5923
aqV2	-9.521723	-39	-24.08921
aqV3	-5	-39	-7.311486
tq0	0.5	310	0.5000002
epsq	564.5843	910	13.82116
deltasq	3.774886	990	90.67936
auV1	-25	-25	-25
auV2	31.09115	14.87297	65
auV3	70	10	70
tu0	6.674401	55	55
epsu	153.4358	3.737746	42.59988
arV1	-56	-44.79507	-55.75689
arV2	11.26361	20.89344	10.98067
arV3	15.90907	55	55
tr0	43.6	3.886651	43.6
epsr	190.2015	0.2	109.5771
asV1	-43.72096	-51.69763	-40.6082
asV2	30.98601	39	29.80298
asV3	57	57	57
ts0	0.9	0.9	0.9
eps5	5.86886	10.16027	4.125393
atV1	-55	-67.09734	-55
atV2	-34	-29.16519	-34
atV3	55	27.12836	25.88619
atV4	55	55	55
tx0	190	5	107.4154
epst	90.24318	11.55454	37.30753
azV1	-51.52867	-65.31613	-78.66565
azV2	-5	-30	-5
azV3	13.52465	10.05557	40
tz0	24.42686	4.550427	500
epsz	230.0445	5000	574.419
rlt	0.1146231	0.3237448	0.01988287

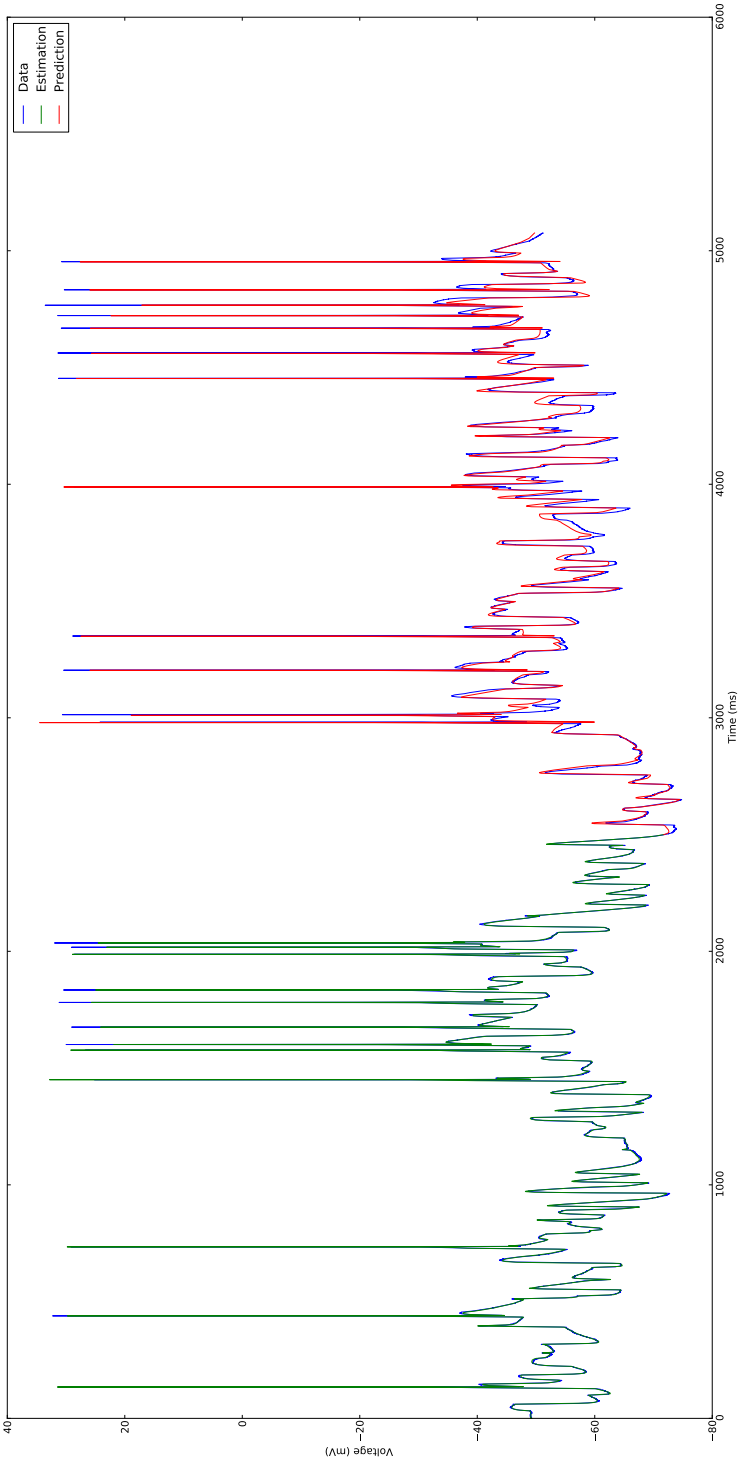

Figure 5.1: Comparison of Data (blue), estimation (green), and prediction for run 1 (sweep 1)

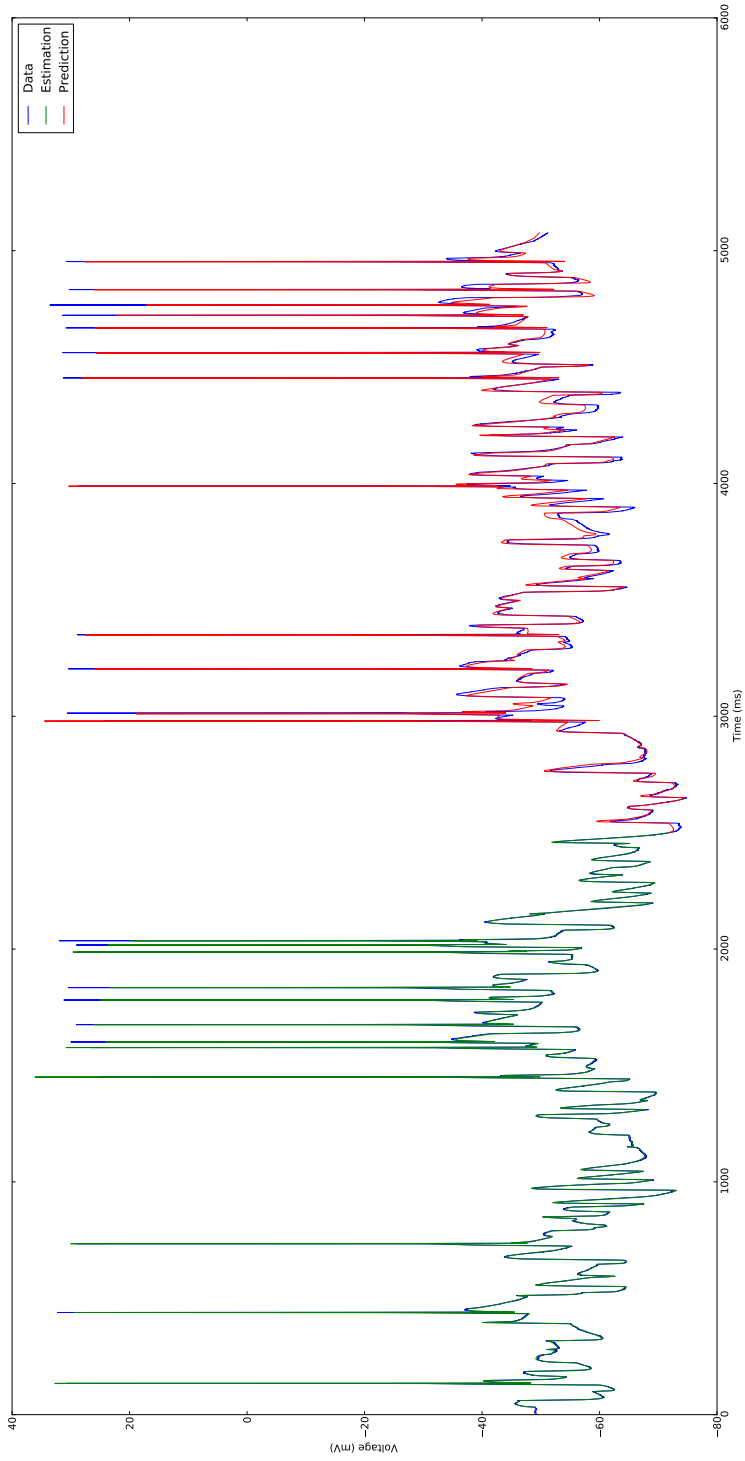

Figure 5.2: Comparison of Data (blue), estimation (green), and prediction for run 7 (sweep 1)

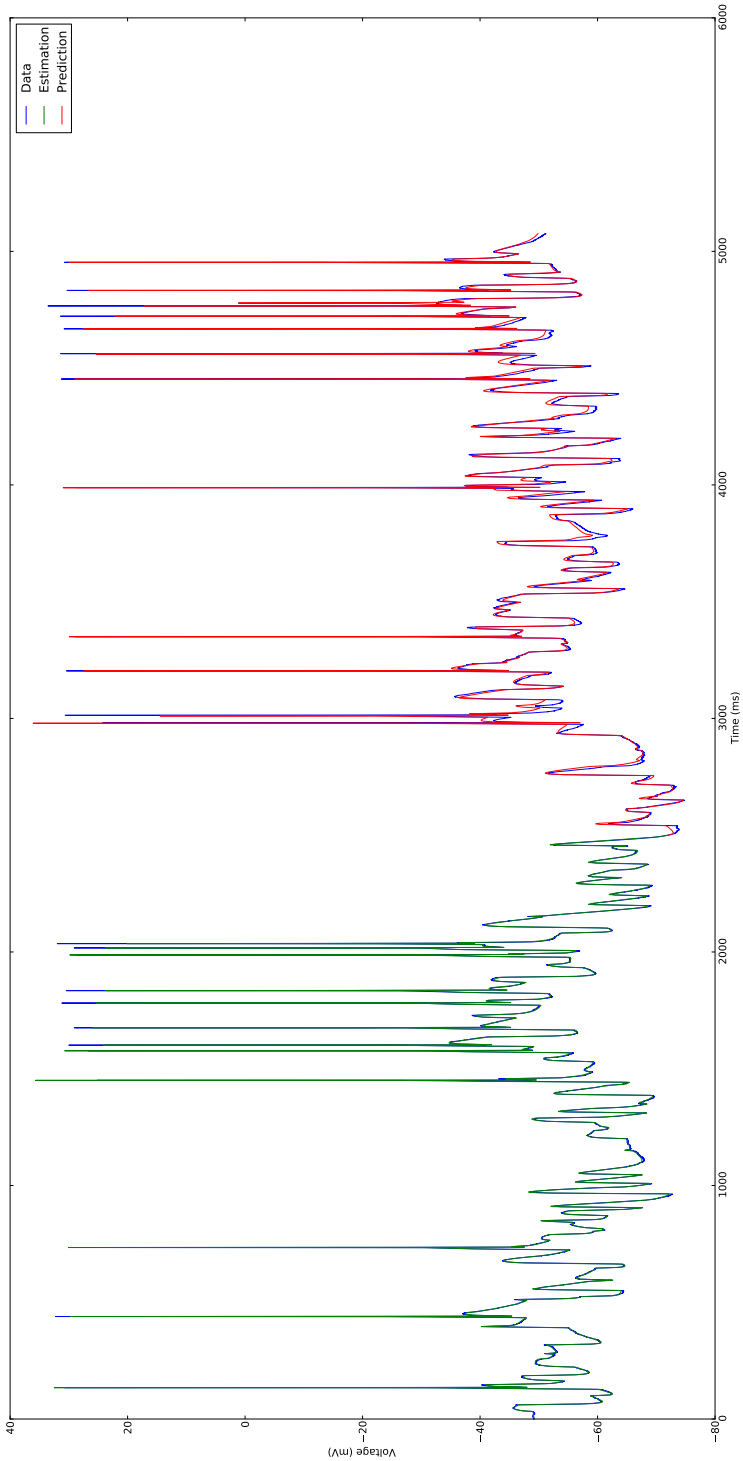

Figure 5.3: Comparison of Data (blue), estimation (green), and prediction for run 8 (sweep 1)

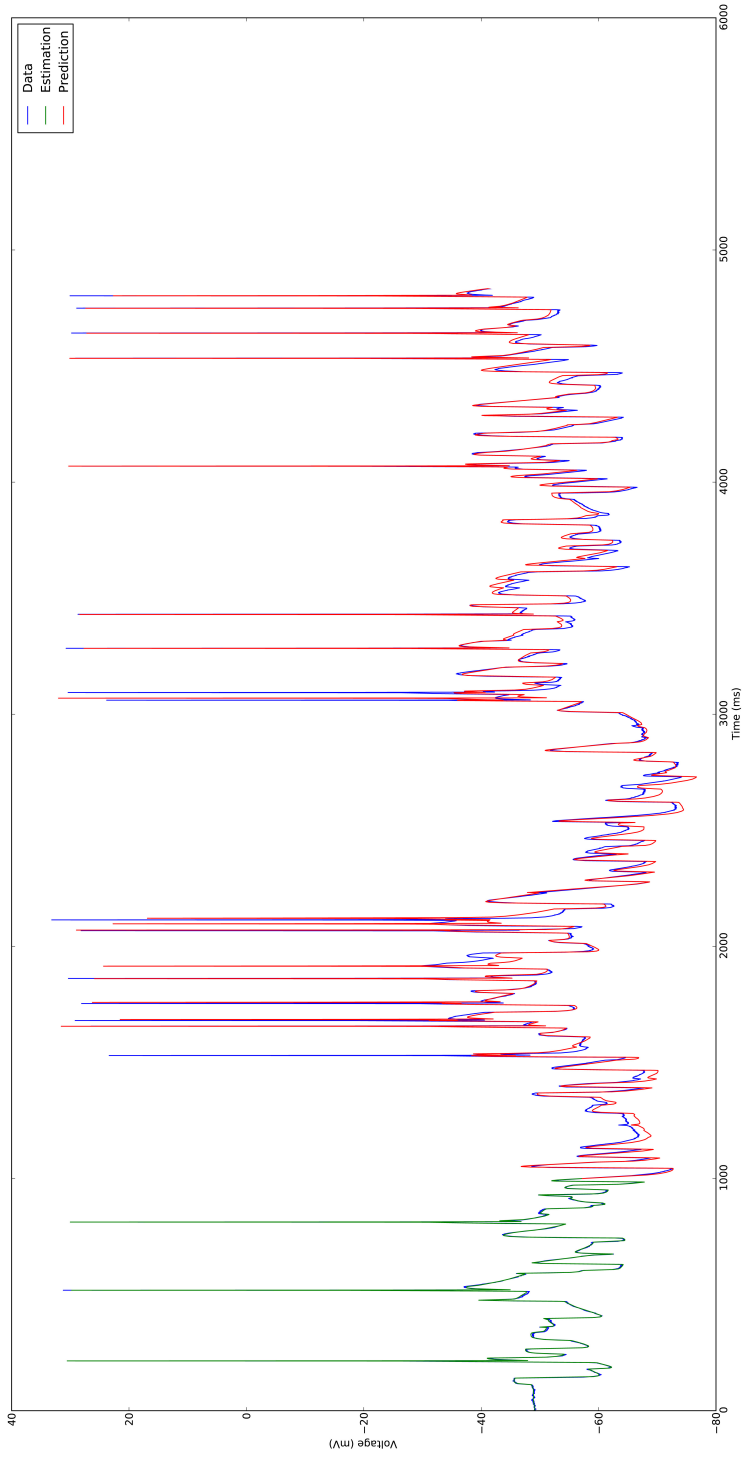

Figure 5.4: Comparison of Data (blue), estimation (green), and prediction for run 9 (sweep 2)

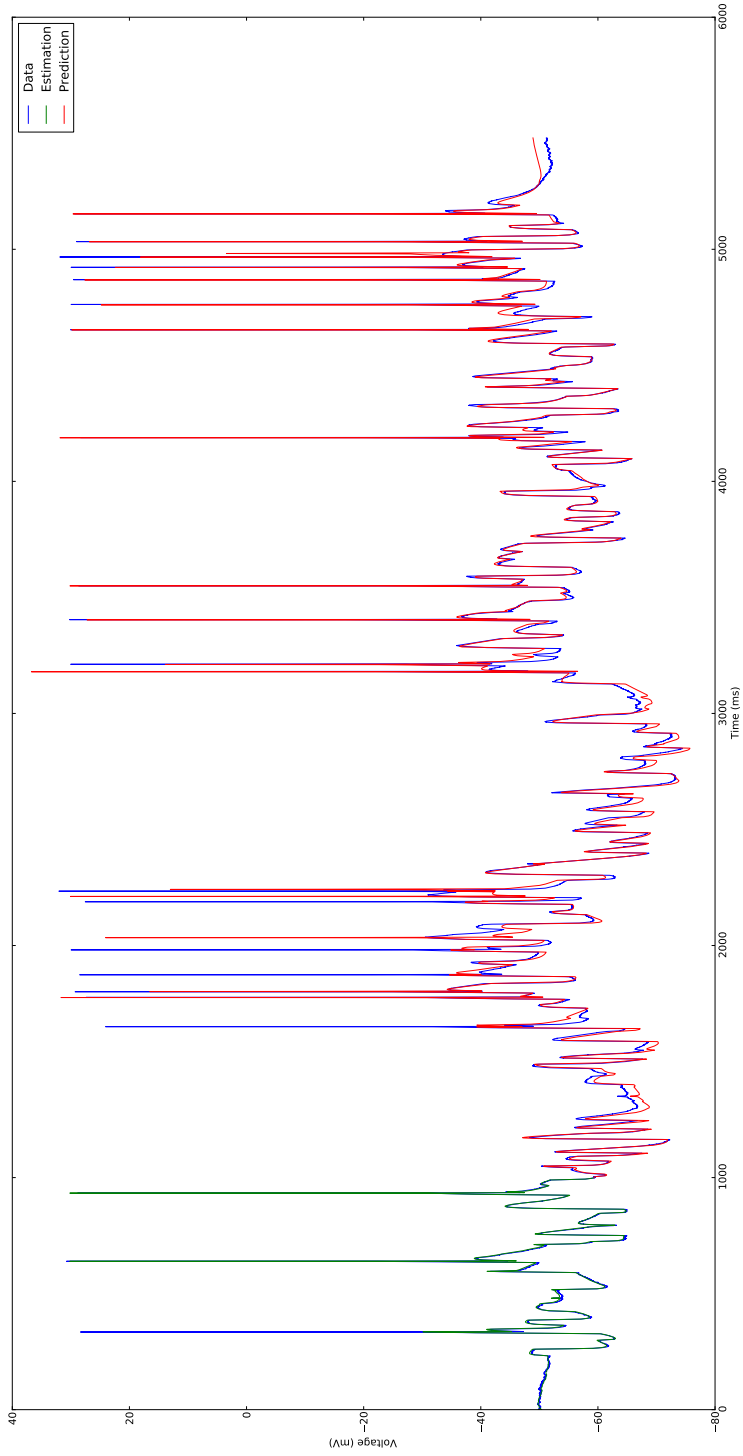

Figure 5.5: Comparison of Data (blue), estimation (green), and prediction for run 11, sweep 4

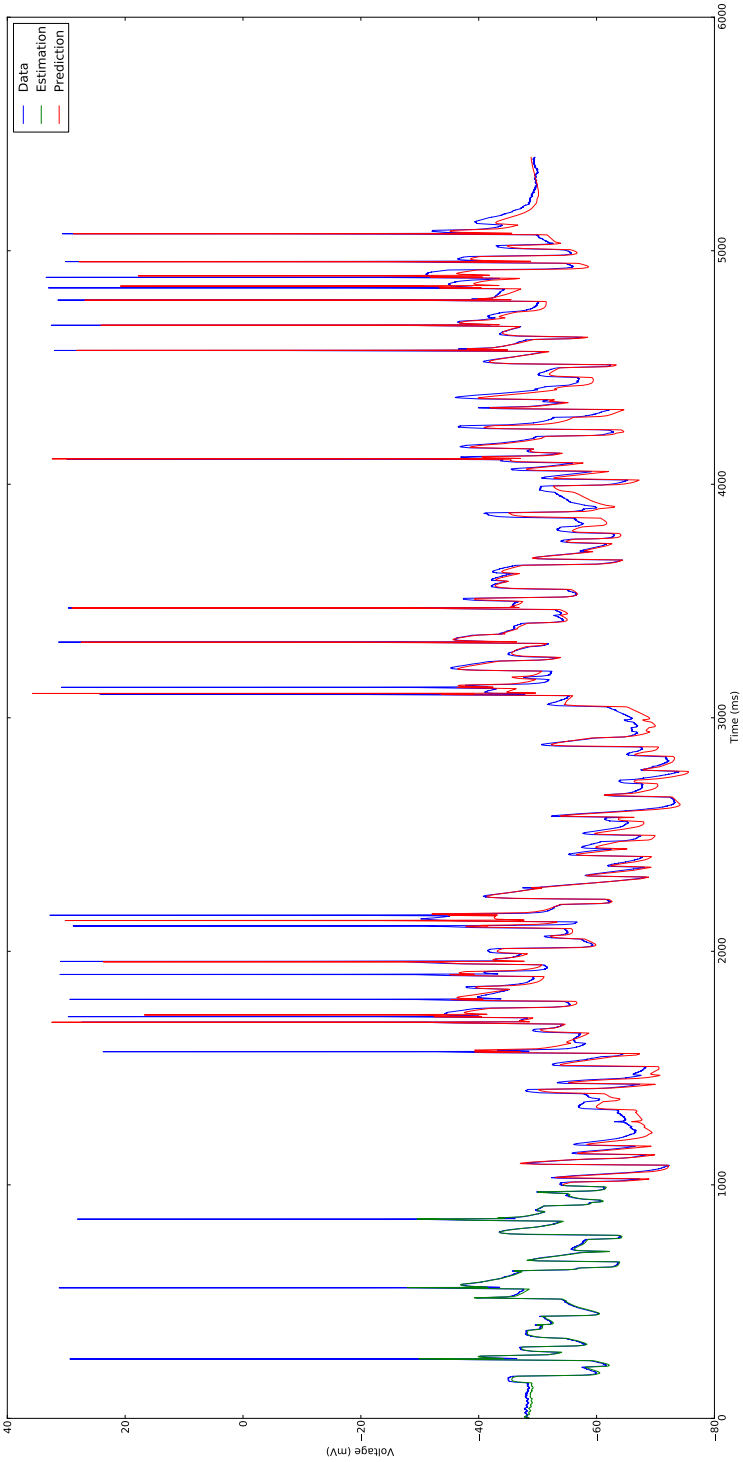

Figure 5.6: Comparison of Data (blue), estimation (green), and prediction for run 13, sweep 3

and then using these initial conditions and the given model from run 1, a forward integration was done. Figure (5.8), (5.9) and (5.10) shows these three runs.

5.7 Summary

The results from two different type II BNST neurons shows that it is possible to estimate all biophysical parameters in a neuron and use their values for forward prediction of the system. The question remains, however, if this is due to the generality of the model that was used for these neurons, and whether it is possible that this general neuron model has enough degrees of freedom that can match any neuron.

These are valid concerns since we have no direct knowledge of the exact dynamics of a neuron, and any model built at best is an approximation. We applied the same model which was used for type II neurons to a type three neuron. These neurons are similar but have different currents present in them, therefore, if our model was general we should have similar results. Figure (5.11) shows estimation and prediction for this type of neuron. Since the specific currents that are present in a type III neuron did not exist in the model the prediction does not match the data.

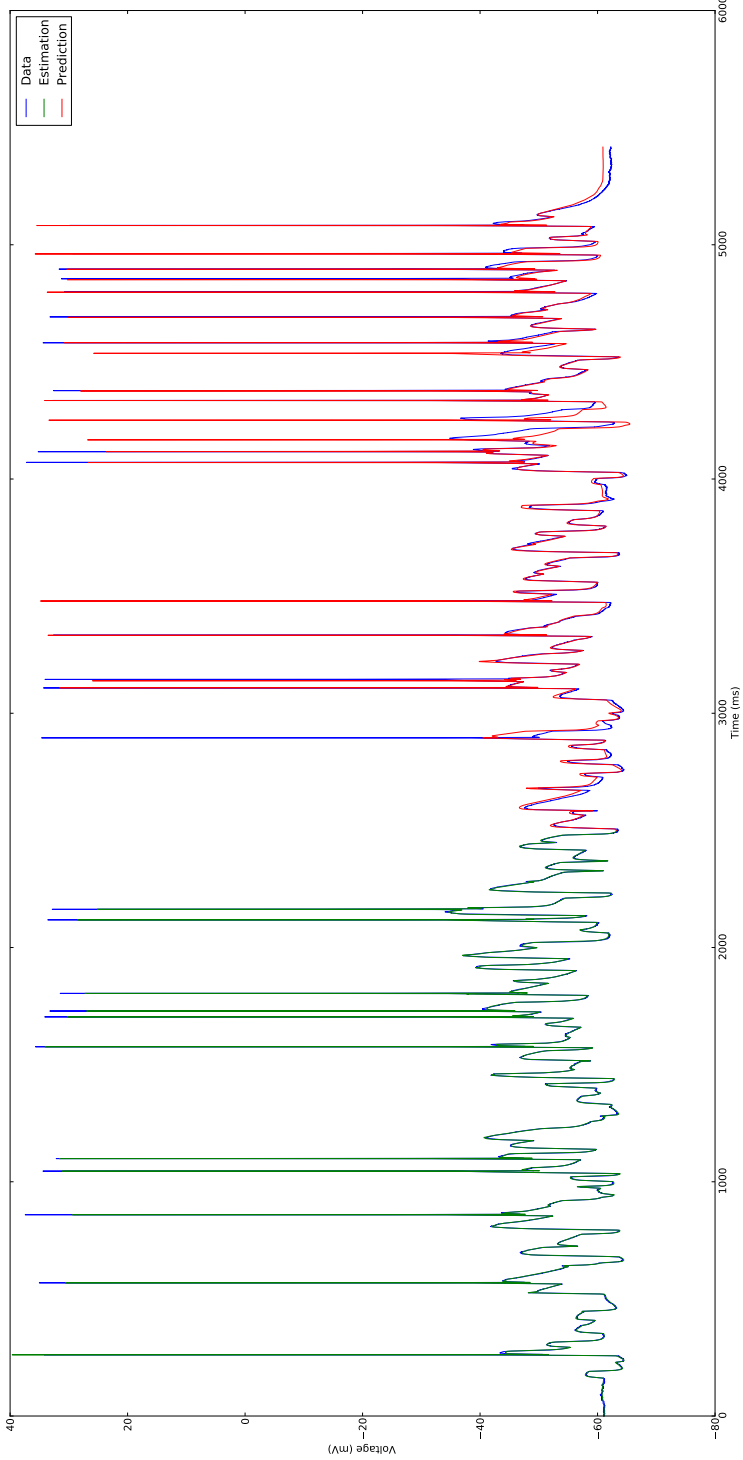

Figure 5.7: Comparison of Data (blue), estimation (green), and prediction for run 1 (sweep 1)

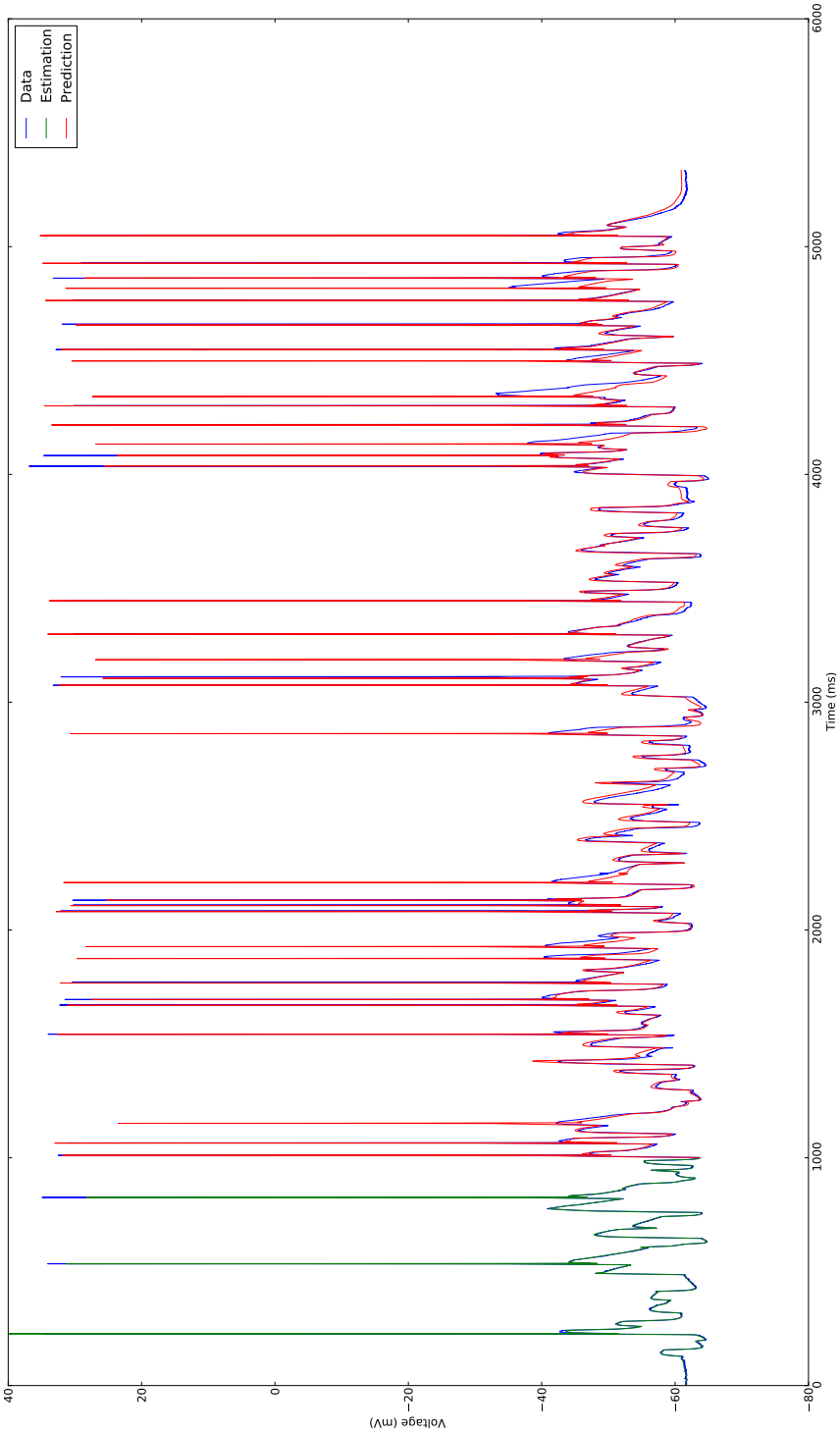

Figure 5.8: Comparison of Data (blue), estimation (green), and prediction for run 2 (sweep 2)

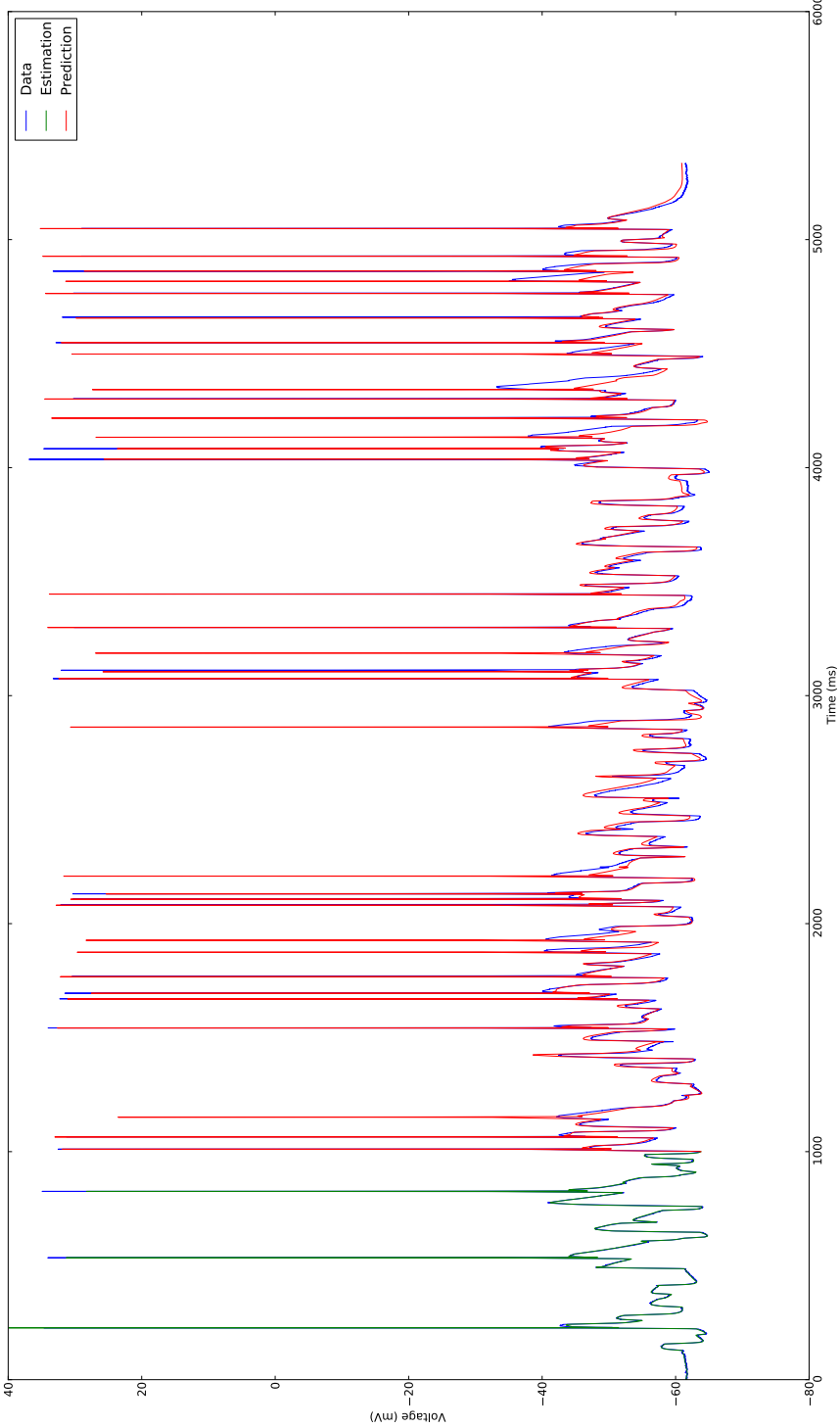

Figure 5.9: Comparison of Data (blue), estimation (green), and prediction for run 3 (sweep 4)

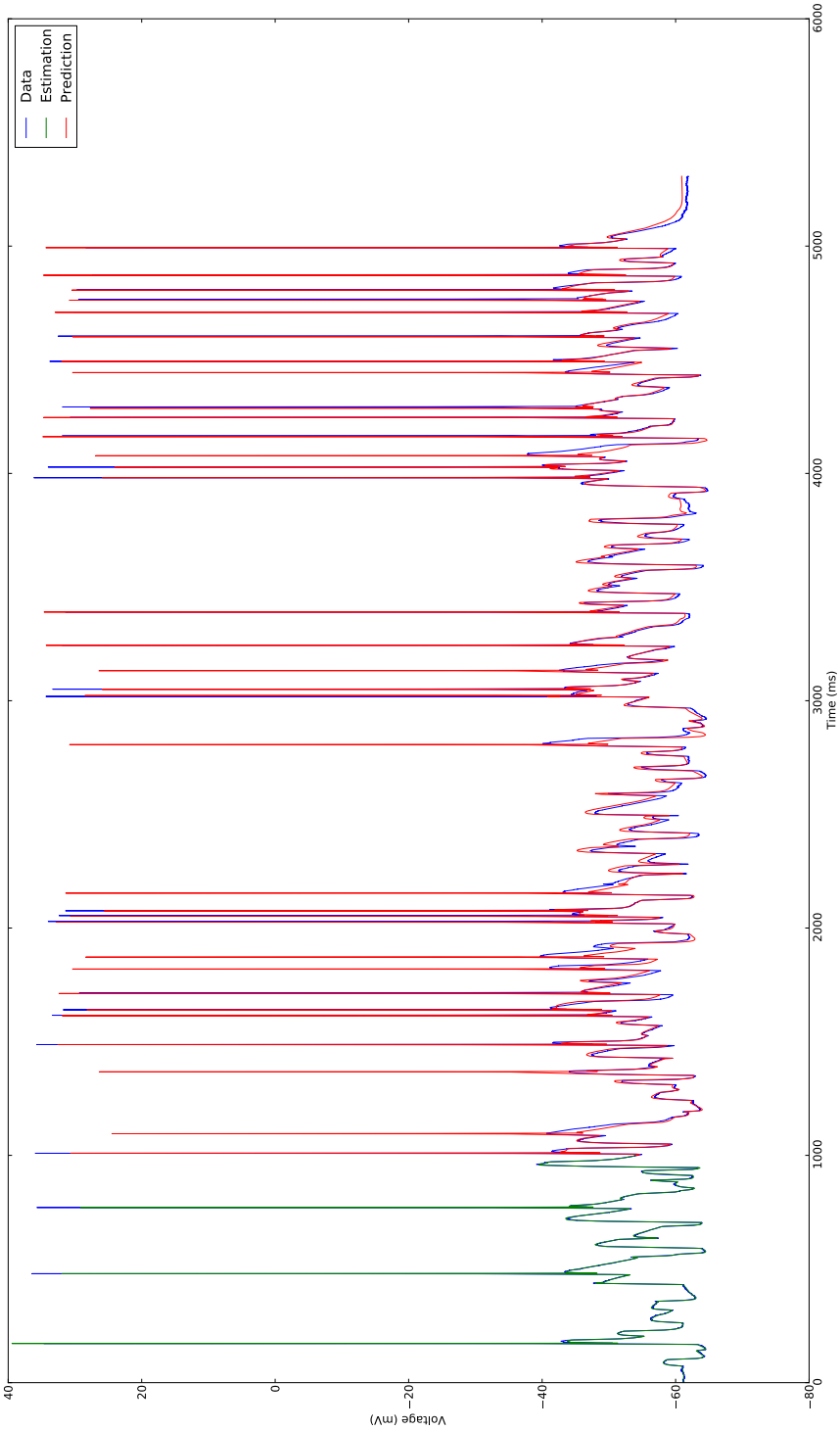

Figure 5.10: Comparison of Data (blue), estimation (green), and prediction for run 4 (sweep 5)

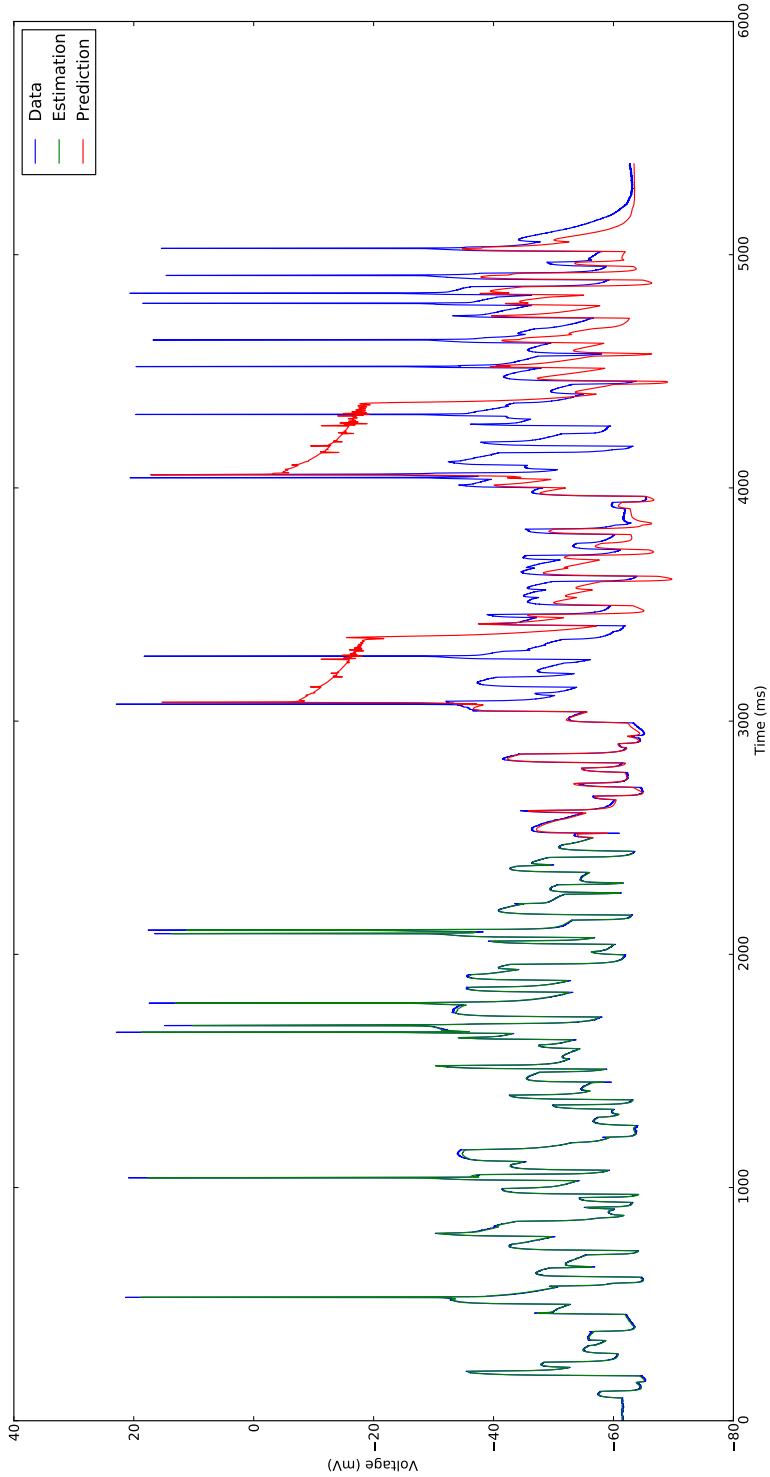

Figure 5.11: Comparison of Data (blue), estimation (green), and prediction for type III BNST neuron

Table 5.6: Summary of runs

Run #	**Sweep #**	**data points used**	**Starting Point**	**Number of States**	**Number of Parameters**
1	1	50,000	0	12	69
2	2	20,000	0	12	0
3	4	20,000	0	12	0
4	5	20,000	0	12	0

Table 5.7: Parameter bounds for run1

Parameter	Unit	Lower Bound	Upper Bound	Initial Guess	Estimation
Cm	pF	0.8	1.2	1	1.2
ENa	mV	45	55	50	55.0
EK	mV	-82	-72	-77	-82.0
El	mV	-60	-50	-55	-60.0

Table 5.8: Estimated parameters in run 1

Parameter	Estimated Value	Parameter	Estimated Value
c1	5	epsp	0.5
Cm	1.2	aqV1	-59.02013
gNa	100	aqV2	-21.36911
gP	1.533136e-12	aqV3	-5
ENa	55	tq0	0.9655148
gA1	0.2128484	epsq	19.76087
gA2	8.269561	deltasq	7.227117
gc	6.93478e-12	auV1	-24.99771
EK	-82	auV2	64.99414
gL	0.1251626	auV3	69.94875
EL	-60	tu0	54.87325
gou	0.2897776	epsu	454.8365
gin	0.0001	arV1	-51.79377
gh	1.510254e-11	arV2	17.50003
Isa	0.0449597	arV3	10.25522
amV1	-27	tr0	4.833438
amV2	18.41729	epsr	14.35102
amV3	5	asV1	-45.33617
tm0	0.0477079	asV2	10.09359
epsm	0.012	asV3	26.92169
ahV1	-71.0094	ts0	0.02
ahV2	-26.17871	eps5	2.686672
ahV3	34.19202	atV1	-55
th0	0.02	atV2	-34
epsh	12.36842	atV3	55
anV1	-54.03087	atV4	55
abV1	-58.04182	tx0	190
abV2	21.0032	epst	7000
abV3	13.73099	azV1	-52.56297
tb0	3.72742	azV2	-25.77637
epsb	23	azV3	31.35153
apV1	-43.31915	tz0	321.4245
apV2	17.15545	epsz	4313.798
apV3	5	rlt	0.4123265
tp0	0.4506331		

Chapter 6

Statistical Path Integral Method

6.1 Introduction

In chapter 3, we discussed a dynamical approach of parameters and states estimation. The following chapter, demonstrated verification of these methods, and in chapter 5 some successful estimation and prediction of biological neurons were discussed. In this chapter, we will formulate and demonstrate a different method of parameter and state estimation. This method uses idea from quantum mechanical path integral formulation, to solve the similar problem of system verification discussed in chapter 3. ([2], [40], [42], [26], [29], [32])

6.2 Probabilistic Formulation

When dealing with a real physical system, there are many hidden characteristics such as the unmeasured parameters and state variables. It is often very important to have a knowledge of these underlying features of the system.

We start with a model that to the best of our knowledge describes a real-world physical system, which is then used to estimate the hidden states and variables of the system. Let us take a model with D dimensions and Ω parameters. Only L of the D state variables are observable, and none of the parameters can be measured directly. The L observable state variables are measured at $M+1$ time points during the measurement time window. Then $L \times (M+1)$ measured points

can be described as the measured path $\mathbf{Y}_{0:M}$:

$$\mathbf{Y}_{0:M} = \Big\{\mathbf{y}(0), \mathbf{y}(1), \ldots, \mathbf{y}(M)\Big\} \tag{6.1}$$

where $\mathbf{y}(n) = \{y_1(n), \ldots, y_L(n)\}$ is point in the L dimensional measurement path $\mathbf{Y}$. Given the measurements $\mathbf{Y}_{0:M}$, we are interested in estimating the parameters and the observed and unobserved state variables path $\mathbf{X}_{0:M}$. This path, $\mathbf{X}_{0:M}$, has a definition similar to that of $\mathbf{Y}_{0:M}$, for the D dimensional model.

$$\mathbf{X}_{0:M} = \Big\{\mathbf{x}(0), \mathbf{x}(1), \ldots, \mathbf{x}(M)\Big\} \tag{6.2}$$

where $\mathbf{x}(n)$ is a point on the D dimensional path of $\mathbf{X}$.

The time evolution of this system is given by a set of rules $\mathbf{f}(\mathbf{x}(t), \theta)$, which is the set of ordinary differential equations below:

$$\frac{d\mathbf{x}}{dt} = \mathbf{f}(\mathbf{x}, \theta) \tag{6.3}$$

where the parameters θ are not changing over the measurement time window. Parameters can be treated as additional state variables with ODEs, $\dot{\theta} = 0$.

The above problem can be formulated statistically. Starting with the measured path $\mathbf{Y}_{0:M}$ and given equations of motion of the system, what is the probability of being in state $\mathbf{x}(M)$? Mathematically, we are interested in finding the conditional probability distribution $\pi(\mathbf{x}(M)|\mathbf{Y}_{0:M})$. Using Bayes' rule:

$$\begin{aligned}
\pi\Big(\mathbf{x}(M)|\mathbf{Y}_{0:M}\Big) &= \frac{\pi\Big(\mathbf{x}(M), \mathbf{y}(M)|\mathbf{Y}_{0:M-1}\Big)}{\pi\Big(\mathbf{y}(M)|\mathbf{Y}_{0:M-1}\Big)} \\
&= \left[\frac{\pi\Big(\mathbf{x}(M), \mathbf{y}(M)|\mathbf{Y}_{0:M-1}\Big)}{\pi\Big(\mathbf{y}(M)|\mathbf{Y}_{0:M-1}\Big)\pi\Big(\mathbf{x}(M)|\mathbf{Y}_{0:M-1}\Big)}\right] \pi\Big(\mathbf{x}(M)|\mathbf{Y}_{0:M-1}\Big)
\end{aligned} \tag{6.4}$$

The first term in the bracket, is nothing but the exponential of the mutual information term, $\mathrm{MI}(\mathbf{x}(m), \mathbf{y}(m)|\mathbf{Y}_{0:M-1})$. Using Chapman-Kolmogorov equation, the second term can be written as:

$$\prod_{n=0}^{M-1} \int d\mathbf{x}(n) \pi\Big(\mathbf{x}(M)|\mathbf{x}(M-1)\Big) \pi\Big(\mathbf{x}(M-1)|\mathbf{Y}_{0:M-1}\Big) \tag{6.5}$$

This term represents the transition probability of going from state $\mathbf{x}(n)$ to state $\mathbf{x}(n+1)$.

Combining all of the above and including all the points in $\mathbf{X}_{0:M}$, we can re-write equation (6.4):

$$\pi\Big(\mathbf{x}(M)|\mathbf{Y}_{0:M-1}\Big) = \prod_{n=0}^{M} \int d\mathbf{x}(n) \exp\Big[- A_0(\mathbf{X}_{0:M}, \mathbf{Y}_{0:M})\Big] \tag{6.6}$$

where A_0 is defined as *action*:

$$\begin{aligned} A_0 \;\; = \;\; & -\sum_{n=0}^{M} \mathrm{MI}\Big[\mathbf{x}(n), \mathbf{y}(n)|\mathbf{Y}_{0:n-1}\Big] - \sum_{n=0}^{M-1} \log\Big[\pi\Big(\mathbf{x}(n+1)|\mathbf{x}(n)\Big)\Big] \\ & - \log\Big[\pi\Big(\mathbf{x}(0)\Big)\Big] \end{aligned} \tag{6.7}$$

The last term, initial path distribution, is taken to be a constant and can be left out. The other two terms can be approximated assuming a Markov process, and Gaussian model and measurement errors.

$$A_0 \approx \frac{R_m}{2} \sum_{n=0}^{M} \Big[\mathbf{x}(n) - \mathbf{y}(n)\Big]^2 + \frac{R_f}{2} \sum_{n=0}^{M} \Big[\mathbf{\Delta}\Big(\mathbf{x}(n)\Big)\Big]^2 \tag{6.8}$$

Where R_m and R_f are the inverse of the square of standard deviations of data and model noise of each state variable. $\mathbf{\Delta}(\mathbf{x}(n))$ depends on the discretization of the dynamics and is the difference between $\mathbf{x}(n)$ and $\mathbf{x}(n+1)$ given the dynamics.

$$\mathbf{\Delta}\Big(\mathbf{x}(n)\Big) = \mathbf{D}\Big(\mathbf{x}(n), \theta\Big) - \mathbf{x}(n+1)$$

where $\mathbf{D}(\mathbf{x}(n))$ is the discretization of $\mathbf{f}(\mathbf{x}(n))$ in equation (6.3). If the ODEs are followed exactly $\mathbf{\Delta}(\mathbf{x}(n))$ would be equal to zero.

The exact form of $\mathbf{\Delta}(\mathbf{x}(n))$ depends on the discretization scheme $\mathbf{D}(\mathbf{x}(n))$ and $\mathbf{f}$. Here, second order Adams-Moulton was used for the discretization of the dynamics, moving from time point n to $n+1$:

$$\mathbf{\Delta}\Big(\mathbf{x}(n)\Big) = \mathbf{x}(n) - \mathbf{x}(n+1) + \frac{h}{2}\Big(\mathbf{f}(\mathbf{x}(n)) + \mathbf{f}(\mathbf{x}(n+1))\Big)$$

6.2.1 Metropolis-Hastings

A common method to sample from a specific distribution is the Metropolis-Hastings method, which is one of the many Markov Chain Monte Carlo (MCMC) methods. In our case, the desired distribution is $\exp(-A_0)$. Once again, the goal is to start with a number of measurements and a model and try to estimate the hidden states and parameters of the system. In the model, $x_i(n)$ represents the nth time point of the ith state variable, and there are Ω parameters. Essentially, one has to work in a $D \times (M+1) + \Omega$ dimensional space, treating the parameters just like the state variables.

In particular, we are interested in solving an integral of the following form, to calculate the expectation value of any function $\chi(\mathbf{x})$:

$$\Big\langle \chi(\mathbf{x}) \Big\rangle = \frac{\int d\mathbf{x} \chi(\mathbf{x}) \exp(-A_0)}{\int \exp(-A_0)} \tag{6.9}$$

using Metropolis-Hastings method. Since this is a Monte Carlo method the above integral is calculated using the following sum:

$$\Big\langle \chi(\mathbf{x}) \Big\rangle \approx \frac{1}{N} \sum_{i=0}^{N} \chi(\mathbf{x}^{(i)}) \tag{6.10}$$

In a simple MCMC methods such as Metropolis Algorithm, one starts with a current path $\mathbf{X}^{(s)}$ and creates a candidate path $\mathbf{X}^*$ by performing a random walk on each element of $\mathbf{X}$. Depending on whether the new path increases or decreases the action, the candidate path is accepted or rejected and a new path $\mathbf{X}^{(s+1)}$ is now created. After this is done many times, the system reaches equilibrium and one can start taking data and calculating the sum in equation (6.10).

The following steps summarizes this method for a specific point on the path, $x(n)$:

1. Start with an initial path $\mathbf{X}^{(0)}$
2. Calculate $A_0\Big(\mathbf{X}^{(0)}\Big)$
3. Add an unbiased random walk to $\mathbf{x}(n)$ (yields new path $\mathbf{X}^*$)

4. Calculate $a = \dfrac{P(\mathbf{X}^*)}{P(\mathbf{X}^{(0)})} = \exp\left[-\Big(A_0(\mathbf{X}^*) - A_0(X^{(0)})\Big)\right]$

   (a) If $a \geqslant 1$ then accept this change ($\mathbf{X}^{(1)} = \mathbf{X}'$)

   (b) Else

$$\mathbf{X}^{(1)} = \begin{cases} \mathbf{X}' & \text{with probability } a \\ \mathbf{X}^{(0)} & \text{with probability } 1 - a \end{cases}$$

5. Back to step 2 using $\mathbf{X}^{(1)}$

This procedure is repeated many times until the system reaches *equilibrium*. At this point, statistics can be gathered for each $\mathbf{x}_k(n)$.

6.2.2 Hybrid Monte Carlo

One of the main problems with this methods is its convergence rate due to its *trial-and-error* nature. Each candidate path is produced by blindly perturbing the states slightly from their current position and deciding whether that was a good or bad move. Hence, this methods uses a lot of its time wandering around in areas that are not statistically interesting before it reaches equilibrium.

Hybrid Monte Carlo is one way to get around this problem of slow convergence rate. In this method a *fake* momentum $\mathbf{p}$ is introduced to form a Hamiltonian:

$$H(\mathbf{p}, \mathbf{x}) = K(\mathbf{p}) + U(\mathbf{x}) \tag{6.11}$$

where the potential energy $U(\mathbf{x})$ is $A_0(\mathbf{x})$ and the kinetic energy has its usual definition, $K(\mathbf{p}) = \mathbf{p}^2/2$. Here, the mass m in the kinetic energy term is equal to unity.

The elements of $\mathbf{x}$ and $\mathbf{p}$ can be treated as position and momentum of particles with potential and kinetic energy given above. Different configuration of these *particles* will result in different values of the Hamiltonian. The evolution of

these particles in *fake* time s is given by the Hamiltonian equations:

$$\begin{aligned} \frac{d\mathbf{x}}{ds} &= \frac{\partial H}{\partial \mathbf{p}} = \mathbf{p} \\ \frac{d\mathbf{p}}{ds} &= -\frac{\partial H}{\partial \mathbf{x}} = -\nabla[A_0(\mathbf{x})] \end{aligned} \tag{6.12}$$

These equations should be discretized in a way that preserves time reversibility and conserves the volume of phase space throughout the transition of $\mathbf{x}$ and $\mathbf{p}$ in time s. Leap-frog is a symplectic numerical integration method that has these properties. In order to iterate $\mathbf{x}$ forward, we need to calculate half-steps and full-steps of $\mathbf{p}$:

$$\begin{aligned} \mathbf{p}(s+\frac{\epsilon}{2}) &= \mathbf{p}(s) - \frac{\epsilon}{2}\nabla\Big[A_0(\mathbf{x}(s))\Big] \\ \mathbf{x}(s+\epsilon) &= \mathbf{x}(s) + \epsilon\mathbf{p}(s+\epsilon/2) \\ \mathbf{p}(s+\epsilon) &= \mathbf{p}(s+\frac{\epsilon}{2}) - \frac{\epsilon}{2}\nabla\Big[A_0(\mathbf{x}(s+\epsilon))\Big] \end{aligned} \tag{6.13}$$

where s is the iteration time and ϵ is the length of the time step.

One needs to calculate the value of of ∇A_0 at each specific time point of each state variable:

$$\frac{dA_0}{dx_i(n)} = R_m \sum_{k,m} \Big(x_k(m) - y_k(m)\Big)\frac{dx_k(m)}{dx_i(n)} + R_f \sum_{k,m} \Delta(x_k(m))\frac{d\Delta(x_k(m))}{dx_i(n)} \tag{6.14}$$

where $\dfrac{dx_k(m)}{dx_i(n)} = \delta_{i,k}\delta_{n,m}$.

All the derivatives for the first term are going to be zero except for one term including $x_i(n)$ in the action. The derivative of the second term, however, depends on how the dynamics is discretized. Using Adams-Moulton as the discretization scheme we can write:

$$
\begin{aligned}
&\sum_{k,m} \Delta(x_k(m)) \frac{d}{dx_i(n)} \Delta(x_k(m)) \\
= &\sum_{k,m} \Delta(x_k(m)) \frac{d}{dx_i(n)} \left[x_k(m) - x_k(m+1) + \frac{h}{2} \Big(f_k(\mathbf{x}(m)) + f_k(\mathbf{x}(m+1)) \Big) \right] \\
= &\sum_{k,m} \Delta(x_k(m)) \left[\delta_{n,m} \Big(\frac{h}{2} \frac{df(x_k(m))}{dx_i(n)} + \delta_{k,i} \Big) + \delta_{n,m+1} \Big(\frac{h}{2} \frac{df_k(m+1)}{dx_l(n)} - \delta_{k,i} \Big) \right] \\
= &\sum_{k} \left[\Big(\frac{h}{2} \Delta(x_k(n)) \frac{df(x_k(n))}{dx_i(n)} + \Delta(x_i(n)) \Big) \right. \\
&\qquad \left. + \Big(\frac{h}{2} \Delta(x_k(n-1)) \frac{df(x_k(n))}{dx_i(n)} - \Delta(x_i(n-1)) \Big) \right] \qquad (6.15)
\end{aligned}
$$

Having all the above formalism, we can now use hybrid Monte Carlo method. Assume we start at a specific position $\mathbf{x}^{(s)}$, we iterate $\mathbf{x}^{(s)}$ and $\mathbf{p}^{(s)}$ forward by L steps using leap-frog integration, equations (6.13). We end up with a new $\tilde{\mathbf{x}}$ which will be accepted or rejected using the following rule:

$$
\mathbf{x}^{(s+1)} = \begin{cases} \tilde{\mathbf{x}} & \text{if } \alpha < \exp(-\Delta H) \\ \mathbf{x}^{(s)} & \text{otherwise} \end{cases} \qquad (6.16)
$$

where α is a random number picked from a standard uniform distribution $U(0,1)$, and $\Delta H = H(\tilde{\mathbf{x}}_{s+1}, \tilde{\mathbf{p}}_{s+1}) - H(\mathbf{x}_s, \mathbf{p}_s)$:

$$
\begin{aligned}
\Delta H &= \sum_{i,n} \left[\frac{\tilde{p}_i^2(n) - p_i^2(n)}{2} + R_m \Big[\Big(x_i^2(n) - y_i^2(n) \Big)^2 - \Big(\tilde{x}_i^2(n) - y_i^2(n) \Big)^2 \Big] \right. \\
&+ \left. R_f \Big[\Big(\tilde{\Delta}^2(x_i(n)) + \tilde{\Delta}^2(x_i(n)) \Big) - \Big(\Delta^2(x_i(n)) + \Delta^2(x_i(n)) \Big) \Big] \right] \qquad (6.17)
\end{aligned}
$$

After these L steps, the new $\tilde{\mathbf{p}}$ is replaced by a new momentum, which $\mathbf{p}^{(s+1)}$is drawn from the following distribution.

$$
P(\mathbf{p}) = \frac{1}{\sqrt{2\pi}} \exp\Big(\frac{-\mathbf{p}^2}{2} \Big) \qquad (6.18)
$$

These steps are repeated several times, and after an initialization phase data can be collected to be used in calculations of the form of equation (6.10).

As described above, the way candidate states are chosen in a hybrid Monte Carlo is different than Metropolis method. However, it is still required that the transitions from $\mathbf{x}$ to $\mathbf{x}^*$ be symmetric so that the target distribution is invariant. In other words, the proposal should be symmetric so that:

$$\pi(\mathbf{x})A(\mathbf{x}, \mathbf{x}^*) = \pi(\mathbf{x}^*)A(\mathbf{x}^*, \mathbf{x}) \tag{6.19}$$

This is shown to be true in [18] and [37].

6.2.3 Langevin Monte Carlo

Langevin Monte Carlo is another stochastic dynamical method which is closely related to hybrid Monte Carlo method. In order to get Langevin Monte Carlo from hybrid Monte Carlo, one needs to choose a new momentum after each leap-frog step and then accept or reject $\mathbf{x}^*$ using equation (6.16) based on the change in H. If the first and second equations in equation (6.13) are combined we get:

$$\mathbf{x}(s+\epsilon) = \mathbf{x}(s) - \frac{\epsilon^2}{2}\nabla\Big[A_0(\mathbf{x}(s))\Big] + \epsilon\eta(s) \tag{6.20}$$

where we have switched $\mathbf{p}(s)$ with $\eta(s)$ which is also drawn from a normal distribution.

Equation (6.20) is the solution to the Langevin diffusion equation:

$$\frac{d\mathbf{x}}{ds} = -\frac{1}{2}\frac{\partial A_0(\mathbf{x}(s))}{\partial \mathbf{x}}ds + dW(s) \tag{6.21}$$

where $W(s)$ is the standard Brownian motion.

Although Langevin Monte Carlo is a special case of hybrid Monte Carlo, it works very differently because of its random generating new steps as it moves down the gradient of action.

6.3 Estimation and Prediction in Colpitts Oscillator

To verify the MCMC methods described in previous sections, Colpitts oscillator was used as a *test* model. Figure (6.1) shows the circuit diagram for this oscillator. The equations from this diagram can be reduced to a simpler form as shown in equations (6.22).

$$\begin{aligned} \dot{x_0} &= \alpha x_1 \\ \dot{x_1} &= -\gamma(x_0 + x_2) - q x_1 \\ \dot{x_2} &= \eta(x_1 + 1 - \exp(-x_0)) \end{aligned} \tag{6.22}$$

(6.23)

This system is chaotic with the following values of parameters:

$$\alpha = 5.0 \quad , \quad \gamma = 0.08 \quad , \quad q = 0.7 \quad , \quad \eta = 6.3$$

This system of equations has three dimensions and four parameters. We would like to measure only x_0 for a total time T, and estimate the other state variables x_1, x_2, and all four parameters. One way to do this is to follow the procedure introduced for twin experiments in chapter 4. As usual, first we integrate the equations for Colpitts oscillator. Only the the first state variable x_0 is then used as a *measurement*.

6.3.1 Number of Measured States

In this specific case, we have used a simple Metropolis-Hastings algorithm to sample from the distribution $\exp(A_0)$. If the system reaches equilibrium after enough iterations, we will get statistics for all measured and unmeasured state variables and parameters. The evolution of action over the course of *iteration time* is given by 6.24.

$$\frac{d\mathbf{X}(s)}{ds} = -\frac{\partial A_0(\mathbf{X}(s))}{\partial \mathbf{X}(s)} + \sqrt{2}\eta(s) \tag{6.24}$$

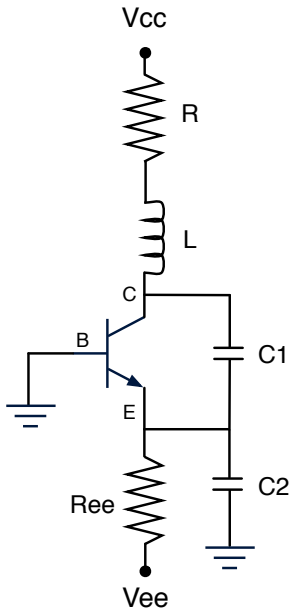

Figure 6.1: Colpitts Oscillator

If we start from different regions of the search space, ideally we should end up in the vicinity of the same value for minimum of A_0. Starting from random initial paths $\mathbf{X}^{(0)}$, we can let the system evolve according to equation (6.24). If we get different minima for A_0, then it is not possible to successfully estimate parameters and states of Colpitts oscillator.

Figure (6.2) shows minima of A_0 starting from different initial path $\mathbf{X}^{(0)}$. If all four parameters are free, it can be seen that the shape of action does not have one well defined minimum. When one of the parameters (α) is fixed, then all initial paths converge to the same minimum of action. This means that it is not possible to find estimate the hidden parameters and states if α is free to change.

6.3.2 Results

After fixing α to its original value, ODEs in equation (6.22) were used to generate synthetic data for estimation method. Time trace of x_0 is used as data to estimate the unobserved states x_1, x_2, and parameters. Figure (6.3) shows the estimation of the hidden states. At the end of the estimation window (yellow line),

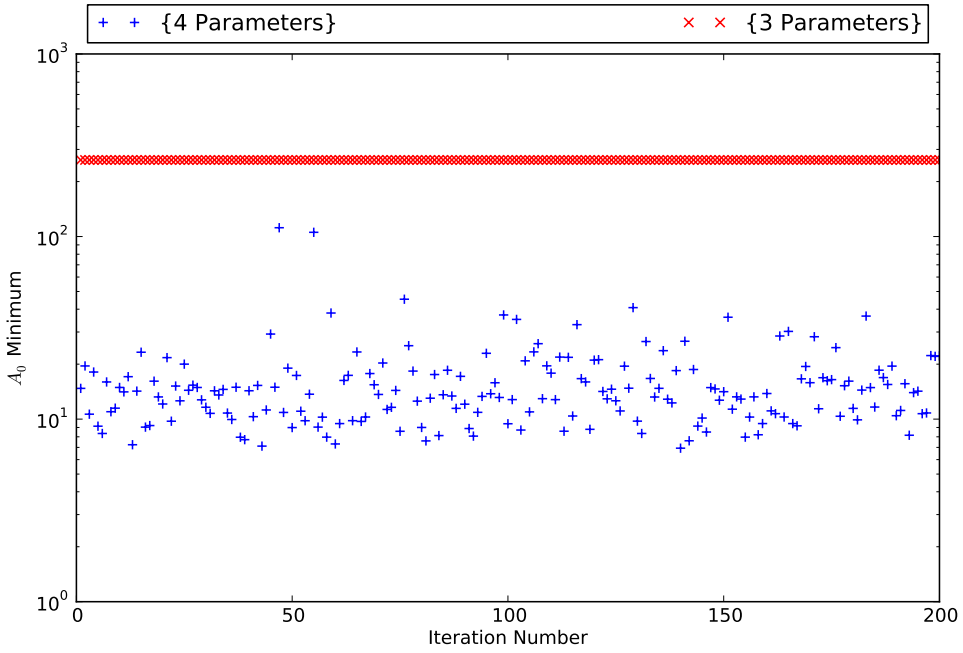

Figure 6.2: Minima of A_0 for Colpitts oscillator with 3 and 4 parameters

the parameters are fixed to their estimated values and integrated forward. Table (6.1) shows the estimated values of these parameters and the error of estimation.

Table 6.1: Estimated Parameters for fixed α. ($\alpha = 5.0$)

Parameter	**Real Value**	**Estimated Value**
γ	8×10^{-2}	$(9.1 \pm 0.5) \times 10^{-2}$
q	7×10^{-1}	$(6.8 \pm 0.4) \times 10^{-1}$
η	6.3	5.7 ± 0.6

6.4 Metropolis Coupled Markov Chain Monte Carlo

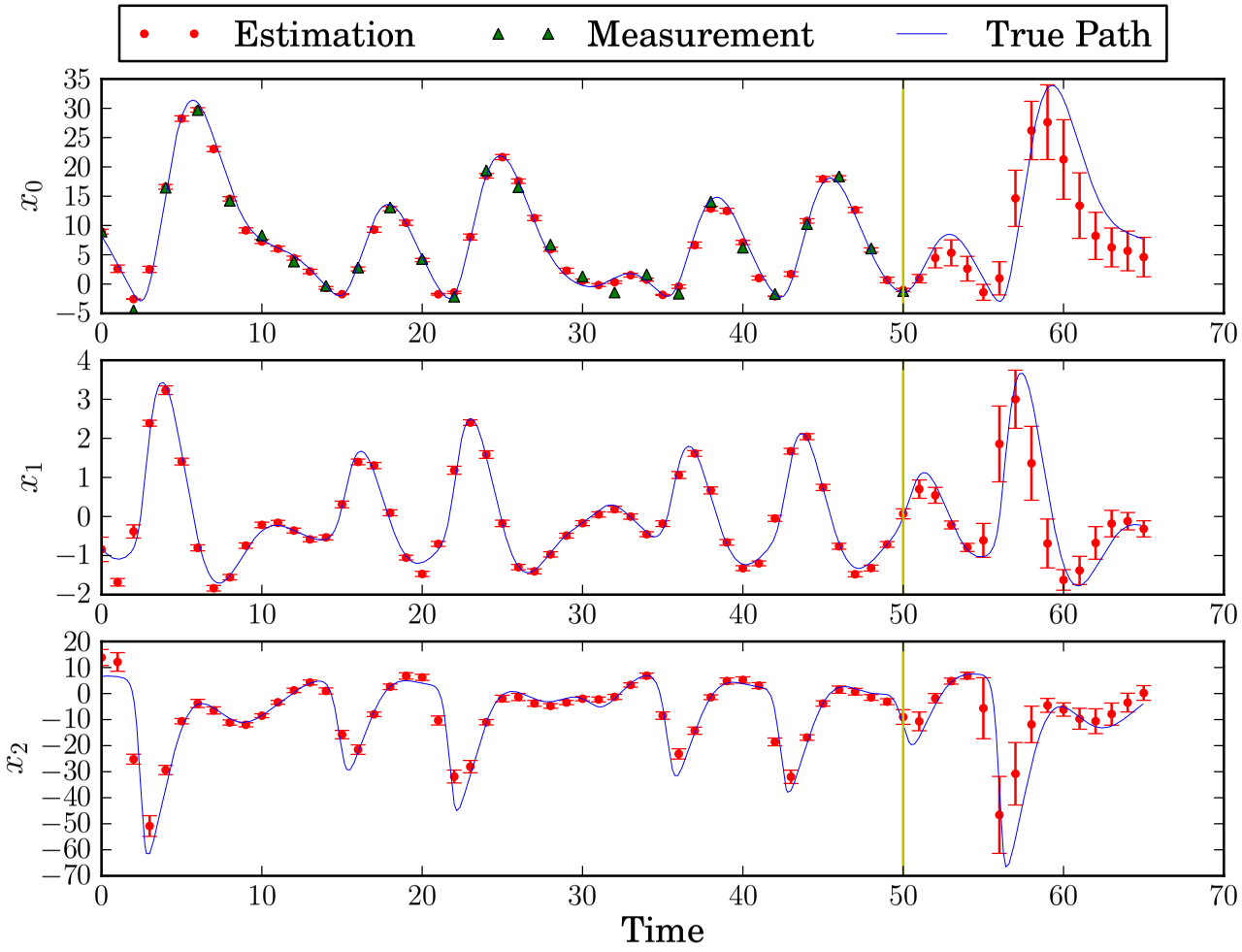

Figure 6.3: Estimation and prediction of state variables of Colpitts oscillator. (All state variables and time have arbitrary units)

Appendix A

Phenomenological Current Equations

A.1 Current List

The currents used in our model are based on the following phenomenological forms.

Current	Description	Source
$I_{Na,t}$	Transient sodium current	[35]
$I_{Na,p}$	Persistence sodium current	[46]
I_K	Delayed rectifier potassium current	[35]
I_A	Transient outward potassium current	[35]
$I_{A,slow}$	Slowly inactivating 'delay' potassium current	[46]
I_{IR}	Inwardly rectifying potassium current	[46]
I_T	Low-threshold calcium current	[35]

A.2 Voltage Equation

Voltage different equation can be written in the following general form, as an addition of currents from different channels (with an exception of calcium currents) and injected current:

$$\frac{dV}{dt} = \frac{1}{C_m}\left[\sum_i \left(\bar{g}_i X^a Y^b (E_x - V)\right) + I_{inj}\right]$$

where $\bar{g}_i$ is the maximal conductance of channel i and X and Y are gating variables for activation and inactivation, respectively. The equations for gating variables of each channel and corresponding parameters are given in the following pages.

A.3 Transient sodium channel $I_{Na,t}$

Current

$$I_{Na,t} = \bar{g}_{Na,t} m^3 h (V - E_{Na})$$

State equations of m and h

$$\begin{aligned} \dot{m} &= (m_\infty(V) - m)/\tau_m(V) \\ \dot{h} &= (h_\infty(V) - h)/\tau_h(V) \end{aligned}$$

where

$$\begin{aligned} m_\infty &= \alpha_m(V)/(\alpha_m(V) + \beta_m(V)) \\ \tau_m &= 1/(\alpha_m(V) + \beta_m(V)) \end{aligned}$$

Kinetics

$$\begin{aligned} \alpha_m(V) &= q_{10} \times 0.32 \text{expM1}(13.1 - V', 4) \\ \beta_m(V) &= q_{10} \times 0.28 \text{expM1}(V' - 40.1, 5) \\ \alpha_h(V) &= q_{10} \times 0.128 \exp((17 - V')/18) \\ \beta_h(V) &= q_{10} \times 4/(1 + \exp\left[(40.0 - V')/5\right]) \\ V' &= V + 65 \\ q_{10} &= 3^{(T-30)/10} = 2.158 \quad (\text{at } 37^\circ\text{C}) \\ \text{expM1}(x, y) &= \begin{cases} y(1 - x/2y) & \text{if } |x/y| < 10^{-6} \\ x/\left[\exp(x/y) - 1\right] & \text{Otherwise} \end{cases} \end{aligned}$$

Units and Parameters

$\bar{g}_{Na} = 0.300$	(S/cm2)
T	(°C)
E_{Na}	(mV)
V	(mV)
I_{Na}	(mA/cm2)

A.4 Persistence sodium channel $I_{Na,p}$

Current

$$I_{Na} = \bar{g}_{Na,P} m h (V - E_{Na})$$

State equations of m and h

$$\begin{aligned} \dot{m} &= (m_\infty(V) - m)/\tau_m(V) \\ \dot{h} &= (h_\infty(V) - h)/\tau_h(V) \end{aligned}$$

Kinetics

$$\begin{aligned} m_\infty(V) &= \frac{1}{1 + \exp\left[(V - m_{vh})/m_{ve}\right]} \\ \tau_m(V) &= \begin{cases} 0.025 + 0.14 \exp\left[(V + 40)/10\right] & \text{If } V < -40 \\ 0.02 + 0.145 \exp\left[(-V - 40)/10\right] & \text{Otherwise} \end{cases} \\ h_\infty(V) &= \frac{1}{1 + \exp\left[(V - h_{vh})/h_{ve}\right]} \\ \tau_h(V) & \quad \text{No functional form provided (from table)} \end{aligned}$$

Units and Parameters

$\bar{g}_{Na,p} = 4 \times 10^{-5}$	(S/cm2)
m_{vh} = -52.6	(mV)
m_{ve} = -4.6	(mV)
h_{vh} = -48.8	(mV)
h_{ve} = 10.0	(mV)
E_{Na}	(mV)
V	(mV)
I_{Na}	(mA/cm2)

A.5 Delayed rectifier potassium current I_K

Current

$$I_K = \bar{g}_K n^3 l (V - E_K)$$

State Equations for n and l

$$\begin{aligned} \dot{n} &= (n_\infty(V) - n)/\tau_n(V) \\ \dot{l} &= (l_\infty(V) - l)/\tau_l(V) \end{aligned}$$

with

$$\begin{aligned} n_\infty(V) &= 1/(1 + \alpha_n^*(V)) \\ \tau_n(V) &= \beta_n^*(V)/\left[q_{10} a_{0n} (1 + \alpha_n^*(V))\right] \\ l_\infty(V) &= 1/(1 + \alpha_l^*(V)) \\ \tau_l(V) &= \beta_l^*(V)/\left[q_{10} a_{0l} (1 + \alpha_l^*(V))\right] \\ q_{10} &= 3^{(T-30)/10} = 2.158 \quad \text{(at 37°C)} \end{aligned}$$

Kinetics

$$
\begin{aligned}
\alpha_n^*(V) &= \exp\left[\frac{10^{-3}\zeta_n(V-V_{hn})9.648\times10^4}{8.315(273.16+T)}\right] \\
&= \exp\left[3.741\times10^{-3}\zeta_n(V-V_{hn})\right] \quad \text{(at 37°)} \\
\beta_n^*(V) &= \exp\left[\frac{10^{-3}\zeta_n g_{mn}(V-V_{hn})9.648\times10^4}{8.315(273.16+T)}\right] \\
&= \exp\left[3.741\times10^{-3}\zeta_n g_{mn}(V-V_{hn})\right] \quad \text{(at 37°)} \\
\alpha_l^*(V) &= \exp\left[\frac{10^{-3}\zeta_l(V-V_{hl})9.648\times10^4}{8.315(273.16+T)}\right] \\
&= \exp\left[3.741\times10^{-3}\zeta_l(V-V_{hl})\right] \quad \text{(at 37°)} \\
\beta_l^*(V) &= \exp\left[\frac{10^{-3}\zeta_l g_{ml}(V-V_{hl})9.648\times10^4}{8.315(273.16+T)}\right] \\
&= \exp\left[3.741\times10^{-3}\zeta_l g_{ml}(V-V_{hl})\right] \quad \text{(at 37°)}
\end{aligned}
$$

Units and Parameters

$\bar{g}_K = 0.003$	(S/cm2)
V_{hn} = -32	(mV)
V_{hl} = -61	(mV)
$a_{0l} = 0.001$	(1/ms)
$a_{0n} = 0.03$	(1/ms)
ζ_n = -5	
$\zeta_l = 2$	
$g_{mn} = 0.4$	
$g_{ml} = 1.0$	
V	(mV)
I_K	(mA/cm2)
E_K	(mV)
T	(°C)

A.6 Transient outward potassium current I_A

Current

$$I_A = \bar{g}_{K,A} nl(V - E_K)$$

State equations of n and l

$$\begin{aligned} \dot{n} &= (n_\infty(V) - n)/\tau_n(V) \\ \dot{l} &= (l_\infty(V) - l)/\tau_l(V) \end{aligned}$$

with

$$\begin{aligned} n_\infty(V) &= 1/[1 + \alpha_n^*(V)] \\ \tau_n(V) &= \beta_n^*(V)/[q_{10} a_{0n}(1 + \alpha_n^*(V))] \\ l_\infty(V) &= 1/[1 + \alpha_l^*(V)] \\ \tau_l(V) &= \beta_l^*(V)/[q_{10} a_{0l}(1 + \alpha_l^*(V))] \\ q_{10} &= 3^{(T-30)/10} = 2.158 \quad (\text{at } 37^\circ\text{C}) \end{aligned}$$

Kinetics

$$\begin{aligned} \alpha_n^*(V) &= \exp\Big[\frac{0.001\zeta_n(V - V_{hn})9.648 \times 10^4}{8.315(273.16 + T)}\Big] \\ &= \exp\Big[3.741 \times 0.001\zeta_n(V - V_{hn})\Big] \quad (\text{at } 37^\circ\text{C}) \\ \beta_n^*(V) &= \exp\Big[\frac{0.001\zeta_n g_{mn}(V - V_{hn})9.648 \times 10^4}{8.315(273.16 + T)}\Big] \\ &= \exp\Big[3.741 \times 0.001\zeta_n g_{mn}(V - V_{hn})\Big] \quad (\text{at } 37^\circ\text{C}) \\ \alpha_l^*(V) &= \exp\Big[\frac{0.001\zeta_l(V - V_{hl})9.648 \times 10^4}{8.315(273.16 + T)}\Big] \\ &= \exp\Big[3.741 \times 0.001\zeta_l(V - V_{hl})\Big] \quad (\text{at } 37^\circ\text{C}) \\ \beta_l^*(V) &= \exp\Big[\frac{0.001\zeta_l g_{ml}(V - V_{hl})9.648 \times 10^4}{8.315(273.16 + T)}\Big] \\ &= \exp\Big[3.741 \times 0.001\zeta_l g_{ml}(V - V_{hl})\Big] \quad (\text{at } 37^\circ\text{C}) \end{aligned}$$

Units and Parameters

T	(°C)
$\bar{g}_{K,A} = 0.01$	(mho/cm2)
V_{hn} = -33.6	(mV)
V_{hl} = -83	(mV)
$a_{0l} = 0.08$	(1/ms)
$a_{0n} = 0.02$	(1/ms)
ζ_n = -3	
$\zeta_l = 4$	
$g_{mn} = 0.6$	
$g_{ml} = 1$	

A.7 Slowly inactivating delay potassium current $I_{A,slow}$

Current

$$I_K = \bar{g}_{A,slow} m^2 \left[ah + (1-a)\right](V - E_K)$$

State equations of m and h

$$\begin{aligned} \dot{m} &= (m_\infty(V) - m)/\tau_m(V) \\ \dot{h} &= (h_\infty(V) - h)/\tau_h(V) \end{aligned}$$

Kinetics

$$\begin{aligned} \tau_m(V) &= 0.378 + 9.91 \exp\left[-((V + 34.3)/30.1)^2\right] \\ m_\infty(V) &= \frac{1}{1 + \exp\left[(V - m_{vh})/m_{ve}\right]} \\ m_\alpha &= \exp\left[-(V + 90.96)/29.01\right] \\ m_\beta &= \exp\left[(V + 90.96)/100\right] \\ \tau_h(V) &= 1097.4/(m_\alpha + m_\beta) \\ h_\infty(V) &= 1/\left[1 + \exp((V - h_{vh})/h_{ve})\right] \end{aligned}$$

Units and Parameters

$\bar{g}_{A,slow} = 9.51\times10^{-4}$	(S/cm2)
m_{vh} = -27	(mV)
m_{ve} = -16	(mV)
h_{vh} = -33.5	(mV)
h_{ve} = 21.5	(mV)
$a = 0.996\ E_K$	(mV)
V	(mV)
I_K	(mA/cm2)

A.8 Inwardly rectifying potassium current I_{IR}

Current

$$I_{IR} = \bar{g}_{IR} m (V - E_K)$$

State equation of m

$$\dot{m} = (m_\infty(V) - m)/\tau_m(V)$$

Kinetics

$$\begin{aligned} m_\infty(V) &= \frac{1}{1 + \exp\left[(V - m_{vh})/m_{ve}\right]} \\ \tau_m(V) &\quad \text{No functional form provided (table)}/q_{10} \end{aligned}$$

with

$$q_{10} = 3^{(T-35)/10} = 1.246 \quad (\text{at } 37^\circ\text{C})$$

Units and Parameters

E_K	(mV)
$\bar{g}$ = 1.4e-4	(S/cm2)
m_{hv} = -82	(mV)
m_{ve} = 13	(mV)
V	(mV)
I_K	(mA/cm2)
m_∞	
τ_m	(ms)
T	(°C)
q_{10}	

A.9 Low-threshold calcium current I_T

Current

$$I_{Ca} = \bar{g}_{Ca,T} m^2 h \mathrm{GHK}(V, Ca_i, Ca_o)$$

with

$$GHK(V, Ca_i, Ca_o) = -f\Big[1 - \frac{Ca_i}{Ca_o}\exp(V/f)\Big] \times \mathrm{efun}(V/f)$$

where

$$\begin{aligned} f &= \frac{25}{293.15}(T + 273.15) = 26.450 \quad \text{(at 37°C)} \\ \mathrm{efun}(x) &= \begin{cases} (1 - \frac{x}{2}) & \text{if } |x| < 10^{-4} \\ \frac{x}{\exp(x)-1} & \text{Otherwise} \end{cases} \end{aligned}$$

State equations of m and h

$$\begin{aligned} \dot{m} &= (m_\infty(V) - m)/\tau_m(V) \\ \dot{h} &= (h_\infty(V) - h)/\tau_h(V) \end{aligned}$$

where

$$\begin{aligned} m_\infty(V) &= \alpha_m(V)/(\alpha_m(V) + \beta_m(V)) \\ \tau_m(V) &= 1/(\alpha_m(V) + \beta_m(V)) \end{aligned}$$

The same equations follow for $h_\infty(V)$ and $\tau_h(V)$.

Kinetics

$$
\begin{aligned}
\alpha_m(V) &= \frac{0.2(-V+19.26)}{\exp\Big[(-V+19.26)/10\Big]-1} \\
\beta_m(V) &= 0.009\exp\big(-V/22.03\big) \\
\alpha_h(V) &= 10^{-6}\exp(-V/16.26) \\
\beta_h(V) &= \frac{1}{\exp\Big[(-V+29.79)/10\Big]+1}
\end{aligned}
$$

Units and Parameters

$T = 6.3$	(°C)
$\bar{g}_{Ca,t} = 0.003$	(S/cm2)
Ca_i	(mM)
Ca_o	(mM)

Appendix B

Standardization of some currents

Standardization of three current I_K, I_A, and I_T is demonstrated here. In each case, the phenomenological form of the current equations is used to convert the parameters into the standard form introduced in section 4.2.

B.1 Delayed rectifier potassium current I_K

Current

$$I_K = \bar{g}_K n^3 l (V - E_K)$$

State Equations for n and l

$$\begin{aligned} \dot{n} &= (n_\infty(V) - n)/\tau_n(V) \\ \dot{l} &= (l_\infty(V) - l)/\tau_l(V) \end{aligned}$$

Steady state and time constants of n and l

$$n_\infty(V) = \frac{1}{2}\left[1 + \tanh\left(\frac{V - va_n}{dva_n}\right)\right]$$

with the following parameters:

va_n = -32
dva_n = 10.6923

$$\tau_n(V) = ta0_n + ta1_n \left[1 - \tanh^2\left(\frac{V - vat_n}{dvat_n}\right)\right]$$

with the following parameters:
$ta0$ = 0
$ta1$ = 7.88
vat = -29.89
$dvat$ = 17

$$l_\infty(V) = \frac{1}{2}\left[1 + \tanh\left(\frac{V - va_l}{dva_l}\right)\right]$$

with the following parameters:
va_l = -61
dva_l = -26.7307

$$\tau_l(V) = ta0_l + ta1_l \tanh\left[\left(\frac{V - vat_l}{dvat_l}\right)\right]$$

with the following parameters:
$ta0$ = 231.7315
$ta1$ = 231.7315
vat = -61
$dvat$ = 26.7

B.2 Transient outward potassium current I_A

Current

$$I_A = \bar{g}_{K,A} nl(V - E_K)$$

State equations of n and l

$$\begin{aligned} \dot{n} &= (n_\infty(V) - n)/\tau_n(V) \\ \dot{l} &= (l_\infty(V) - l)/\tau_l(V) \end{aligned}$$

Steady state and time constants of n and l

$$n_\infty(V) = \frac{1}{2}\left[1 + \tanh\left(\frac{V - va_n}{dva_n}\right)\right]$$

with the following parameters:

va_n	= -33.6
dva_n	= 17.8205

$$\tau_n(V) = ta0_n + ta1_n\left[1 - \tanh^2\left(\frac{V - vat_n}{dvat_n}\right)\right]$$

with the following parameters:

$ta0_n$	= 0
$ta1_n$	= 11.8222
vat_n	= -37.20
$dvat_n$	= 25.5

$$l_\infty(V) = \frac{1}{2}\left[1 + \tanh\left(\frac{V - va_l}{dva_l}\right)\right]$$

with the following parameters:

va_l	= -83
dva_l	= -13.3654

$$\tau_l(V) = ta0_l + ta1_l \tanh\left[\left(\frac{V - vat_l}{dvat_l}\right)\right]$$

with the following parameters:

$ta0_l$	= 2.8966
$ta1_l$	= 2.8966
vat_l	= -83
$dvat_l$	= 13.35

B.3 Low-threshold calcium current I_T

Current

$$I_{Ca} = \bar{g}_{Ca,T} m^2 h \mathrm{GHK}(V, Ca_i, Ca_o)$$

with

$$GHK(V, Ca_i, Ca_o) = -f\Big[1 - \frac{Ca_i}{Ca_o}\exp(V/f)\Big] \times \mathrm{efun}(V/f)$$

where

$$f = \frac{25}{293.15}(T + 273.15) = 26.450 \quad \text{(at 37°C)}$$

$$\text{efun}(x) = \begin{cases} (1 - \frac{x}{2}) & \text{if } |x| < 10^{-4} \\ \frac{x}{\exp(x)-1} & \text{Otherwise} \end{cases}$$

State equations of m and h

$$\dot{m} = (m_\infty(V) - m)/\tau_m(V)$$
$$\dot{h} = (h_\infty(V) - h)/\tau_h(V)$$

Steady state and time constants of m and h

$$m_\infty(V) = \frac{1}{2}\left[1 + \tanh\left(\frac{V - va_m}{dva_m}\right)\right]$$

with the following parameters:

va_m = -35.65
dva_m = 16

$$\tau_m(V) = ta0_m + ta1_m\left[1 - \tanh^2\left(\frac{V - vat_m}{dvat_m}\right)\right]$$

with the following parameters:

$ta0_m$ = 0
$ta1_m$ = 11.494
vat_m = -40.4
$dvat_m$ = 24

$$h_\infty(V) = \frac{1}{2}\left[1 + \tanh\left(\frac{V - va_h}{dva_h}\right)\right]$$

with the following parameters:

va_h = -67.1
dva_h = -12.39

$$\tau_h(V) = ta0_h + ta1_h\left[1 - \tanh^2\left(\frac{V - vat_h}{dvat_h}\right)\right]$$

with the following parameters:

$ta0_h$ = 0
$ta1_h$ = 8303.5
vat_h = -70.1
dva_ht = 18

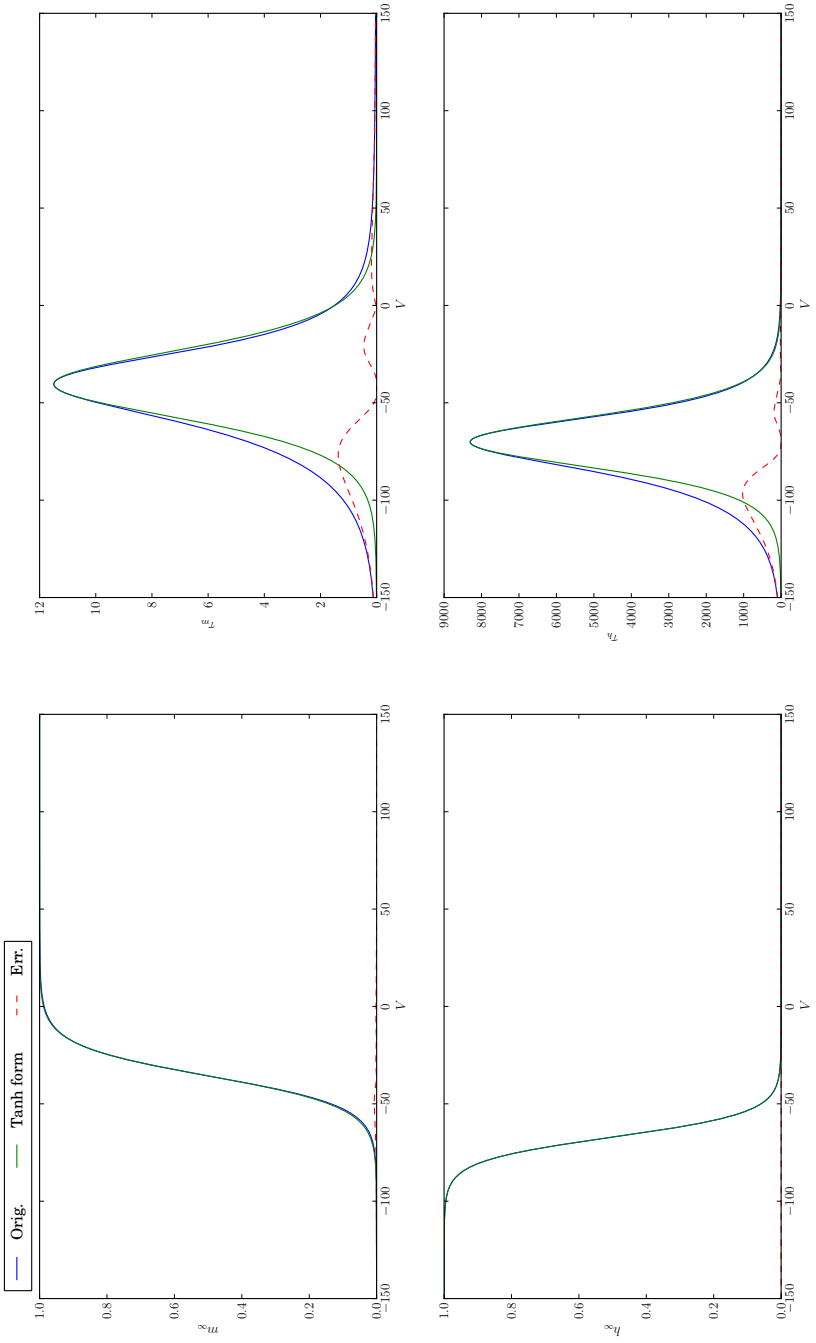

Figure B.1: Comparison of phenomenological and standardized curves for I_K

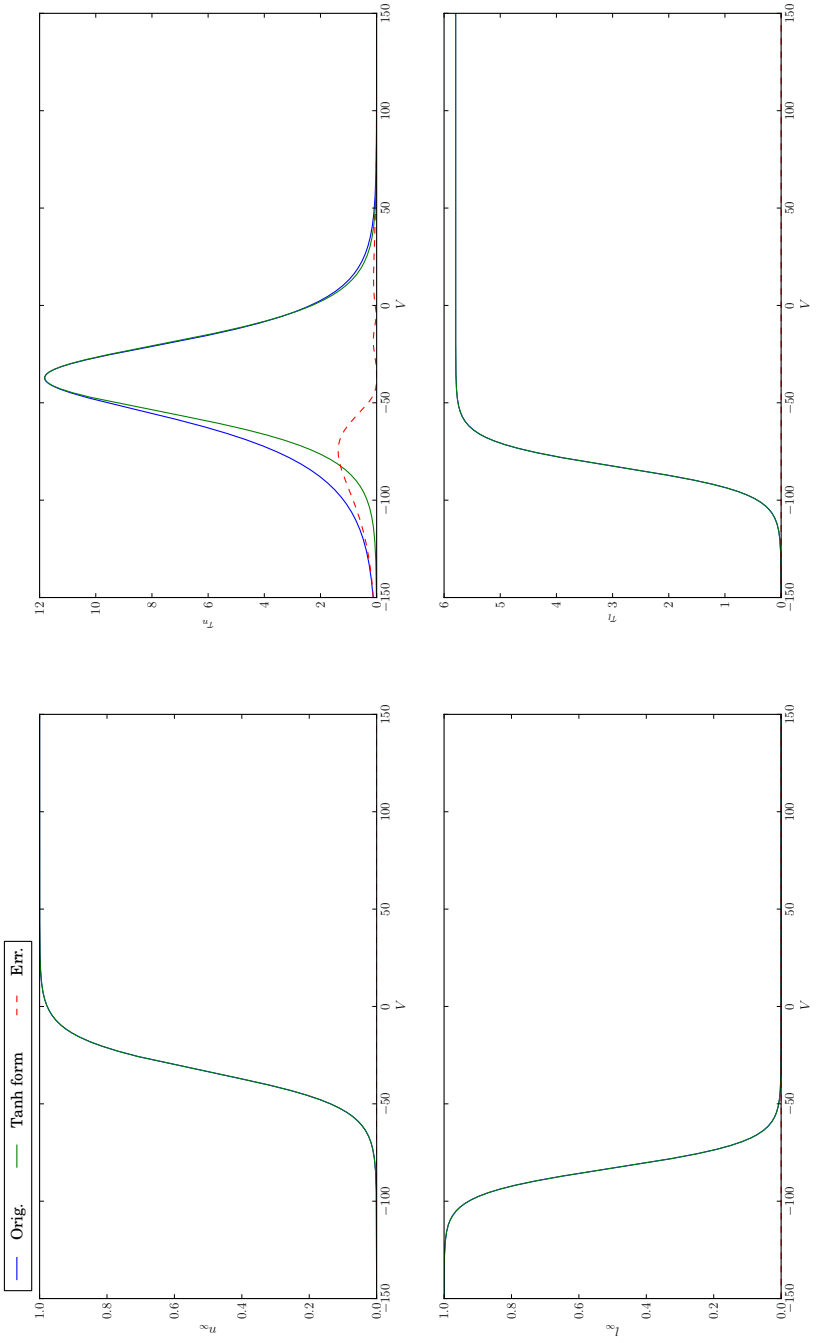

Figure B.2: Comparison of phenomenological and standardized curves for I_A

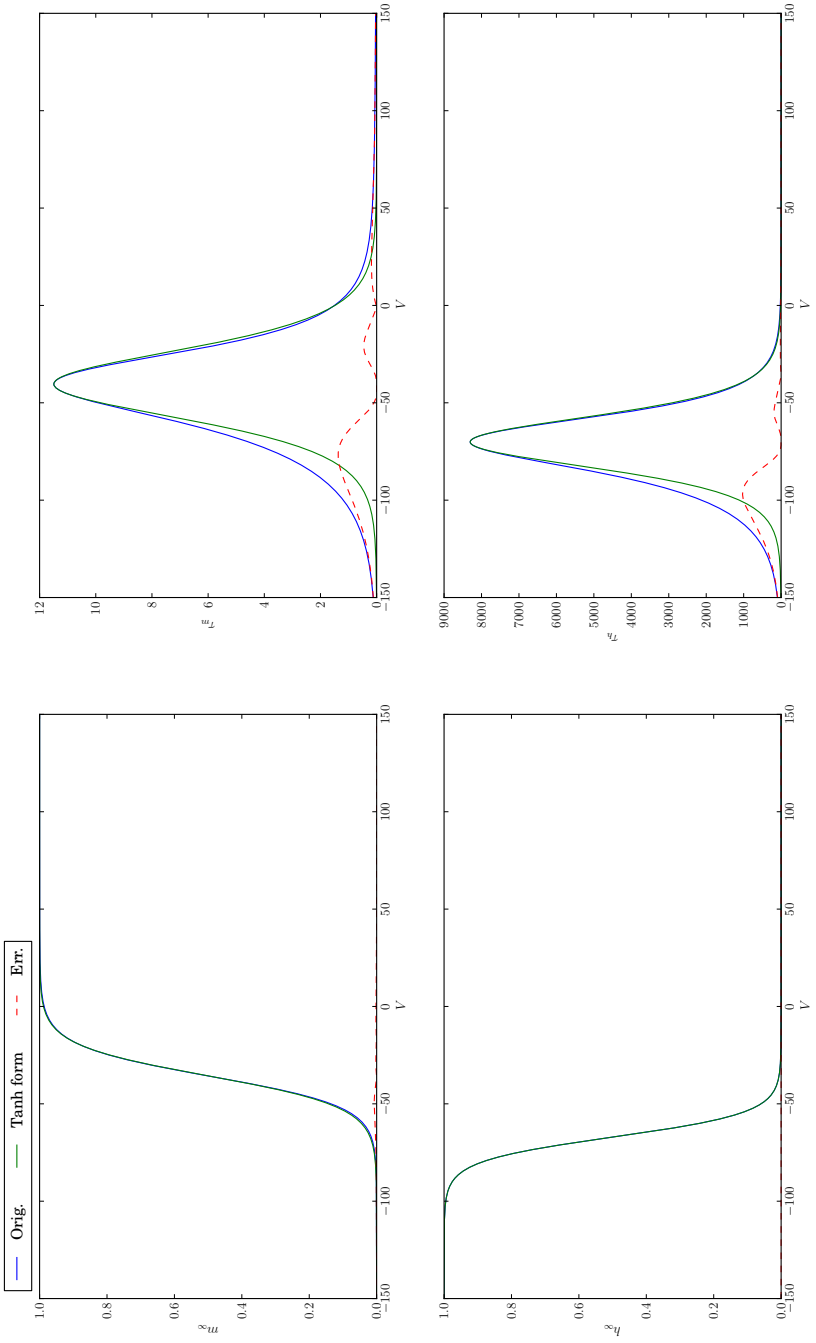

Figure B.3: Comparison of phenomenological and standardized curves for I_T

Appendix C

Detailed Model for Type II BNST Neurons

C.1 Steady states

$$
\begin{aligned}
m_\infty &= \frac{1}{2}\Big[1+\tanh[(V-amV1)/amV2]\Big] \\
h_\infty &= \frac{1}{2}\Big[1+\tanh[(V-ahV1)/ahV2]\Big] \\
n_\infty &= \frac{1}{2}\Big[1+\tanh[(V-anV1)/amV2]\Big] \\
b_\infty &= \frac{1}{2}\Big[1+\tanh[(V-abV1)/abV2]\Big] \\
p_\infty &= \frac{1}{2}\Big[1+\tanh[(V-apV1)/apV2]\Big] \\
q_\infty &= \frac{1}{2}\Big[1+\tanh[(V-aqV1)/aqV2]\Big] \\
u_\infty &= \frac{1}{2}\Big[1+\tanh[(V-auV1)/auV2]\Big] \\
r_\infty &= \frac{1}{2}\Big[1+\tanh[(V-arV1)/arV2]\Big] \\
s_\infty &= \frac{1}{2}\Big[1+\tanh[(V-asV1)/asV2]\Big] \\
t_\infty &= \frac{1}{2}\Big[1+\tanh[(V-atV1)/atV2]\Big] \\
z_\infty &= \frac{1}{2}\Big[1+\tanh[(V-azV1)/azV2]\Big]
\end{aligned}
\tag{C.1}
$$

C.2 Time constant

$$
\begin{aligned}
\tau_m &= tm0 + epsm\Big(1 - \tanh^2[(V - amV1)/amV3]\Big) \\
\tau_h &= th0 + epsh\Big(1 - \tanh^2[(V - ahV1)/ahV3]\Big) \\
\tau_n &= tm0 + epsm\Big(1 - \tanh^2[(V - anV1)/amV3]\Big) \\
\tau_b &= tb0 + epsb\Big(1 - \tanh^2[(V - abV1)/abV3]\Big) \\
\tau_p &= tp0 + epsp\Big(1 - \tanh^2[(V - apV1)/apV3]\Big) \\
\tau_q &= tq0 + deltasq + \frac{1}{2}\Big[1 - \tanh(V - aqV1)\Big] \\
&\quad [epsq(1 - \tanh^2((V - aqV1)/aqV3)) - deltasq)] \\
\tau_u &= tu0 + epsu\Big(1 - \tanh^2[(V - auV1)/auV3]\Big) \\
\tau_r &= tr0 + epsr\Big(1 - \tanh^2[(V - arV1)/arV3]\Big) \\
\tau_s &= ts0 + eps5\Big(1 - \tanh^2[(V - asV1)/asV3]\Big) \\
\tau_t &= tx0 + epst\Big[1 + \tanh((V - atV1)/atV3)\Big]\Big[1 - \tanh((V - atV1)/atV4)\Big] \\
&\quad \times \frac{1 - \tanh(V - atV1)\tanh\Big[(1/atV3 + 1/atV4)(V - atV1)\Big]}{1 + \tanh((V - atV1)/atV3)\tanh((V - atV1)/atV4)} \\
\tau_z &= tz0 + epsz\Big(1 - \tanh^2((V - azV1)/azV3)\Big)
\end{aligned}
\tag{C.2}
$$

Bibliography

[1] H.D.I. Abarbanel. *Analysis of observed chaotic data*. Springer Verlag, 1996.

[2] H.D.I. Abarbanel. Effective actions for statistical data assimilation. *Physics Letters A*, 373(44):4044–4048, 2009.

[3] H.D.I. Abarbanel, D.R. Creveling, R. Farsian, and M. Kostuk. Dynamical state and parameter estimation. *SIAM Journal on Applied Dynamical Systems*, 8:1341, 2009.

[4] H.D.I. Abarbanel, D.R. Creveling, and J.M. Jeanne. Estimation of parameters in nonlinear systems using balanced synchronization. *Physical Review E*, 77(1):016208, 2008.

[5] H.D.I. Abarbanel and M.I. Rabinovich. Neurodynamics: nonlinear dynamics and neurobiology. *Current opinion in neurobiology*, 11(4):423–430, 2001.

[6] H.D.I. Abarbanel, S.S. Talathi, G. Mindlin, M. Rabinovich, and L. Gibb. Dynamical model of birdsong maintenance and control. *Physical Review E*, 70(5):051911, 2004.

[7] F.J. Alexander, G.L. Eyink, and J.M. Restrepo. Accelerated monte carlo for optimal estimation of time series. *Journal of Statistical Physics*, 119(5):1331–1345, 2005.

[8] G. Altekar, S. Dwarkadas, J.P. Huelsenbeck, and F. Ronquist. Parallel metropolis coupled markov chain monte carlo for bayesian phylogenetic inference. *Bioinformatics*, 20(3):407–415, 2004.

[9] Y.F. Atchadé, G.O. Roberts, and J.S. Rosenthal. Towards optimal scaling of metropolis-coupled markov chain monte carlo. *Statistics and Computing*, 21(4):555–568, 2011.

[10] A. Beskos, N.S. Pillai, G.O. Roberts, J.M. Sanz-Serna, and A.M. Stuart. Optimal tuning of the hybrid monte-carlo algorithm. *Arxiv preprint arXiv:1001.4460*, 2010.

[11] A. Beskos, FJ Pinski, JM Sanz-Serna, and AM Stuart. Hybrid monte carlo on hilbert spaces. *Stochastic Processes and their Applications*, 2011.

[12] M.S. Brainard and A.J. Doupe. Auditory feedback in learning and maintenance of vocal behavior. *Nature Reviews Neuroscience*, 1(1):31–40, 2000.

[13] M.S. Brainard and A.J. Doupe. What songbirds teach us about learning. *Nature*, 417(6886):351–358, 2002.

[14] L. Chen, Z. Qin, and J.S. Liu. Exploring hybrid monte carlo in bayesian computation. *sigma*, 2:2–5, 2001.

[15] D.R. Creveling, J.M. Jeanne, and H.D.I. Abarbanel. Parameter estimation using balanced synchronization. *Physics Letters A*, 372(12):2043–2047, 2008.

[16] O. De Feo, G.M. Maggio, and M.P. Kennedy. The colpitts oscillator: Families of periodic solutions and their bifurcations. *International Journal of Bifurcation and Chaos*, 10(5):935–958, 2000.

[17] A. Destexhe and T.J. Sejnowski. *Thalamocortical assemblies*. Oxford University Press Oxford, 2001.

[18] S. Duane, A.D. Kennedy, B.J. Pendleton, and D. Roweth. Hybrid monte carlo. *Physics letters B*, 195(2):216–222, 1987.

[19] C.W. Gardiner. *Stochastic methods*. Springer, 1985.

[20] J. Geweke. Monte carlo simulation and numerical integration. *Handbook of computational economics*, 1:731–800, 1996.

[21] C.J. Geyer. Practical markov chain monte carlo. *Statistical Science*, 7(4):473–483, 1992.

[22] A.J. Gruber, S.A. Solla, D.J. Surmeier, and J.C. Houk. Modulation of striatal single units by expected reward: a spiny neuron model displaying dopamine-induced bistability. *Journal of neurophysiology*, 90(2):1095–1114, 2003.

[23] J. Guckenheimer and R.A. Oliva. Chaos in the hodgkin-huxley model. *SIAM J. Appl. Dyn. Syst*, 1(1):105–114, 2002.

[24] S.E. Hammack, I. Mania, and D.G. Rainnie. Differential expression of intrinsic membrane currents in defined cell types of the anterolateral bed nucleus of the stria terminalis. *Journal of neurophysiology*, 98(2):638–656, 2007.

[25] R. Hazra, J.D. Guo, S.J. Ryan, A.M. Jasnow, J. Dabrowska, and D.G. Rainnie. A transcriptomic analysis of type i-iii neurons in the bed nucleus of the stria terminalis. *Molecular and Cellular Neuroscience*, 2011.

[26] D. Hochberg, C. Molina-Paris, J. Perez-Mercader, and M. Visser. Effective action for stochastic partial differential equations. *Physical Review E*, 60(6):6343, 1999.

[27] Q.J.M. Huys, M.B. Ahrens, and L. Paninski. Efficient estimation of detailed single-neuron models. *Journal of neurophysiology*, 96(2):872–890, 2006.

[28] E.M. Izhikevich. *Dynamical systems in neuroscience: the geometry of excitability and bursting*. The MIT press, 2007.

[29] B. Jouvet and R. Phythian. Quantum aspects of classical and statistical fields. *Physical Review A*, 19(3):1350, 1979.

[30] M.P. Kennedy. Chaos in the colpitts oscillator. *Circuits and Systems I: Fundamental Theory and Applications, IEEE Transactions on*, 41(11):771–774, 1994.

[31] N.F. Lepora, P.G. Overton, and K. Gurney. Efficient fitting of conductance-based model neurons from somatic current clamp. *Journal of computational neuroscience*, pages 1–24, 2012.

[32] J.S. Liu. *Monte Carlo strategies in scientific computing*. Springer Verlag, 2008.

[33] D.J.C. MacKay. *Information theory, inference, and learning algorithms*. Cambridge Univ Pr, 2003.

[34] G.M. Maggio, O. De Feo, and M.P. Kennedy. Nonlinear analysis of the colpitts oscillator and applications to design. *Circuits and Systems I: Fundamental Theory and Applications, IEEE Transactions on*, 46(9):1118–1130, 1999.

[35] M. Migliore, EP Cook, DB Jaffe, DA Turner, and D. Johnston. Computer simulations of morphologically reconstructed ca3 hippocampal neurons. *Journal of neurophysiology*, 73(3):1157–1168, 1995.

[36] R.M. Neal. Bayesian training of backpropagation networks by the hybrid monte carlo method. *Dept. of Computer Science, University of Toronto, Tech. Rep. CRG-TR-92-1*, 1992.

[37] R.M. Neal and University of Toronto. Department of Computer Science. Probabilistic inference using markov chain monte carlo methods. 1993.

[38] IP Omelyan, IM Mryglod, and R. Folk. Symplectic analytically integrable decomposition algorithms: classification, derivation, and application to molecular dynamics, quantum and celestial mechanics simulations. *Computer Physics Communications*, 151(3):272–314, 2003.

[39] A. Pikovsky, M. Rosenblum, and J. Kurths. *Synchronization: A universal concept in nonlinear sciences*, volume 12. Cambridge Univ Pr, 2003.

[40] J.C. Quinn and H.D.I. Abarbanel. State and parameter estimation using monte carlo evaluation of path integrals. *Quarterly Journal of the Royal Meteorological Society*, 136(652):1855–1867, 2010.

[41] J.C. Quinn and H.D.I. Abarbanel. Data assimilation using a gpu accelerated path integral monte carlo approach. *Journal of Computational Physics*, 2011.

[42] J.M. Restrepo. A path integral method for data assimilation. *Physica D: Nonlinear Phenomena*, 237(1):14–27, 2008.

[43] T. Sauer, J.A. Yorke, and M. Casdagli. Embedology. *Journal of Statistical Physics*, 65(3):579–616, 1991.

[44] JC Sexton and DH Weingarten. Hamiltonian evolution for the hybrid monte carlo algorithm. *Nuclear Physics B*, 380(3):665–677, 1992.

[45] G.M. Shepherd. *The synaptic organization of the brain*. Oxford University Press, USA, 2004.

[46] J.E. Steephen and R. Manchanda. Differences in biophysical properties of nucleus accumbens medium spiny neurons emerging from inactivation of inward rectifying potassium currents. *Journal of computational neuroscience*, 27(3):453–470, 2009.

[47] A.M. Stuart, J. Voss, and P. Wilberg. Conditional path sampling of sdes and the langevin mcmc method. *Communications in Mathematical Sciences*, 2(4):685–697, 2004.

[48] A. Szücs, F. Berton, T. Nowotny, P. Sanna, and W. Francesconi. Consistency and diversity of spike dynamics in the neurons of bed nucleus of stria terminalis of the rat: A dynamic clamp study. *PloS one*, 5(8):e11920, 2010.

[49] T. Takaishi and P. De Forcrand. Testing and tuning symplectic integrators for the hybrid monte carlo algorithm in lattice qcd. *Physical Review E*, 73(3):036706, 2006.

[50] N.G. van Kampen. *Stochastic processes in physics and chemistry*. North holland, 2007.

[51] H.U. Voss, J. Timmer, and J. Kurths. Nonlinear dynamical system identification from uncertain and indirect measurements. *International journal of bifurcation and chaos in applied sciences and engineering*, 14:1905–1934, 2004.

[52] G. Zhong and J.E. Marsden. Lie-poisson hamilton-jacobi theory and lie-poisson integrators. *Physics Letters A*, 133(3):134–139, 1988.